Hadronization Effects in the Strong Interaction

Patrik Edén

Department of Theoretical Physics
Lund University, Sweden

Thesis for the degree of Doctor of Philosophy

Thesis Advisor: Gösta Gustafson

Faculty Opponent: Valery A. Khoze

To be presented, with the permission of the Faculty of Mathematics and Natural Sciences of Lund University, for public criticism in Lecture Hall A of the Department of Physics on Friday, the 15th of January 1999, at 10.15 a.m.

Organization **LUND UNIVERSITY** Department of Theoretical Physics Helgonavägen 5 223 62 LUND	**Document Name** **DOCTORAL DISSERTATION** **Date of issue** December 1998 **CODEN:** ISBN 91-628-3331-6
Author(s) Patrik Edén	**Sponsoring organization**

Title and subtitle
Hadronization Effects in the Strong Interaction

Abstract

Different hadronization effects in high energy interactions are investigated. The frame-work is the Lund model for the strong interaction.
A model for baryon production in jet fragmentation is presented and extended to baryon remnant fragmentation in deep inelastic scattering and hadron–hadron collisions.
Observables designed to probe hadronization effects on $p_\perp$ correlations are shown to be sensitive to model assumptions, provided a strong two-jet cut is imposed on the data sample. A cut on high-$p_\perp$ jets also improves the similarity between quark jets in deep inelastic scattering and e^+e^- annihilation, and is thus suitable for an investigation of quark fragmentation universality.
The scale dependencies in jets are discussed and emphasis is put on the virtuality dependence rarely considered in theoretical calculations. Jet definitions corresponding to the theoretically considered jets are presented.
The ratio of multiplicities in quark and gluon jets are calculated within the frame-work of the Colour Dipole cascade. Energy conservation together with preconfinement implies a numerically large NNLO correction, which gives a result in agreement with data.

DOKUMENTDATABLAD
enl SIS 61 41 21

Key words
QCD, hadronization, string fragmentation, baryon production, jets

Classification system and/or index terms (if any)

Supplementary bibliographical information		**Language** English
ISSN and key title		**ISBN** 91-628-3331-6
Recipient's notes	**Number of pages** 147	**Price**
	Security classification	

Distribution by (name and address)
Patrik Edén, Dept. of Theoretical Physics
Helgonavägen 5, S-223 62 LUND

Signature ______________________ **Date** 1998-12-06

To Tomasine

This thesis is based on the following publications:

I P. Edén and G. Gustafson
Baryon Production in the String Fragmentation Picture
Zeitschrift für Physik **C 75** (1997) 41

II P. Edén
A Program for Baryon Generation and Its Applications to Baryon Fragmentation in DIS
LU TP 96-29

III P. Edén and G. Gustafson
Using Two-jet Events to Understand Hadronization
LU TP 98-25 (Submitted to *European Physical Journal* **C**)

IV P. Edén
Investigation of Quark Fragmentation Universality
LU TP 98-22 (Submitted to *European Physical Journal* **C**)

V P. Edén and G. Gustafson
Energy and Virtuality Scale Dependence in Quark and Gluon Jets
Journal of High Energy Physics **09** (1998) 015

Contents

Introduction

> I understand that you belong to some kind of jet-set eating popcorn on your way to Monte Carlo, while looking at photos of fragmented violins. Funny business, that not immediately comes to mind. But research is best when it is free.
> *K. Modigh*

I expect this thesis to be read only by a few people, who can be divided into two categories. Some of the readers will be colleagues in the field who immediately skip the first pages and start browsing the papers. The other readers are relatives and friends who politely starts reading the introduction, slightly discouraged by the fact that half of the words already in the title of the thesis were unknown to them.

In the beginning of the introduction, it is my intention to make these polite efforts of the latter category worthwhile. I will try to give some insight to the concepts "strong interaction" and "hadronization". If no such insight is gained by reading these pages, I am the only one to blame. However, if some reader also would like a clarification of the title words "effects", "in" and "the", I recommend him or her to immediately lay down this book and start reading a thesis in philosophy instead.

The major part of the thesis is the second, consisting of five papers. At the end of this introduction I give an overview of these, and before that a brief description of the Lund model for strong interactions, which is the theoretical frame-work in the papers.

From atoms to jets

A motivation for the strong interaction

This thesis is about particles inside particles inside the atom, and I will use the atom as a starting point for the introduction. Some decades into this century the model of the atom was well established. It consists of a nucleus with positive electric charge surrounded by negative electrons. The nucleus of the atom is

Figure 1: **a)** *Two protons with positive charge repel each other by the electric force.* **b)** *Nevertheless, protons together with neutral neutrons can be bound together into a nucleus. There must be some strong attractive force keeping the nucleus together.*

built up by protons and neutrons. The proton is positive, while the neutron is neutral (which gave the particle its name).

This model for the atom describes well what we see in nature, but it raises one important question: What keeps the nucleus together? The positively charged protons should repel each other, but instead they are closely packed together into the nucleus, as illustrated in Fig 1. Thus it seems as if there is also a stronger attractive force between them.

The first attractive force that comes to mind is gravity, but it is definitely not stronger. Instead we must expect that there is some other strong and attractive force between protons and neutrons. This force has been given the a-metaphoric name “strong force”.

QCD

So far we have just replaced the words “something that keeps the nucleus together” by some other words: “strong force”. The latter is simpler to say, but not in any way clarifying. When a physicist prefers one expression before the other, it is because a mathematical definition, not easily misinterpreted, is associated with his favourite expression. There are also mathematical equations describing what can happen in different situations, which can be used to predict previously untested experiments. Thanks to Newton, Einstein and others, we therefore consider “gravitational force” a better expression than “something that keeps the moon in its orbit around the earth”, and thanks mainly to Maxwell we prefer “electric force” before “something that binds atoms into molecules and can create sparks between antennas”. (In contrast to these examples, remarkably little is clarified by changing expressions from “funny feeling that you can guess what someone else is thinking” to “telepathic force”.)

The mathematical description of the strong force is called Quantum Chromo Dynamics, QCD. In QCD there are three charges, and one charge of each kind put together becomes neutral. Here an analogy to colours can be made. There are three basic colours – red, green and blue – and combining them all gives white (colour-neutral). The strong charge is due to this analogy called "colour" and is either "red", "green" or "blue". The analogy is however purely pedagogical, there is no physical relation between colours and strong charges.

For each strong charge there is also an anti-charge. In some popular descriptions of QCD, the colour analogy is continued, so that the anti-charge to red is called "cyan" or whatever, but the properties of the charge "opposite" to red is just as well (or even better) illustrated by the name anti-red, which is used among particle physicists.

Anti-charge is not a unique feature of QCD. They also appear in the mathematical formalism for electromagnetism, Quantum Electro Dynamics (QED). One of the main features of QED (and also QCD) is the existence of *anti-particles.* A particle and anti-particle have the same mass but opposite charges. It is then natural to say that the anti-particles carry anti-charge. The anti-particles are necessary to introduce for the mathematical formalism to be consistent, but a perhaps more persuasive motivation for their existence is that they have been observed.

Quarks

In QCD the proton itself is not colour charged. Instead it is assumed that the proton has an inner structure and that it is the components of the proton, called "quarks", which carry colour charge. I will here give a simple motivation for this assumption.

Our model for how the nucleus keeps together must explain why the strong force dominates over the electric force for the protons within one nucleus, but not for two protons some distance apart. In other words, the proton appears colour neutral at large distances and therefore does not interact strongly, while two protons very close to each other can be bound together by the strong force.

This behaviour of protons is in a sense similar to the properties of the atom: The atom as a whole is electrically neutral, but the charges inside the atom are dislocated with respect to each other. This separation of charges can be used to create electric bonds between two atoms close to each other, thus forming a molecule.

One possible explanation for the proton properties is thus that the proton – just as the atom – has an inner structure. The components of the proton, called "quarks", carry colour charge. The proton consists of three quarks whose colour charges cancel each other, so that the proton as a whole is colour neutral. However, two protons very close to each other can feel a strong force, due to the slightly different locations of the colour charges inside the protons.

More particles and forces

The quarks in the proton must also carry electric charge, so that the sum of them becomes the proton charge. Similarly the three quarks in the neutron should add up to be electrically neutral. Thus we need at least two different types of quarks, with different electric charges. Different combinations of these quarks can then give protons or neutrons.

It is possible to combine three quarks of two different kinds in more than two ways. Thus it should be possible to create other particles than the proton and the neutron. Indeed, many "relatives" to the proton and neutron have been found. There are actually so many relatives that two quark types are not enough. Instead six quarks are needed to explain all the different forms of observed particles.

There is a common name for all particles built up by three quarks. They are called baryons, from the Greek word for "heavy": *barýs*. Indeed they are very heavy in the subatomic world, much heavier than the electron.

A quark and an antiquark can also form a colour neutral particle. Most of these particles weigh less than the baryons, but still significantly more than an electron. They are called mesons, from the Greek word *mesós*, intermediate. Baryons and mesons which all are built up by strongly interacting quarks and antiquarks are also referred to as hadrons, from *hadrós*: strong.

Heavier baryons and mesons decay into lighter particles and send out different forms of radiation. Many of these decays are possible due to the so-called weak force, which I will not discuss much here. As the name suggests, the weak force appears in most situations much weaker than the electro-magnetic force.

Experiments with the strong force

Our discussion has led to the assumption of a strong force, acting on particles called quarks inside the proton and neutron. It is then reasonable to expect that a collision of two protons at very high energies could kick out the quarks. Since the quarks have electric charge, it should also be possible to kick them out of the proton by sending very high energy electrons towards the proton. Another method to produce quarks is in collisions between electrons and anti-electrons (called "positrons", since they have positive charge). An electron and a positron can destroy each other, and the resulting radiation is sometimes transformed into a quark–antiquark pair. If the energy in the electron–positron collision is very high, the quark and antiquark will move in opposite directions with very high energies. The different forms of experiments are illustrated in Fig 2.

Though many experiments of these different types have been performed, isolated quarks have never been observed. Instead a bunch of colour neutral hadrons move in the direction the quark was expected to have. Thus it seems

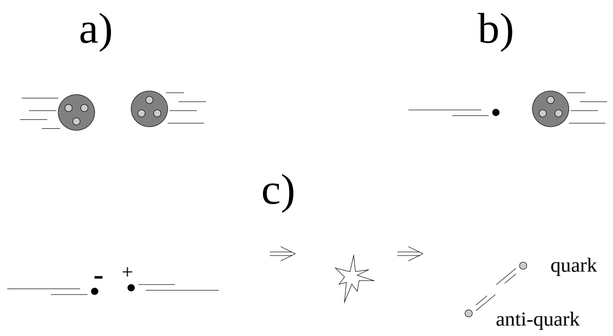

Figure 2: *Different experiments trying to kick out quarks with high energy. Hadron–hadron collisions (a), electron–proton collisions (b) and electron–positron annihilation (c). However, isolated quarks have never been seen. Instead a set of colour neutral hadrons move in the expected direction of the quark.*

impossible for quarks to be isolated, a feature which is called "confinement". The process where the off-spring of a struck quark becomes hadrons is called "hadronization".

Pair production in electro–magnetism

To give a motivation for why it is easier to form a lot of hadrons than to separate a quark from other quarks, I will here make an detour into electromagnetism.

As discussed previously, there is for each particle a corresponding anti-particle with opposite charge. If a particle and an anti-particle meet, they will in general destroy each other, creating some form of radiation in the process. E.g., an electron and a positron can annihilate each other and their energy can then be turned into electro–magnetic radiation. *This process can also be reversed*: In a strong electric field, an electron–positron pair can be produced.

Imagine e.g. an electric field between two oppositely charged capacitor plates, as shown in Fig 3, and let us assume that the capacitor plates do not let go of their charges. We can then make the charge difference between the plates very large, without creating any sparks between them. The electric field can then be so strong that electron–positron pairs are produced. The two differently charged particles are dragged towards opposite capacitor plates, which implies that the total charge of each plate is slightly reduced. If the field is strong enough, we gain more energy by reducing the field strength than it costs to create the pair, and a lot of electron–positron pair production will occur. The process is illustrated in Fig 3.

Electric fields strong enough for pair production are however very rare. The

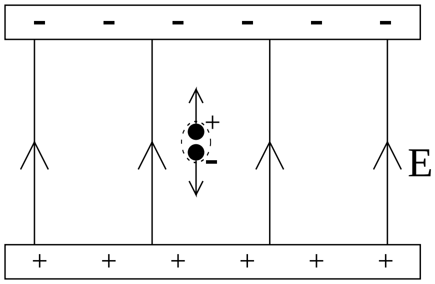

Figure 3: *Between two oppositely charged capacitor plates there is an electric field E. If the field is strong enough, an electron–positron pair can be produced. When they move apart, the field strength is reduced, and the energy gained is larger than the energy it costs to produce the pair.*

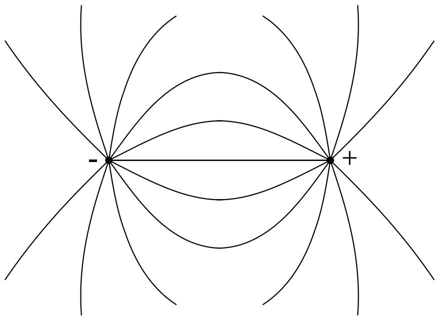

Figure 4: *The electric field between two charges spreads out over the whole space. The field energy in a small region is therefore not high enough for electron–positron pair production.*

field between a positive and negative charge spreads out over the whole space, as shown in Fig 4. The field energy in any small region between the charges is then in general very low, and pair production does not occur.

Confinement and hadronization

Just as for the electric force, the strong force can be represented by a field, going between different strong charges. The strong field is however quite different. The exact properties of the field are not known, but in one successful model thoroughly investigated in Lund, the field is assumed to be compressed into a

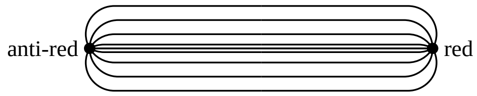

Figure 5: *The strong field between two colour charges can be assumed to be compressed into a tube. The field energy in a small region can be used to create quark–antiquark pairs.*

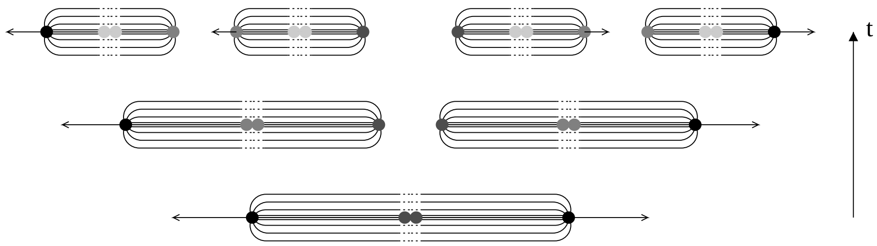

Figure 6: *The colour charge and its anti-charge move apart, several break-ups of the colour field tube can occur via quark-antiquark production. The final result is a set of mesons, moving approximately in the same direction as the original charges.*

tube as shown in Fig 5, instead of spreading out like the electric field. The strong field is as the name suggests strong, and since the field does not spread out, the energy available in a small region of the field tube is enough to create a quark-antiquark pair.

If the quark and antiquark move apart with very high energy, spanning a strong field between them, several pairs can be produced. As seen in Fig 6 the antiquark of one pair and the quark of the neighbouring pair then form a colour neutral system, a meson. All produced quarks and antiquarks will be accelerated by the field, and thus move approximately in the direction specified by the colour field tube. When we try to kick out a quark from a proton in a high energy collision, or create a quark–antiquark pair moving apart with high energy, we do not see isolated quarks and antiquarks. Instead we see a bunch of hadrons moving approximately in the direction of the struck quark. These bunches are called “jets”.

This thesis

In the discussion above, the statement “We never see isolated quarks, instead we produce a lot of different hadrons” is replaced by some other expressions, like "confinement", "hadronization", "colour field tube" and "pair production". The main reason, from a physicist's point of view, to change expressions is to introduce words related to firm mathematical definitions and equations. There are indeed mathematical constraints on all these new concepts, and also many mathematically formulated relations. However, the picture is not complete, and it contains many free parameters.

One branch of particle physics today searches for better theoretical understanding of hadronization, and observables that can be used to put constraints on the existing phenomenological models. This thesis is supposed to be a little contribution in this search, and though the impression may be that it happened several pages ago, it is with this short statement about how the introduction is related to the questions addressed in the thesis that I end my efforts in being comprehensive to a generic reader.

The Lund model

In general, hadronic processes are described in terms of two phases. The hard part of the interaction can be understood from perturbative QCD calculations, exploiting the asymptotic freedom of the non-Abelian gauge theory. The complete perturbative calculations are today typically available only to second order, but an approximate extension of the validity can be obtained via parton cascades, based on leading log resummations. The perturbative phase is complemented by a phenomenological description of soft hadronization, which models the important and yet so sparsely understood confinement mechanism.

In this section I will briefly describe the Lund models for the two phases: The Colour Dipole cascade [1] and the String Fragmentation picture [2]. In the end a subsection devoted to baryon production is added, as it is a main topic in two of the papers.

Colour dipole cascade

Perturbative QCD calculations are only completed up to finite orders. The exact expression for gluon radiation from a $q\overline{q}$ system is e.g. only known for one or two gluons [3]. The formation of multiparton states can however be well approximated by iterative cascades. The colour dipole model is such a cascade.

The expression for the probability to emit one gluon shows that this gluon radiation is very similar to classical radiation from an electric dipole. Thus the $q\overline{q}$ pair can be regarded a colour dipole emitting a gluon.

The exact expression for two gluon emission can be well approximated by a two-step procedure. First the $q\overline{q}$ dipole emits one gluon. This gluon is a colour octet, which implies that two colour dipoles are formed, one between the quark and the anti-colour charge of the gluon, the other between the antiquark and

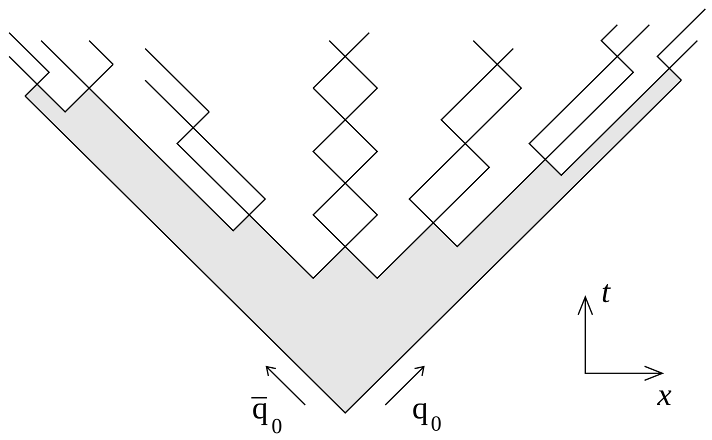

Figure 7: *String fragmentation in x-t space.*

the colour charge of the gluon. The second gluon is emitted by either one of these two dipoles, which are assumed to emit independently of each other. This stepwise emission of two gluons gives a very good description of the process, provided the transverse momentum $k_\perp$ for the second emission is significantly smaller than for the first.

In the Colour Dipole Model, this stepwise procedure is assumed to generalize for an arbitrary number of gluons. Each gluon emission splits a dipole into two new ones. These continue to emit more gluons independently of each other, with the constraint that the $k_\perp$ of every new emission is smaller than the preceding one.

The Colour Dipole Model is a parton cascade model in agreement with the Modified Leading Log approximation [4], and includes the important coherence effect for soft gluon emission, which in other formalisms is described by angular ordering [5]. The cascade is terminated by an infrared cut-off in $k_\perp$. Below this cut-off, the perturbative description breaks down due to the large running coupling. The result of the parton cascade is a chain of dipoles spanned from the quark via all the gluons (in an order specified by the cascade) to the antiquark.

In the colour dipole model, it is also possible to include photon radiation and $g \to q\overline{q}$ splittings, thus giving a complete picture of the parton cascade.

String fragmentation

In the Lund model, the colour field between a quark and an anti-quark is assumed to be compressed to a vortex line or a flux tube in a semiconductor. The energy stored in the string is proportional to the length, with the proportionality given by the string tension $\kappa \approx 1$ GeV/fm. A massless quark and anti-quark moving apart will loose kinetic energy as the string between them gets longer, and when all their energy is lost they will change direction and be pulled towards each other by the string. This results in a yo-yo motion of the partons.

If the string gets long enough, $q\overline{q}$ pair production can split the string in two colour singlet string pieces. These two pieces can then split again. The space time points for subsequent splittings in the two segments are causally disconnected, and the two string segments can therefore be assumed to decay independently of each other. The final result of the string splittings are small quark and anti-quark string segments, that are identified with mesons (cf. Fig 7).

The string break-up by the creation of a $q\overline{q}$ pair can be described in terms of a tunneling mechanism [6]. If the quarks are not massless a $q\overline{q}$ pair can not be produced in one point. Instead they can exist classically at a separation d, if the energy κd stored in the string between them is at least equal the sum of their transverse masses. Thus the $q\overline{q}$ production can be described as a tunneling from a common origin out to the classically allowed region. The result is a suppression of heavy quarks, and a Gaussian $k_\perp$ spectrum.

In a multiparton state after a cascade, there is a colour flow specified by the dominating planar diagram. This is in the dipole cascade represented by a chain of dipoles from the quark via gluons to the anti-quark. The same colour flow also specifies the string configuration. The string is stretched from the quark to the anti-quark, with the gluons acting as kinks on the string. One important feature of this model is infrared stability, in the sense that soft gluons give very small changes to the string configuration and do not affects the hadronic final state.

Baryon production

In e^+e^- hadronic events, most of the created particles are mesons which contain a quark and an antiquark. Mesons are also the natural products of string fragmentation, where a quark and an antiquark from adjacent string breakups join to to form a meson. However, a non-negligible rate of (anti-)baryons, consisting of three (anti-)quarks, is also seen in experiments. One way to include baryon production in the string fragmentation picture is to allow for a stepwise production of diquark-antidiquark pairs. Part of this thesis concerns this so called “popcorn mechanism” for baryon production [7], and it will therefore be described in some detail here.

The formation of effective diquarks can be seen as an effect of $q\overline{q}$ induced colour fluctuations in the string. A $q\overline{q}$ pair breaks string *if* they have the right colour. For pairs with wrong colour, the field does not vanish between them, instead there are colour states of the pair which generates the same kind

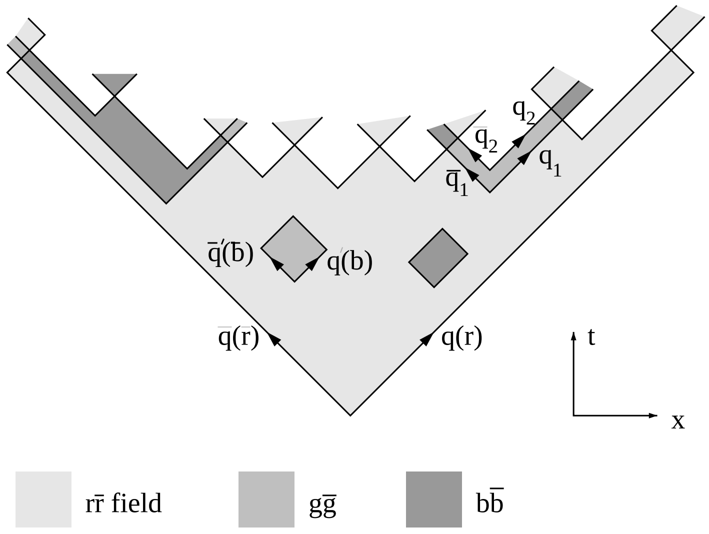

Figure 8: *If a vertex pair* $q_2\overline{q}_2$ *is produced inside a colour fluctuation region spanned by* $q_1\overline{q}_1$, *an effective diquark-antidiquark pair has "popped out" in a stepwise manner. The model allows for several breakups in the colour fluctuation region, creating one or several mesons in between the baryon and antibaryon, as shown to the left.*

of triplet-antitriplet string between the partons of the pair as outside them. Consider e.g. the $b\overline{b}$ pair $q'\overline{q}'$ produced in the $r\overline{r}$ string spanned by an original pair $q\overline{q}$ in Fig 8. If the quark q' moves towards q and the blue and red charges form an antitriplet $\overline{g}$ state, a $g\overline{g}$ string field is stretched between the partons in the $q'\overline{q}'$ pair. In such a case energy is neither gained nor lost as the partons move around and they can slide smoothly back and forth in the string. We call these quarks curtain quarks, from the picture of a curtain ring sliding back and forth on a rod.

The partons in the curtain $q'\overline{q}'$ pair leave the string energy unaffected but violates energy conservation due to their own transverse mass. The time they can exist is determined by the Heisenberg uncertainty principle. Some of these curtain pairs thus only appear as temporary colour fluctuations in the string, which does not affect the final state particles. This is e.g. the case for the $b\overline{b}$ coloured $q'\overline{q}'$ curtain pair shown in Fig 8.

However, the energy-violating colour fluctuation need not end its existence with a reabsorbtion of the curtain pair. It is also possible that the string between the members of the pair breaks inside the colour fluctuation. As illustrated for the $q_1\overline{q}_1$ and $q_2\overline{q}_2$ pairs in Fig 8, this implies that an effective diquark is created in a stepwise manner. Within this model, it is also possible to have several breakups inside the colour fluctuation region. Then a meson is formed between the baryon and antibaryon, as shown to the left in Fig 8.

The production of different diquarks and popcorn mesons is to a large extent determined by the probability for large colour fluctuation regions. The strong suppression of long lifetimes for the curtain pair also implies a suppression of large separations. Thus the formation of heavier spin 1 diquarks is suppressed relative to spin 0 states, and the formation of many popcorn mesons in the same colour fluctuation region is strongly suppressed.

The papers

In this section I give a brief overview of the papers presented in the second part of the thesis.

We have investigated observables available in existing high energy experiments which can be used to learn more about the hadronization phase. Some structure to these investigations can be obtained by separating the observables into three classes:

1) Observables predominantly determined by the hadronization phase.

2) Observables depending both on perturbative and non-perturbative QCD, where the different dependences can be enhanced in different event samples.

3) Observables in general considered well described by perturbative calculations alone.

In the papers a variety of different observables are considered, which cover these three classes.

Paper I

The flavour composition of the hadronic final state is an example of the first category of observables. E.g., the baryon flavour composition and the locality of baryon number conservation can be used to learn more about hadronization. In the first paper, we discuss the popcorn model for baryon production in e^+e^- annihilation [7].

The effective parton masses – for curtain quarks, vertex quarks and effective diquarks – which through the tunneling mechanism determine the relative production rates of different hadrons, are not known. In the baryon production model these production rates are instead represented by a set of parameters. As

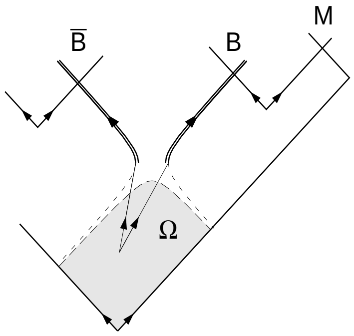

Figure 9: *Curtain pair production can occur anywhere in region Ω.*

the same colour fluctuation mechanism determines the suppression of heavy diquarks and of popcorn mesons, many parameters should however be correlated. In the paper we revise and reformulate the model so that these expected correlations are embedded in the algorithm. We also relate some of the parameters to the mass differences in the constituent parton model.

In the paper we also discuss another implication of heavy curtain quarks. Massive particles do not move with the speed of light, which implies that there is a limited region of possible production points for the curtain pair, as shown in Fig 9. The total probability for a colour fluctuation region to surround a vertex is then proportional to the integral of the proper curtain production weight, taken over the allowed region. The result is a suppression of diquark vertices near the string ends, which implies a suppression for baryons taking a large fraction of the available energy. This resulting suppression of high energy baryons is in agreement with data [8].

With a reduced number of free parameters, the revised model gives an improved description of energy spectra and an equally good description of hadron multiplicities, as compared to the preceding model.

Paper II

In the second paper, I discus how baryon fragmentation can be related to the mechanism behind baryon production in e^+e^-. In deep inelastic scattering and hadron-hadron collisions, a quark is kicked out of a baryon, leaving a baryon remnant. The fragmentation of the baryonic system can be described by a Lund string spanned from the triplet colour charge of the struck quark to the matching anticolour of the baryon remnant. This remnant is very similar to the effective diquarks that occur in baryon production in e^+e^- annihilation.

Thus, if we split a q$\overline{\text{q}}$ string by an (effective) diquark–antidiquark pair, the resulting quark-diquark string piece has similarities to a baryonic string formed by the same quark-diquark configuration in deep inelastic scattering or hadron-hadron collisions. The similarity is strengthened by the fact that, in e^+e^- annihilation, a vertex in general splits the string into two causally disconnected string pieces, which continue to fragment independently of each other. In paper two I discuss how far this relation can be expected to hold, and exploit it to obtain a model for baryon fragmentation which is related to the baryon production model in paper one.

The second paper also contains a more technical description of a computer program implementing the models of paper I and II. However, the Monte Carlo computer program PYTHIA [9], implementing the Lund string fragmentation model, is continuously developing, and the implementation of the revised popcorn model is now modified and merged with the latest version of PYTHIA. Nevertheless, the main features of the algorithm presented in paper II are still valid.

Paper III

While the flavour composition in the hadronic final state is mainly depending on hadronization, the properties of transverse momentum, $p_\perp$, is determined both by perturbative and non-perturbative effects. In the third paper we examine the possibility to observe the hadronization effects on transverse momentum properties.

Benefiting from the huge statistics available at the Z^0 experiments, it is possible to obtain a significant amount of events which are accepted by a rather extreme two-jet cut. In these "soft" events the perturbative activity is heavily suppressed and differences between different models for soft $p_\perp$ generation may emerge. We have analysed two-jet cuts applied to Monte Carlo generated events in terms of efficiency and purity, where efficiency is the acceptance rate of soft events, while purity is the rate of soft events in the final event sample. ("Soft events" are defined as those where no gluon emission occurred with a transverse momentum above 2 GeV.) Using the cuts that perform well, we find that predictions on $p_\perp$-related observables differ for different hadronization models, and thus that these could be distinguished in a confrontation with two-jet data.

One observable that we examine is the $p_\perp$ transfer over the rapidity y, i.e. the vectorial sum of $\mathbf{p}_\perp$ for all particles with a rapidity smaller than y. This observable is sensitive to the locality of $p_\perp$ conservation in the hadronization phase. In most successful hadronization models, locality is a word of honour. The hadron multiplicity is assumed to be related to the parton multiplicity locally in phase space (local parton–hadron duality) [10]. Furthermore, charge, baryon number and flavour is in most models assumed to be locally conserved. Data in general strongly support these assumptions. A consistent picture of local hadronization would then naturally imply a local conservation of $p_\perp$ in the hadronization phase. Our investigations show that it is possible to test this assumption against data from hadronic Z^0 decays.

Paper IV

The fourth paper also concerns the separation of hadronization effects from perturbative properties. I discuss how quark fragmentation universality can be tested by comparing quark jets in deep inelastic scattering (DIS) and e^+e^-. In a high energy interaction, the perturbative QCD activity creates quark and gluon jets, which fragment into a set of hadrons going approximately in the same direction as the parton. Quark fragmentation universality means that the properties of a quark jet is independent of the process generating the jet. This can be tested by comparing quark jets in e^+e^- and DIS.

For a reliable interpretation of the comparison, it is important that the event samples from the two processes are characterized by the same kinematics. This is in general not the case in the comparisons of e^+e^- and DIS presented so far. Higher order corrections in DIS allow high $p_\perp$ gluon emissions which have no correspondence in the e^+e^- process. I have examined the possibility to exclude such DIS events by reconstructing the $p_\perp$ scale with jets. This is shown to be a fruitful approach, significantly improving the expected similarity between e^+e^- quark jets and the DIS current jet.

Quark fragmentation universality is best examined using far forward current data from DIS, where the results are independent of most target properties, e.g. the mechanism behind the initial state parton evolution. In the fourth paper, I also investigate a current jet definition which extends the considered phase space region to become sensitive to the dynamics of initial state radiation. The new jet definition probes a relatively "clean" target region, being more sensitive to rather fundamental properties (like the status of BFKL versus DGLAP evolution) than to proton remnant fragmentation effects. An equivalent jet definition can be applied to e^+e^- data, which again enables a comparison between the two processes, thus facilitating the interpretation of the results. The method has not yet been applied on experimental data, but the Monte Carlo studies in the paper show that the observable can be used to distinguish different models for DIS.

Paper V

In the last paper of this thesis, we discuss one major example of the third category of observables: the ratio $N_\mathrm{q}/N_\mathrm{g}$ of multiplicities in quark and gluon jets. The predicted asymptotic value is given by the colour factor ratio $C_F/C_A = 4/9$. The experimental results are however significantly larger ($\sim 2/3$) [11], why higher order corrections are needed. The $1/\sqrt{\ln(s)}$ correction is however numerically small [12]. Attempts to systematically include all $1/\ln(s)$ corrections have been made [13], but there is still a discrepancy between theory and data. Yet higher orders are unfortunately not easily derived in a way which is independent of the chosen renormalization scheme.

In the paper, we stress the fact that hadronization effects introduce $1/\ln(s)$ corrections to the ratio $N_{\mathrm{q}}/N_{\mathrm{g}}$, and thus that a complete calculation of $1/\ln(s)$ terms cannot be made from perturbative considerations alone. In general, analytical predictions are based on parton level calculations followed by the assumption of local parton–hadron duality (LPHD) [10]. This implies e.g. that the hadron multiplicity in some part of the phase space is expected to be proportional to the parton multiplicity in the same region. In the parton level calculation, a cut-off must be imposed to avoid the infrared divergences of QCD. Since LPHD is applied on partons that survived a infrared cut-off, the value and form of this cut-off is an implicit assumption about the relevance at hadron level for different parton emissions.

For LPHD to be applicable, the cascade cut-off must be local, and of course Lorentz invariant. It also seems reasonable that it reflects the colour flow of the parton configuration. Many successful hadronization models are based on colour flow, which implies that the colour singlet cluster between a colour charged parton and the matching anti-charge of another parton is a more relevant hadronization quantity than the partons themselves. Such models – like the cluster fragmentation model [14] or the Lund string fragmentation model [2] – are quite successful in describing data, while schemes based on independent fragmentation of partons are less accurate.

If the colour singlet clusters are the relevant hadronization quantities, the average hadron multiplicity given by a parton emission is a function of the cluster invariant mass. For LPHD to be fully applicable in the parton state, we should then apply an infrared cut-off in the cluster mass, which is just the virtuality of the emitting parton. The virtuality cut-off is local, Lorentz invariant and reflects colour flow, and is thus a strong candidate for a proper infrared cut-off.

Virtuality is a commonly used cut-off quantity in cascades and analytical calculations, but there are other options. We may take into account other consequences of the colour flow argument. If a, say, blue quark emits a $\mathrm{b\bar{r}}$ gluon changing its own colour to red as illustrated in Fig 10, there is not only a $\mathrm{r\bar{r}}$ cluster created. The blue charge must be associated with a corresponding anticharge, and in the emission the mass of the $\mathrm{b\overline{b}}$ cluster is changed. If we call the squared mass of the cluster before the emission $\hat{s}_0$ and the squared masses after the emissions $\hat{s}_1$ and $\hat{s}_2$, the gluon emission as in Fig 10 changes the average multiplicity N according to

$$\Delta N = N(\hat{s}_1) + N(\hat{s}_2) - N(\hat{s}_0). \tag{1}$$

To define a cut-off which excludes emissions with negligible ΔN, we need to

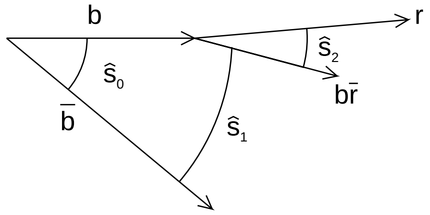

Figure 10: *When a blue colour charge emits a* $\mathrm{b}\bar{\mathrm{r}}$ *gluon, the* $\mathrm{b}\overline{\mathrm{b}}$ *colour dipole with squared mass* $\hat{s}_0$ *is split into two, with squared masses* $\hat{s}_1$ *and* $\hat{s}_2$*, respectively.*

know the form of $N(\hat{s})$. In the Lund string fragmentation picture $N(\hat{s})$ behaves as $\ln(\hat{s})$, which implies that $\Delta N \sim \ln(\hat{s}_1\hat{s}_2/\hat{s}_0)$. This motivates a cutoff in the quantity $\hat{s}_1\hat{s}_2/\hat{s}_0$, which is the squared transverse momentum of the gluon w.r.t. the emitting colour dipole, measured in its restframe [1].

As for the virtuality, this dipole-$k_\perp$ is locally invariant and reflects the importance of colour flow. It is thus a full-worthy alternative to the virtuality cut-off, for LPHD to be applicable. For collinear emissions, the two cut-offs are essentially equivalent, which implies that they give the same leading order results. Predictions for the cut-offs may however differ in terms suppressed by a relative factor of $1/\ln(s)$. Hadronization is today not fully understood, and a complete calculation of $1/\ln(s)$ correction terms to quantities like $N_\mathrm{q}/N_\mathrm{g}$ is therefore not easily obtained. However, much can be learned by studying effects which give rise to numerically large terms, hopefully dominating over the unknown ones. For $N_\mathrm{q}/N_\mathrm{g}$, energy conservation is such an effect. In the fifth paper we show that the recoil effects in the cascade are particularly simple to calculate in the colour dipole formalism. The result for $N_\mathrm{q}/N_\mathrm{g}$, using the dipole-$k_\perp$ cut-off, is indeed a correction which is numerically large, though formally suppressed by $1/\ln(s)$. (It dominates over the MLLA $1/\sqrt{\ln(s)}$ corrections for energies up to 10^7 GeV.) The presented analytical relation has only Λ_QCD as a free parameter and agrees well with available data [11].

Finally, we discuss in the fifth paper how this ratio and other jet properties can be observed in experimental data. In QCD the properties of a jet in general depend on two scales, the energy and virtuality of the jet. Theoretical predictions mostly apply to a situation where these scales coincide, while for experimental data they are often different. We present some new jet definitions which are applicable to an experimental situation and correspond better to the theoretically considered jets. The performance of the jet definitions are examined using MC simulations.

Acknowledgments

First, I want to thank Gösta, who with patience has lead me into an exciting field of physics and probably taught me more than I am aware of. I thank Torbjörn and Leif for their cooperation in various projects and their guidance into Monte Carlo generators. I owe a lot of gratitude to Jari and Markus, who have answered all my computer questions, starting with how the power button works.

I thank Markus for making the three different offices we have shared such great places, perfect for discussing physics... and everything else. I also want to thank everybody at the department, who during the years I've been around to measure it made "atmosphere" such a pleasant macroscopic social quantity.

Finally, a very special thanks goes to Tomasine, for being supportive and understanding during the months when I so rarely left the office, and my brain never did.

References

[1] G. Gustafson, *Phys. Lett.* **B175** (1986) 453;
G. Gustafson, U. Pettersson, *Nucl. Phys.* **B306** (1988) 746;
B. Andersson, G. Gustafson, L. Lönnblad, *Nucl. Phys.* **B339** (1990) 393

[2] B. Andersson, G. Gustafson, G. Ingelman, T. Sjöstrand, *Phys. Rep.* **97** (1983) 31

[3] R.K. Ellis, D.A. Ross, A.E. Terrano, *Nucl. Phys.* **B178** (1981) 421

[4] A.H. Mueller, *Nucl. Phys.* **B213** (1983) 85 [Erratum , **B241** (1984) 141]; *ibid.* **B228** (1983) 351;
Yu.L. Dokshitser, S.I. Troyan, *in* Proc. XIX Winter School LNPI, v.I. 144 (1984); preprint LNPI-922 (1984)

[5] A.H. Mueller, *Phys. Lett.* **B104** (1981) 161;
B.I. Ermolaev, V.S. Fadin, *JETP. Lett.* **33** (1981) 269;
A. Bassetto, M. Ciafaloni, G. Marchesini, A.H. Mueller, *Nucl. Phys.* **B207** (1982) 189

[6] H. Bohr, H.B. Nielsen, *NBI-HE-78-3* (1978)

[7] B. Andersson, G. Gustafson, T. Sjöstrand, *Phys. Scripta* **32** (1985) 574

[8] OPAL Collaboration, R. Akers et al., *Z. Phys.* **C63** (1994) 181;
OPAL Collaboration, P.D. Acton et al., *Phys. Lett.* **B291** (1992) 503;
DELPHI Collaboration, P. Abreau et al., *Phys. Lett.* **B318** (1993) 249

[9] M. Bengtsson, T. Sjöstrand, *Comp. Phys. Comm.* **39** (1986) 347;
T. Sjöstrand, *Comp. Phys. Comm.* **82** (1994) 74

[10] Ya.I. Asimov, Yu.L. Dokshitser, V.A. Khoze, S.I. Troyan, *Z. Phys.* **C27** (1985) 65

[11] OPAL Physics Note PN344, preliminary results, contributed paper 296 to the ICHEP'98 Conference, Vancouver

[12] A.H. Mueller, *Nucl. Phys.* **B228** (1983) 351

[13] J.B. Gaffney and A.H. Mueller, *Nucl. Phys.* **B250** (1985) 109;
I.M. Dremin and V.A. Nechitailo, *Mod. Phys. Lett.* **A9** (1994) 1471

[14] G. Marchesini, L. Trentadue, G. Veneziano, *Nucl. Phys.* **B181** (1981) 335

Baryon Production in the String Fragmentation Picture

Paper I

Baryon Production in the String Fragmentation Picture

Patrik Edén, Gösta Gustafson
Department of Theoretical Physics
Lund University

An improved version of the “pop-corn” model for baryon production in quark and gluon jets is presented. With a reduced number of parameters the model reproduces well both production rates for different baryon species and baryon momentum distributions. Predictions are presented for a set of baryon-antibaryon correlations.

1.1 Introduction

The string fragmentation model [1] is able to give a generally very good description of the distribution of hadrons in quark and gluon jets [2]. The abundance of mesons with different flavour and spin can be described with a limited number of parameters, which have a natural interpretation. Thus the production of a $q\overline{q}$ pair can be understood as a tunneling phenomenon [3], which gives a suppression of strange quarks compared to the lighter u- and d-quarks. Also the relation between vector and pseudo-scalar mesons and the suppression of tensor mesons can be understood within the string model.

Baryon production is a more complex process than the production of mesons. $B\overline{B}$ correlations in rapidity are in agreement with the assumption that the B and the $\overline{B}$ are produced as neighbours or next to neighbours in a string breakup. The distribution in the angle between the baryon and the thrust axis (i.e. the general string direction) in the $B\overline{B}$ cms is not spherically symmetric [4, 5]. Furthermore, recent data from polarized e^+e^- annihilations show that baryons are more frequent in quark jets than in antiquark jets [6]. Thus baryon-antibaryon pairs do not originate from isotropically decaying clusters. Instead the distribution can be understood if the B and the $\overline{B}$ are pulled in opposite directions at the string breakup. The simplest possibility would be that the string breaks by the production of a diquark-antidiquark pair, which become constituents in the baryon and the antibaryon, and a model based on this assumption was presented in ref [7]. In particular data on transverse momentum correlations [4] do not agree with expectations from this simple model, but indicate that occasionally one or a few mesons may be produced in between the baryon and the antibaryon along the string. This idea was developed in the so called popcorn model [8]. Because of the limited experimental information on baryon production, in particular concerning multi-strange baryons, some simplifying approximations were used when the model was implemented in the JETSET Monte Carlo [2, 9]. Thus it was e.g. assumed in the MC that at most one meson could be produced between the B and the $\overline{B}$. Until recently this version of the MC was in fair agreement with most experimental data on baryon production.

With the advent of new data with very high statistics from LEP it is however now possible to achieve a better understanding of the baryon production mechanism. In this paper we will present an improved model for baryon production. This model is based on the same general principles as the popcorn model in ref [8], but takes better account of the detailed kinematics of the process. The result agrees well with experimental data both for production rates for different baryons and for energy spectra. We also show here some predictions for a set of different correlations, which can be used to test the model.

We want to mention that also other approaches to jet fragmentation have been presented, in particular where the production rates are mainly determined by the different hadron masses. This is the case for the UCLA model [10], which is based on the Lund string fragmentation scheme, but in which the production rates are determined by the hadron masses rather than by the quark properties. This model gives a fair description of meson production with few parameters. However, it is not trivial to get a unique prediction for baryon production within this approach, and the most recent publication concentrates on meson production. Chliapnikov et al. [11] have observed regularities between production rates and masses, spin and isospin for different hadrons. However, in this analysis the production of e.g. protons and Λ include decay products from heavier resonances, and it is not clear to us whether it is possible to find a similar relation for the directly produced hadrons. Also the cluster fragmentation model as implemented in the HERWIG MC [12], in which hadron rates are mainly determined by their masses, has difficulties to reproduce the experimental data. This further supports our assumption that dynamical properties deeper than just the hadron masses are important in the production of baryons.

In section 2 we review the ideas of the Lund string fragmentation model and of the popcorn model, and also discuss its shortcomings within the default version. In section 3 we describe our revised model, and in section 4 we present some comparisons with experimental data.

1.2 String Fragmentation and the Popcorn Model

1.2.1 String fragmentation

Longitudinal momentum distribution

In the string model the confining field is assumed to behave like a relativistic string, i.e. like a vortex line in a superconductor. The model contains first a description of the decay of a straight string, and secondly the assumption that gluons behave as transverse excitations or kinks on the string. As gluon kinks have no inherent influence on particle composition, we will in the following discuss the fragmentation of a simple straight string. The string can break by the production of $q\overline{q}$ pairs, which are pulled apart by the string tension. When a quark meets an antiquark from a neighbouring pair, they can form a final state meson, as shown in Fig 1.1. The production points lie around a hyperbola in x-t space, which means that on the average the mesons are evenly distributed in rapidity. When a $q\overline{q}$ pair is produced, the system is split in two causally disconnected pieces, and assuming that these pieces decay independently, one finds a unique solution [13]. The probability to find a definite final state with meson momenta p_i is given by the following relation, if we assume that there

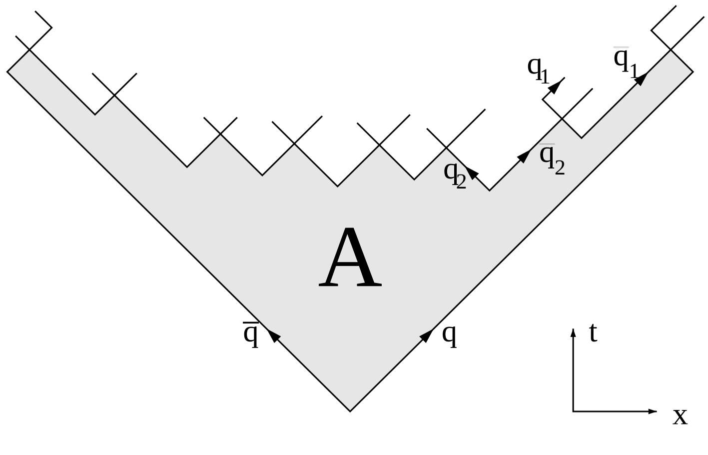

Figure 1.1: *String fragmentation in x-t space.*

is only one meson species with mass m,

$$\text{Prob.} \propto \prod_i (N d^2 p_i \delta({p_i}^2 - m^2)) \delta(\sum_k p_k - p_{\text{tot}}) \exp(-bA\kappa^2). \tag{1.1}$$

Here A is the (colour coherence) area indicated in Fig 1.1, κ is the string tension and N and b are two free parameters. This expression has the form of a phase space factor (determined by the parameter N) times an exponential term which has the form or a Wilson area law (with the scale parameter b). The distribution in Eq (1.1) can be generated iteratively from one end of the meson system in Fig 1.1. Thus, if a set of mesons are generated and each one takes a fraction z of the remaining light cone momentum $E+p$ (or $E-p$ if the system is generated from the other end) then z is given by the following distribution

$$f(z) = N\frac{(1-z)^a}{z}\exp(-bm^2/z). \tag{1.2}$$

The parameters N, b and a are related by normalization, leaving two free parameters. With different quark and hadron species a larger freedom is consistent with the assumptions given above. Different quark flavours can be produced at different average proper times. For a meson with transverse mass $m_\perp$, built up by flavours α and β, the distribution in Eq (1.2) is then replaced by the expression

$$f_{\alpha\beta}(z) \propto \frac{1}{z} z^{a_\alpha} \left(\frac{1-z}{z}\right)^{a_\beta} \exp(-bm_\perp^2/z). \tag{1.3}$$

Here α is the flavour of the previously produced $q\overline{q}$ pair, and β the flavour of the new $q\overline{q}$ pair. The proper time, τ, of the break-up points, or the variable Γ defined by

$$\Gamma \equiv \kappa^2\tau^2, \tag{1.4}$$

is given by the probability distribution

$$H(\Gamma) \propto \Gamma^{a_\alpha} e^{-b\Gamma}. \tag{1.5}$$

From this relation we get the mean value

$$\langle\Gamma_\alpha\rangle = \frac{1+a_\alpha}{b}. \tag{1.6}$$

Thus with different parameters a_α, the proper time for the breakup points may depend on the flavour α of the $q\overline{q}$ pair produced. In fits to experimental data different a-values have usually only been introduced for effective diquarks in connection with baryon production.

Flavour and transverse momentum

Quarks with mass μ and transverse momentum $k_\perp$ must classically be produced in the string at a certain distance, d, so that the string energy between them can be transformed into the transverse mass of the pair $2\mu_\perp = 2\sqrt{\mu^2+k_\perp^2} = \kappa d$. Quantum mechanically this production can be described as a tunneling process [3, 1]. The wave functions of the quark and the antiquark are exponentially damped in the classically forbidden region, and the production probability is proportional to the square of the product of these wave functions. Using the WKB approximation we find that this is approximately given by

$$|\psi_{\overline{q}}\psi_q|^2 \sim \exp(-\frac{\pi}{\kappa}\mu_\perp^2) = \exp(-\frac{\pi}{\kappa}\mu^2)\exp(-\frac{\pi}{\kappa}k_\perp^2) \tag{1.7}$$

if the wave functions ψ are normalized to 1 at the classical boundary. This expression factorizes in a flavour factor (s-quarks will be suppressed by about 1/3, while charm and heavier quarks can be neglected) and a Gaussian $k_\perp$ distribution.

Vector meson suppression

The result in Eq (1.7) was obtained if the wave functions were normalized to 1 at the classical boundary. The produced quark must however fit into the wave function of a final state meson. A spin-spin interaction implies e.g. that the wave function for a ρ-meson is more spread out then that of a pion, see Fig 1.2. Thus the wave function at the boundary is smaller for ρ, and it has been estimated that [1]

$$\psi^2(\text{class. boundary}) \sim 1/m_\perp \tag{1.8}$$

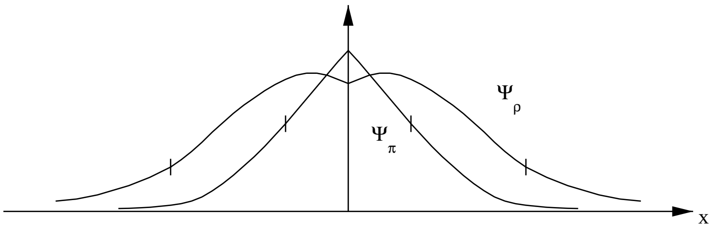

Figure 1.2: *Wave functions for ρ and π, showing the different normalization at the classical turning point, which is marked with a dash.*

where $m_\perp$ is the transverse mass of the meson.

In this way we can understand why the ρ/π ratio is suppressed from 3:1, as obtained from spin counting, to something closer to 1:1. The $p_\perp$ dependence in Eq (1.8) is weak for most mesons except for the pions, which have very small mass. For pions we expect from Eq (1.8) an enhancement for small $p_\perp$ values and a more narrow $p_\perp$ distribution. Due to the small pion mass we also expect further correlations in $p_\perp$ between neighbouring pions, see further ref [14].

1.2.2 Baryon production

As mentioned in the introduction the simplest model for baryon production would follow from the assumption that the string can break by the production of a diquark-antidiquark pair in a $\overline{3}$-3 colour state. An antidiquark with specified flavour and spin would then appear as a new quark flavour in Eqs (1.3,1.5,1.7), and different production rates would be determined by effective diquark masses and spin suppression factors. (Because baryons are symmetric three-quark states, extra weights have also to be applied in order to guarantee SU(6) symmetry.) As the effective masses are difficult to determine theoretically, they were represented by a set of free parameters in the MC implementation. These parameters determine the relative production ratios qq/q, $\mathrm{ud}_1/\mathrm{ud}_0$, us/ud. The MC also includes a possibility to further suppress the decuplet baryon states relative to the octet states, but the corresponding parameter is usually set equal to one.

To improve agreement with experiments a more general framework for baryon production was presented in the "popcorn" model [8]. In this model a diquark is produced in a stepwise manner and not as a single unit. Assume that a colour field is stretched between e.g. a red quark and an antired antiquark. The string can break if a $\mathrm{r}\overline{\mathrm{r}}$ $\mathrm{q}\overline{\mathrm{q}}$ pair is produced and pulled apart by the string tension. We can also imagine that a $\mathrm{b}\overline{\mathrm{b}}$ pair is produced as a virtual fluctuation. If the rb ($\overline{\mathrm{r}}\overline{\mathrm{b}}$) is in a colour antitriplet $\overline{\mathrm{g}}$ (triplet g) state, the colour field

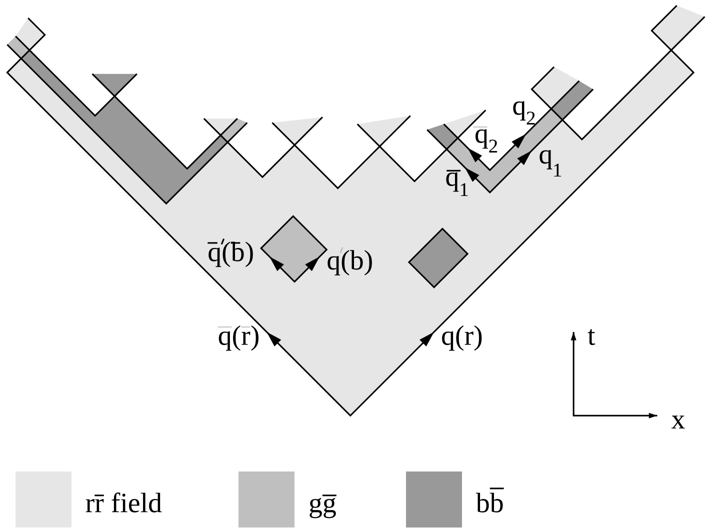

Figure 1.3: *If a vertex pair* $q_2\overline{q}_2$ *is produced inside a colour fluctuation region spanned by* $q_1\overline{q}_1$*, an effective diquark-antidiquark pair has "popped out" in a stepwise manner. The model allows for several breakups in the colour fluctuation region, creating one or several mesons in between the baryon and antibaryon, as shown to the left.*

between the produced quark and antiquark will correspond to a triplet colour field with the same strength as the original field. Thus equal forces in opposite directions act on the new quark and the new antiquark, leaving no net force on either of them. In accordance with the uncertainty principle they can move around freely for a time inversely proportional to their energy. These quarks are in the present paper called "curtain quarks", from the picture of rings on a curtain-rod, sliding back and forth with no frictional losses and without changing the properties of the rod. In distinction to curtain quarks, the quarks that cause the string to break are in this paper called "vertex quarks". If the string breaks within the colour fluctuation region, an effective diquark-antidiquark pair is produced, see Fig 1.3.

As no net force is acting on the curtain quarks they appear as free particles. Therefore it was in ref [8] expected that the probability to find such a $q\overline{q}$ pair with transverse mass $\mu_\perp$ at a separation d in space is proportional to $|\Delta_F(d, \mu_\perp)|^2$. To produce an intermediate meson system with invariant mass M between the baryon and antibaryon, the distance d must be larger than M/κ. As Δ_F falls off exponentially for large d-values, a strong suppression is obtained for large masses M. For this reason the possibility to have more than one intermediate meson was neglected in the MC implementation. The probability for one intermediate meson was in the program determined by the so called popcorn parameter. In the popcorn model the production ratios between different baryon species become slightly modified since a specific diquark is not always accompanied by a corresponding antidiquark. Thus Ω production is somewhat less suppressed, as the antiquark partners of the ss diquark not necessarily go together in a $\overline{\mathrm{s}}\overline{\mathrm{s}}$ antidiquark.

Turning to the momentum distribution we note that baryon spectra in the default JETSET program is harder than the experimental results [15-19]. In the popcorn model the two quarks in an effective diquark are produced at different proper times (cf. Fig 1.3). The relevant time in Eqs (1.4) and (1.6) is the latest one, the one corresponding to the "vertex quark", and it is natural that on average this is larger than the time for the $\mathrm{q}\overline{\mathrm{q}}$ production associated with meson production outside the colour fluctuation region. Thus we could expect a larger value of a for the effective diquark production (cf. Eq (1.6)), which according to Eq (1.3) results in a softer baryon spectrum. This effect is however not large enough, and in attempts to describe experimental data it has been suggested that first rank baryons might be suppressed [20]. (Rank denotes the order in which the hadrons are produced, counting from the string end. Thus in Fig 1.1, the meson built up by the original quark q and the antiquark $\overline{\mathrm{q}}_1$ has rank 1, the meson build up by q_1 and $\overline{\mathrm{q}}_2$ has rank 2 etc.) In the string model heavy baryons like Λ_c or Λ_b are only created as first rank particles (or decay products of these), and in order to get enough of these heavy baryons, the suppression of the first rank baryons should not apply to c or b jets. If the curtain quarks move along the light-cones as indicated in Fig 1.3, a special suppression of first rank baryons may not appear natural, but, as we will show in the following section, it can indeed be dynamically understood in a more detailed analysis of the kinematics.

1.3 The Revised Model

1.3.1 Baryon flavours

In the revised model we take the separate production of the curtain quarks and the vertex quarks more seriously. Thus we assume that the production of a vertex $\mathrm{q}\overline{\mathrm{q}}$ pair, which breaks the string, is always determined by the expression in Eqs (1.7), irrespective of whether it is ending up in an effective diquark or not. The s-quark suppression of all *vertex* quarks is therefore essentially determined by the K/π ratio.

Turning to curtain quarks we assume, following ref [8], that the production probability for these quarks is determined by the function $\Delta_F(d, \mu_\perp)$. Here $\mu_\perp$

is the transverse mass of the curtain quark and d is the minimal separation of the pair. If a meson system with invariant (transverse) mass M is produced between the baryon and the antibaryon, d is given by the sum of M and the effective diquark masses (called m_1 and m_2) entering the baryon and the antibaryon. Thus

$$\kappa d = M + m_1 + m_2. \tag{1.9}$$

For large values of d, Δ_F is exponentially suppressed and as in the previous implementation we use the approximation

$$|\Delta_F(d, \mu_\perp)|^2 \sim \exp(-2\mu_\perp d). \tag{1.10}$$

The relative production rates for different diquarks are thus governed by their mass differences. Even though diquark masses must be considered unknown, we assume that the differences in mass can be determined from the constituent masses, as derived in the parton model.

As the quantity $\mu_\perp$ in Eq (1.10) is the transverse mass of the curtain quark, we note that large transverse momenta are strongly suppressed. Thus $k_\perp$ for the curtain quarks are generally small compared to the $k_\perp$ of the vertex quarks, and has therefore been neglected in the MC implementation. Consequently the transverse momentum of the hadron will essentially be given by two vertex quarks, and – like the earlier versions – the new model predicts a similar $p_\perp$ distribution for primary baryons and mesons [1]. This approximation should be very good for inclusive distributions, but may be somewhat too crude for correlations in $\bar{p}_\perp$ or azimuthal angle. In the implementation, we let two parameters

$$\beta_{\rm q} \equiv 2\,\langle\mu_{\perp{\rm q}}\rangle\,/\kappa, \quad \text{or} \quad \beta_{\rm u} \text{ and } \Delta\beta \equiv \beta_{\rm s} - \beta_{\rm u}, \tag{1.11}$$

represent $\langle\mu_\perp\rangle$ in Eq (1.10) for light and strange curtain quarks.

From Eqs (1.10) and (1.11), the relative production rate for different diquarks with the same type of curtain quark (light or strange) can be expressed by diquark mass differences and two β parameters. The ratio between diquarks with different types of curtain quarks depends not only on mass differences but also on $m_{{\rm ud}_0}$. Thus e.g.

$$\begin{aligned}\frac{P({\rm us}_0,{\rm s})}{P({\rm ud}_0,{\rm u})} &= \exp(-2(\beta_{\rm s} m_{{\rm us}_0} - \beta_{\rm u} m_{{\rm ud}_0})) \\ &= \exp(-2\beta_{\rm s}(m_{{\rm us}_0} - m_{{\rm ud}_0}))\exp(-2\Delta\beta m_{{\rm ud}_0}).\end{aligned} \tag{1.12}$$

At first this seems to call for a new free parameter. It turns out, however, that by changing the $\beta_{\rm s}$ value and the decuplet suppression discussed below, one

[1] Neglecting the rest mass of the quarks and using a typical value for $\kappa d \approx 1{\rm Ge}V$, we find $P(k_\perp) \propto \exp(-2dk_\perp) \Rightarrow \langle k_\perp\rangle \sim 0.1{\rm Ge}V$. As the $k_\perp$-contributions to a hadron are essentially added in quadrature, this is very small compared to the transverse momenta of the vertex quarks, for which we have $\langle k_\perp\rangle_{(vertex)} \sim 0.4{\rm Ge}V$.

can compensate all effects of a variation in m_{ud_0}, apart from a small variation on the Δ production rate. In view of the experimental uncertainty regarding Δ production, we find little need to introduce m_{ud_0} as a free parameter, and in the MC its value is therefore fixed to 0.2GeV.

In the same way as for mesons, we also for baryon production expect a spin dependent factor related to the normalization of the hadronic wave function. Also the earlier MC contains one parameter for suppression of the decuplet states compared to the octet states, but in the default version this parameter is set to 1, because the decuplet is sufficiently suppressed by smaller weights for production of the heavier spin 1 diquarks. In our model the three quarks in a baryon are produced essentially independently. Thus we expect a suppression of higher spin states, in a similar way for baryons as for mesons, due to the normalization of the total three-particle wavefunction. Following the arguments in ref [1] we assume that this factor is approximately linear in the baryon mass (cf. also with the π^0-η-η' ratios discussed in ref [14]). Thus in addition to a suppression factor for the decuplet states compared to the octet states, we also expect a suppression of Σ compared to Λ due to the larger spin-spin interaction in ud quark pairs compared to us or ds pairs. In the MC program we have introduced one parameter for the decuplet/octet suppression while the extra Σ/Λ suppression from the mass differences ($M_\Sigma - M_\Lambda \sim 70\mathrm{GeV}, \quad M_{\mathrm{decuplet}} - M_{\mathrm{octet}} \sim 200\mathrm{GeV}$) is fixed by the decuplet/octet suppression through the relation

$$\frac{P(\mathrm{decuplet})}{P(\mathrm{octet})} = \frac{1}{1+Q} \quad \Rightarrow \quad \frac{P(\Sigma)}{P(\Lambda)} = \frac{1}{1+Q/3}. \tag{1.13}$$

This suppression is implemented in such a way that the total production of Λ and Σ is kept constant.

Popcorn mechanism

Using the two β parameters, Eq (1.9) and (1.10), the popcorn mechanism has been implemented without the introduction of any new parameter.

When the popcorn model was implemented in the JETSET MC it was assumed that the production of two or more mesons between the baryon and the antibaryon could be neglected, and there was no extra vector meson suppression in spite of the larger mass compared to the pion mass. This was a deliberate approximation assuming that the overestimated ρ and ω production could simulate the neglected production of two or three uncorrelated pions. In the new MC this approximation is not used, and the probability for a "popcorn meson system" is determined by the invariant mass of this system. In table 1.1 we show the rate of popcorn systems with different number of popcorn mesons for different values of β_{u}.

β_{u} (GeV^{-1})	relative rate of popcorn systems with N primary mesons N=0	N=1	N=2	N=3	N>3	mean number of primary mesons in a popcorn system
1.0	0.69	0.23	0.06	0.01	0.01	0.42
0.6	0.60	0.26	0.10	0.03	0.02	0.62
0.2	0.46	0.27	0.14	0.07	0.05	1.05

Table 1.1: *The rate of popcorn systems with different number of popcorn mesons for the same tune as in table 1.3 where* β_{u} *is* $0.6\mathrm{GeV}^{-1}$*, and similar tunes with* $\beta_{\mathrm{u}} = 1\mathrm{GeV}^{-1}$ *and* $0.2\mathrm{GeV}^{-1}$.

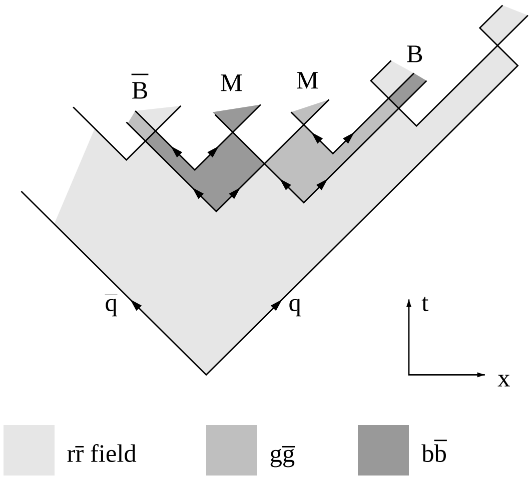

Figure 1.4: *A popcorn example with two curtain quark pairs.*

Popcorn systems with more than one meson could also be formed by two separate colour fluctuations as illustrated in Fig 1.4. In such a situation the baryon and antibaryon need not have any flavour in common. We expect this production mechanism to be suppressed, and it is neglected in the MC. If the production rate for each curtain quark pair is determined by the ratio $P(\mathrm{qq})/P(\mathrm{q}) \sim 0.1$, the "double curtains" should be suppressed cf. to the "single curtains" with multiple popcorn mesons by this factor. As the latter is only a small fraction of the total baryon production (15% for β_{u}, cf. tab 1.1), we believe the double curtains to give a very small contribution, even if they are somewhat less suppressed by the factors on Eqs (1.9) and (1.10). In principle this kind of baryon production can be experimentally indicated if one can observe e.g.

correlated $\Omega^-\overline{\mathrm{p}}$ or $\Delta^{++}\overline{\Xi}^+$ pairs, which can only be produced by the double curtain mechanism.

Summarizing, apart from the s/u parameter determined by the meson rates and the diquark probability parameter (qq/q), the baryon multiplicities are in our model essentially determined by three tunable parameters, β_u, $\Delta\beta$ and the decuplet/octet suppression, giving a total of five parameters. This should be compared to the earlier model and its implementation in JETSET, in which all together seven parameters govern baryon production (if the decuplet suppression is not included): The s/u and qq/q parameters plus five more, one suppressing strangeness in effective diquarks, one suppressing spin 1 diquarks, and three related to the popcorn mechanism.

1.3.2 Momentum distributions

We have assumed that the curtain quarks appear as massive particles. This implies that they cannot move along light-cones as in the illustration in Fig 1.3. Since the curtain quarks behave as free particles we assume that the curtain quark and its antiquark partner move along straight lines from a common starting point. We would then expect a suppression if some of the potential starting points lie outside the color field region. To estimate this effect we will be guided by a simple semi-classical model. (We use the semi-classical model mainly to estimate the relative suppression when the extension of the colour field is reduced. The overall normalization is determined by the quantum mechanical expression Δ_F in Eq (1.10).) As we will see, the net result is first a larger effective a-parameter for baryon production (cf. Eq (1.3)), second a suppression of first rank baryons. This suppression is stronger for light baryons, but rather weak for baryons containing heavy c- or b-quarks. Thus this model provides a dynamical interpretation of the phenomenological observations in ref [20].

Let us first study a situation with only one vertex quark, i.e. a situation with no meson between the baryon and the antibaryon. Assume that a curtain quark-antiquark pair is produced in a point (called A in Fig 1.5a) at an invariant distance τ from the vertex point C for the effective diquark-antidiquark pair. Fig 1.5b illustrates the situation in a frame where the space distance between A and C is zero. (Consequently the time distance equals τ.) We assume that the curtain quark and antiquark combine with their vertex quark partners in the points D and E to form an effective diquark and antidiquark. This diquark (antidiquark) is not massless, and thus it moves along a hyperbola with centre in the vertex point C. If the mass of the diquark-antidiquark pair is $2m_\perp$ the distance d between D and E is given by $d = 2m_\perp/\kappa$ (cf. Eq (1.9)). In the model we assume that the probability for this process is proportional to $\exp(-S)$, where S is the action. Thus, if $\mu_\perp$ is the transverse mass of the

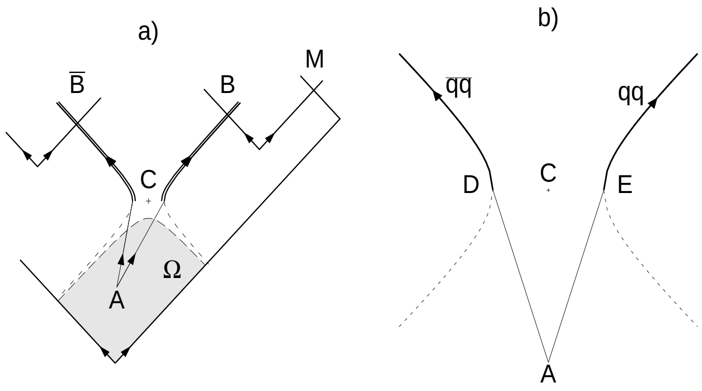

Figure 1.5: *Curtain pair production at point A, and a diquark vertex at point C. Figure b is boosted to the frame where A and C are at a common space point.*

curtain quarks we get a relative weight

$$\begin{aligned} w &= \exp(-S) \\ S &= E * t \\ E &= 2\mu_\perp/\sqrt{1-v^2} = 2\mu_\perp/\sqrt{1-d^2/4t^2}. \end{aligned} \tag{1.14}$$

We note that the curtain quark and the vertex quark could also combine at a different point along the hyperbola, and similarly for the antiquarks. Also the two recombinations do not have to be at the same time in the particular frame chosen in Fig 1.5b. Other possibilities would generally give smaller weights, and therefore we use for the general situation in Fig 1.5a the weight in Eq (1.14) with t replaced by the proper time τ between the points A and C.

In a situation with more than one vertex $\mathrm{q\overline{q}}$ pair, we have an intermediate meson system with (transverse) mass M. The minimum distance between the "combination points" is now given by $d = (M + m_{\perp 1} + m_{\perp 2})/\kappa$ (cf. Eq (1.9)), and we will assume that also here the weight for the curtain quark production is given by Eq (1.14) with this value of d.

In a situation as illustrated in Fig 1.5a, the total weight W is obtained by summing over all production points A inside the kinematically allowed region Ω, defined by the condition $\tau > m_\perp/\kappa$.

$$W = \int_\Omega w \mathrm{d}x \mathrm{d}t. \tag{1.15}$$

The result is a total weight $W(\Gamma, \mu_\perp, d)$ which is a function of the three variables Γ (the square of the proper time for the effective diquark vertex), $\mu_\perp$ (the

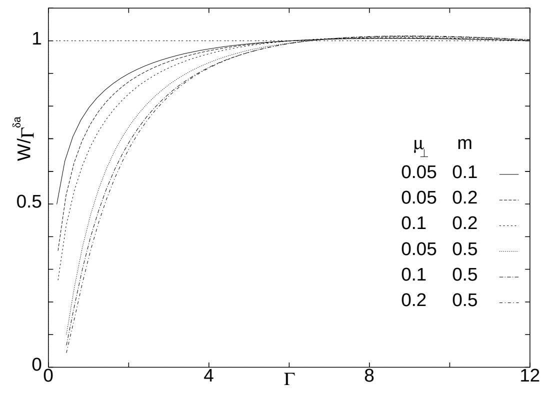

Figure 1.6: *Extra suppression* $P(\Gamma) \equiv W/\Gamma^{\delta a}$ *as a function of* Γ *for different values of* m *and* $\mu_\perp$*.* W *is normed so that* $P \approx 1$ *for large* Γ*.*

transverse mass of the curtain quark) and d (the minimum separation for the curtain quark-antiquark pair).

The effect of this ansatz can be anticipated: The action in Eq (1.14) becomes large both for large t and small t (which implies large velocities) and has a minimum for $t^2 = d^2/2$. Thus the most favoured region for the production point A lies at some finite distance from C. The result in Eq (1.10) should correspond to a situation when Ω is large enough to contain most of this region, while the production probability should be further suppressed for small regions Ω.

A numerical calculation shows that for large vales of Γ the weight W scales with Γ in the following way

$$W \sim \Gamma^{\delta a(\mu_\perp, d)} \quad ; \ \Gamma \text{ large.} \tag{1.16}$$

The power $\delta a(\mu_\perp, d)$ has the effect of shifting the a-parameter in Eq (1.3) and (1.5). The δa dependence on d and $\mu_\perp$ implies a unique shift of a for each diquark system. However, the differences are not large, and for relevant values of $\mu_\perp$ and d we find $\delta a \approx 0.5$.

The scaling result in Eq (1.16) is valid only when Γ is large compared to $(\kappa d)^2$. The weight W goes to zero when the area of possible production points Ω is small. As seen from the numerical results shown in Fig 1.6 the extra suppression for small Γ differs for different diquark masses and curtain quark masses. From these differences, and the total normalization of W for different d and $\mu_\perp$, production probabilities for diquarks could in principle be estimated within the semi-classical framework.

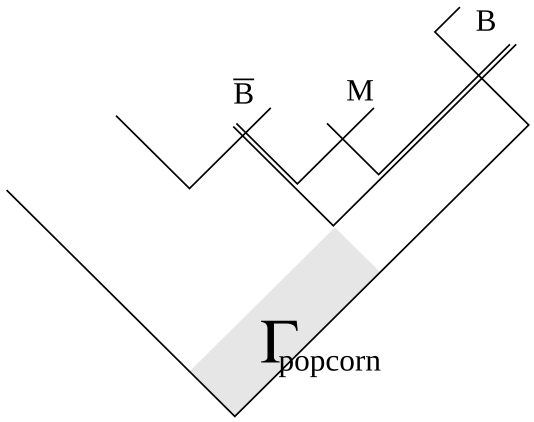

Figure 1.7: *The Γ value for a popcorn system.*

In the semiclassical model the production probability goes to zero when

$$\Omega = \Gamma - (\kappa d/2)^2 \left(1 + \ln \frac{\Gamma}{(\kappa d/2)^2}\right) \tag{1.17}$$

goes to zero, i.e. when Γ goes to $(\kappa d/2)^2$. In a proper quantum mechanical treatment the probability should go to zero when $\Gamma \to 0$. Γ-values below $(\kappa d/2)^2$ should be suppressed but not totally excluded. Thus we feel that using the exact result in Eq (1.15) would be to stretch the semiclassical model too far, and instead we use for all values of $\mu_\perp$ and d the following suppression factor for small Γ-values

$$P(\Gamma) = 1 - \exp(-\rho\Gamma) \quad \text{with} \quad \rho \approx \ln(2)\text{GeV}^{-2}. \tag{1.18}$$

This is further motivated by the phenomenological observation that the result is not very sensitive to the exact value of the parameter ρ.

In the case of popcorn mesons, it is not obvious how to choose the corresponding effective Γ-value to be used in the suppression factor Eq (1.18). In our simulations we have used the area indicated in Fig 1.7 which is the largest possible area when the curtain quarks do not exceed the speed of light. This assumption implies that these Γ-values are in general much smaller than corresponding values for diquark vertices without popcorn, which consequently influences the popcorn probability.

An important effect of the suppression for small Γ is a suppression of rank 1 baryons (the effect being stronger for light baryons than for baryons with heavy c or b quarks). For low rank hadrons, $\langle\Gamma\rangle$ is smaller than the result in

hadron	rank 1	rank 3
p	1.9	2.9
Λ_s	1.9	2.9
Λ_c	2.6	(only created as rank 1)
Λ_b	2.7	(only created as rank 1)

Table 1.2: $\langle\Gamma\rangle$ *for light baryons and* $\langle\Gamma_{\mathrm{eff}}\rangle$ *for heavy baryons.* JETSET *7.4 default simulation of* e^+e^- *collisions at* Z^0 *energies (using Bowler correction to* $f(z)$ *for heavy flavours).*

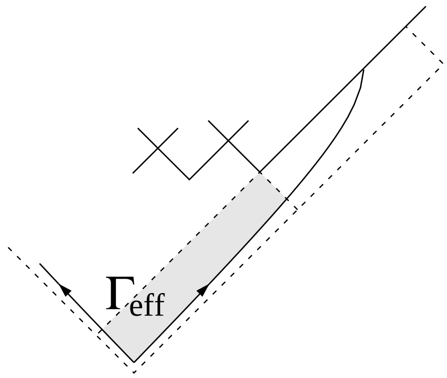

Figure 1.8: *In the case of heavy end quarks of mass* μ_q*, the curtain pair production area* Γ *is cut by the hyperbolic motion of the quarks, giving rise to a smaller* $\Gamma_{\mathrm{eff}} \approx \Gamma - \mu_\mathrm{q}^2 \ln(1/z)$.

Eq (1.6), which is a limiting value in the centre. The average values $\langle\Gamma\rangle$ for rank 1 and rank 3 baryons are shown in table 1.2, and for the light baryons (represented by p and Λ) we see a significant difference. This suppression of low rank (light) baryons obviously results in softer momentum spectra, and the results will be further discussed in the following section.

For heavy baryons with a c- or a b-quark, the large quark mass automatically implies larger values for Γ. This is the case also if we take into account the fact that the heavy quark moves along a hyperbola and not along the light-cone, as illustrated in Fig 1.8. (Remember that in the string model these heavy hadrons can only be produced as first rank particles including an initial heavy quark.) Thus the whole area Γ as defined in momentum space is not available for quark pair production but only the smaller area Γ_{eff}, marked in the figure. In table 1.2 we have for Λ_c and Λ_b presented corresponding average values,

$\langle \Gamma_{\text{eff}} \rangle$, and we note that these have approximately the same size as the $\langle \Gamma \rangle$-values in the central region for light baryons. To obtain the values in table 1.2 we have been using a heavy quark fragmentation function which reproduces the experimental momentum spectra. This is the case for the fragmentation function suggested by Morris and Bowler [21], which is obtained if the space-time area indicated in Fig 1.8 is interpreted as a "colour coherence area" in the Lund string model. This fragmentation function is in very good agreement with charm and bottom momentum spectra [22], and is the default option in JETSET version 7.4. Similar results are obtained if we use the Peterson fragmentation function [23] fitted to the data.

At this stage, no new tunable parameter is introduced in the model. The values of both ρ and δa are determined by model predictions. However, the shift of the a-parameter is more complicated. The δa value obtained above suppresses diquark vertices with large z values, i.e. vertices close to the string ends. Thus it describes the very small probability for a curtain quark pair to be produced around such vertices. A similar suppression is expected also for ordinary $\mathrm{q\overline{q}}$ production if the pair is not massless with zero transverse momentum [24, 1]. The massive $\mathrm{q\overline{q}}$ pair is produced somewhere along two hyperbolae around the vertex and the range of possible production points on these hyperbolae decreases when the vertex is close to the string ends. This effect is taken into account when tuning the a parameter in the MC. Thus for baryon production there are two different effects which suppress small Γ-values, resulting in larger effective a-values. It is not at all obvious that the combined effect can be well described by simply adding the corresponding δa-shifts. For this reason we have in our MC (as in the original JETSET MC) left δa as a tunable parameter, with expected best values in the range 0-0.5.

1.4 Results

We have implemented our model in a revised version of the JETSET Monte Carlo, and we will here discuss some results for e^+e^- annihilation at the Z^0 energy. The results are also compared with default JETSET 7.4.

Flavour composition

We have made a preliminary tuning of the flavour production parameters and in table 1.3 we present the particle multiplicities obtained for $\beta_{\mathrm{u}} = 0.6\mathrm{GeV}^{-1}$, $\Delta\beta = 1.2\mathrm{GeV}^{-1}$, decuplet/octet= 0.19 and $\delta a = 0.5$. We note a very good agreement between our model and experimental data. The discrepancy is less than 1.5 standard deviations in all cases except for $\Sigma^{\pm}$ (-1.7σ). Thus compared with JETSET default we get with fewer parameters an equally good or better agreement with data.

hadron	Multiplicity experiments	JETSET7.4 default	modified
p	0.98±0.10	1.20	0.87
Λ	0.371±0.015	0.387	0.363
Σ^0	0.071±0.015	0.074	0.070
$\Sigma^\pm$	0.177±0.023	0.141	0.137
Ξ^-	0.0257±0.0014	0.0271	0.0274
Δ^{++}	0.124±0.065	0.189	0.118
$\Sigma(1385)^\pm$	0.044±0.008	0.074	0.056
$\Xi(1530)^0$	0.0061±0.0011	0.0053	0.0062
Ω^-	0.0016±0.0005	0.0007	0.0010
Λ_c	0.075±0.024	0.059	0.034
All c baryons		0.083	0.056
Λ_b		0.033	0.020
All b baryons		0.058	0.039
$\Lambda\overline{\Lambda}$	0.089±0.007	0.090	0.106
$\Lambda\overline{\Xi}^-$		0.019	0.021

Table 1.3: *Average multiplicities from* JETSET *7.4 simulations of* $1.6*10^6$ e^+e^- *events at* Z^0 *energies, compared to experimental data. The parameter values used in the new baryon production model are* $\beta_u = 0.6\text{GeV}^{-1}$, $\Delta\beta = 1.2\text{GeV}^{-1}$, *decuplet suppression* $= 0.19$ *and* $\delta a = 0.5$. *Experimental data are from ref* [2] Λ_c *data are from ref* [26] . *No extensive tune of the meson parameters have been made.*

At high energies the effective suppression of first rank baryons does not affect noticeably the total multiplicity of light baryons. It does however reduce the production of heavy baryons containing a c- or a b-quark, which in the string model can only be produced as first rank particles. Compared to the default JETSET version these particles are reduced to about 70% (For Λ_c and Λ_b the reduction is somewhat larger, around 60%). Due to the large experimental uncertainties both the larger and the smaller results are consistent with data.

Momentum distribution

Baryons with large momenta are suppressed for two reasons. The most important one is the Γ-suppression in Eq (1.18). High momenta are also suppressed by a large value for the parameter δa. This suppression is, however, less effective. In Fig 1.9 we show momentum distributions for protons and Λ-particles for two values of δa, 0 and 0.5. We note that a very good agreement with pro-

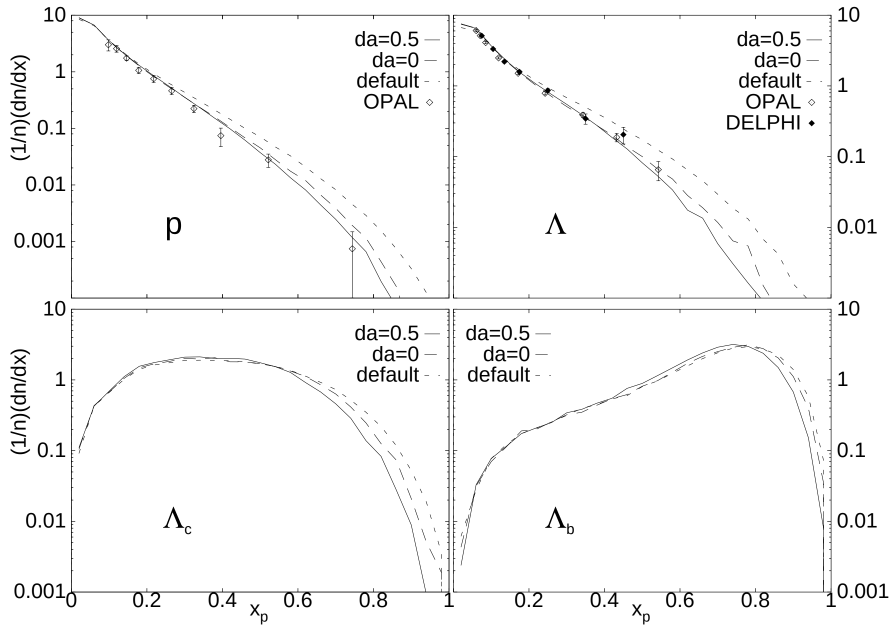

Figure 1.9: *Momentum distribution* $\frac{1}{n}\frac{dn}{dx_p}$ *for* p, Λ, Λ_c *and* Λ_b. $x_p = p_\mathrm{hadron}/p_\mathrm{beam}$. *Results from Monte Carlo simulations with* Γ *suppression model are shown for two different values of* δa, *and compared to* JETSET *default and experiments. OPAL data are from refs* [15]. *DELPHI data are from ref* [17].

ton and Λ-data is obtained for both δa values. In Fig 1.9 we also show that the effect of Γ suppression is rather small on Λ_c and Λ_b momentum distributions.

Even if inclusive baryon spectra are fairly insensitive to the value of δa, this parameter can be restricted if we separate the quark and antiquark jets. In Fig 1.10 we show baryon-antibaryon asymmetries compared with data from SLD [6]. We note that data seem to favour a δa value larger than 0, and that future studies with better statistics could be used to restrict the range of possible values for the δa parameter.

Correlations

Correlation data can be used as a more thorough test of the model. As examples, multiplicity correlations for $\Lambda\overline{\Lambda}$ and $\Lambda\overline{\Xi}^-$ pairs are also presented in table 1.3. The number of correlated $\Lambda\overline{\Lambda}$ pairs (0.106 per event) is in fair agreement with data, and the number of $\Lambda\overline{\Xi}^-$ pairs predicted to be 0.021 per event.

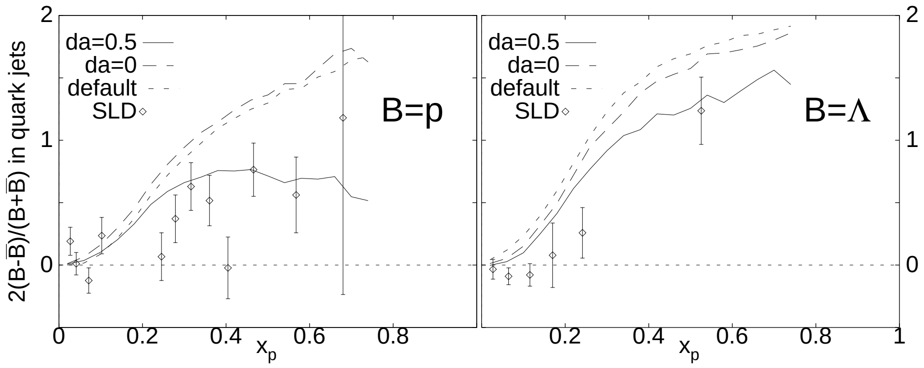

Figure 1.10: *The x_p distribution of* $2*(\mathrm{B}-\overline{\mathrm{B}})/(\mathrm{B}+\overline{\mathrm{B}})$ *for baryons and antibaryons in the same hemisphere as the outgoing quark. The model predicts more hard baryons than antibaryons in quark jets, as has been observed. Quantitatively, the predictions are sensitive to the δa value. The plots show* p *and* Λ *asymmetry for $\delta a = 0$ and* 0.5*,* JETSET *default and SLD preliminary data* [6].

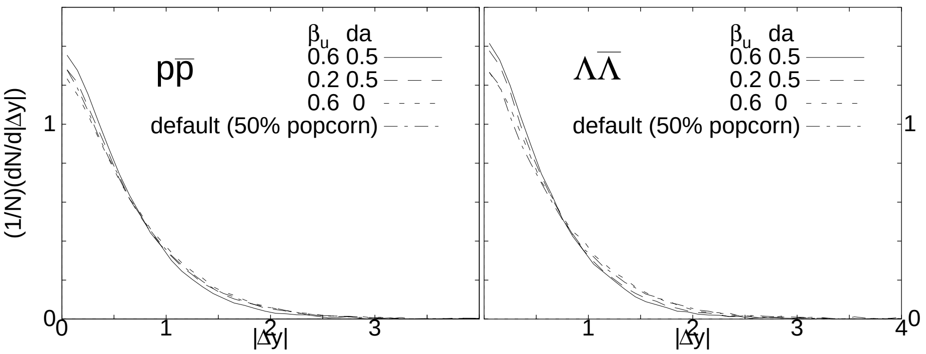

Figure 1.11: $\Lambda\overline{\Lambda}$ *and* $\mathrm{p}\overline{\mathrm{p}}$ *rapidity correlations.* $N \equiv N_{\mathrm{B}\overline{\mathrm{B}}} + N_{\overline{\mathrm{B}}\mathrm{B}} - N_{\mathrm{BB}} - N_{\overline{\mathrm{BB}}}$. *The curves corresponds, as indicated, to different values of β_{u} and δa and to the traditional* JETSET *MC with default parameters and 50% popcorn.*

Some results for rapidity correlations are presented in Fig 1.11, which shows distributions in $N \equiv N_{\mathrm{B}\overline{\mathrm{B}}'} - \frac{1}{2}(N_{\mathrm{BB}'} + N_{\overline{\mathrm{BB}}'})$ vs. $|\Delta y|$. We have compared our results with default JETSET and not directly with experimental data, because it is difficult to implement exactly the same experimental cuts. Experimental results, which have been compared with the JETSET MC, appear to be conflicting, as OPAL results favour a large popcorn parameter around 95% [25], while DELPHI data agree with 50% popcorn [17]. As seen in Fig 1.11 there are only small differences between the theoretical curves, but we note that to some extent the result does depend on the value of δa. This is of interest because in published comparisons between experimental data and the JETSET MC only the popcorn parameter has been tuned.

As mentioned above correlations in $\bar{p}_\perp$ or azimuthal angle can be affected by the neglected small transverse momentum of the curtain quarks. For this reason we do not present predictions for these correlations. If wanted the $p_\perp$ of the curtain quarks could be implemented with one more parameter, which does not affect any other observable. One should note, though, that at higher energies, e.g. at LEP, correlations in $\bar{p}_\perp$ or azimuthal angle are mainly determined by jet production, while transverse momentum contributions from the fragmentation contributes very little.

Energy dependence

Due to the suppression of first rank baryons one could expect that the energy dependence of the baryon production might be slightly changed. This could follow from the fact that at lower energies a larger fraction of the hadrons are first rank. The energy dependence of the baryon rate depends also on the amount of popcorn, and it turns out that for the parameter values presented above the energy variation between 10 GeV and 91 GeV is not noticeably different from the original default JETSET MC.

We end by noting that our model contains two features which can be treated separately in the MC, first the new scheme for flavour compositions and second the suppression in Eq (1.18) leading mainly to a softer momentum spectrum. Thus in order to understand which features are essential for the result, it is e.g. possible to make simulations with the old model for flavour generation but include the suppression for small Γ. For heavy baryons this gives a smaller suppression than our full model, as the rate is reduced to ~85% of the standard JETSET value.

1.5 Summary

A revised version of the "pop-corn" model for baryon production is presented, in which the stepwise production of the quarks in a baryon is carried through consistently. As in the popcorn model it is assumed that a $q\bar{q}$ pair with "wrong colour" (i.e. not with the colour which makes the string break) can be produced as a quantum fluctuation. One or more secondary $q\bar{q}$ pairs can be produced within the fluctuation causing the string to break and producing a $\mathrm{B}\overline{\mathrm{B}}$ pair plus possibly also mesons. We assume here that these secondary $\mathrm{q}\overline{\mathrm{q}}$ pairs are produced in just the same way as ordinary meson-producing $\mathrm{q}\overline{\mathrm{q}}$ breakups in the string. In this way the number of free parameters can be reduced, and yet the experimental production ratios for different baryon species can be reproduced.

Describing the initial "wrong colour" $\mathrm{q}\overline{\mathrm{q}}$ pair with a semiclassical model, we find a suppression of hard baryons, in particular of hard first rank baryons. This implies that the model reproduces well experimental momentum distributions for p and Λ.

Finally a set of predictions for $\mathrm{B}\overline{\mathrm{B}}$ correlations are presented.

Acknowledgments

We want to thank Torbjörn Sjöstrand for many valuable discussions, and for his guidance into the JETSET Monte Carlo code.

References

[1] B. Andersson, G. Gustafson, G. Ingelman, T. Sjöstrand, *Phys. Rep.* **97** (1983) 31

[2] A. De Angelis, CERN-PPE-95-135 (and references therein), presented at the 1995 EPS-HEP meeting, Brussels, Belgium.

[3] H. Bohr, H.B. Nielsen, *NBI-HE-78-3* (1978)

[4] TPC collaboration, H. Aihara et al., *Phys. Rev. Lett.* **55** (1985) 1047

[5] ALEPH collaboration, EPS-422, presented at the 1995 EPS-HEP meeting, Brussels, Belgium.

[6] SLD collaboration, SLAC-PUB-95-6920, presented at the 1995 EPS-HEP meeting, Brussels, Belgium.

[7] B. Andersson, G. Gustafson, T. Sjöstrand, *Nucl. Phys.* **B197** (1982) 45;
B. Andersson, G. Gustafson, G. Ingelman, T. Sjöstrand, *Z. Phys.* **C13** (1982) 361

[8] B. Andersson, G. Gustafson, T. Sjöstrand, *Phys. Scripta* **32** (1985) 574

[9] M. Bengtsson, T. Sjöstrand, *Comp. Phys. Comm.* **39** (1986) 347;
T. Sjöstrand, *Comp. Phys. Comm.* **82** (1994) 74

[10] C.D. Buchanan, S.B. Chun, *PhysṘev. Lett.* **59** (1987) 1997;
C.D. Buchanan, S.B. Chun, *Phys. Lett.* **B308** (1993) 153;
C.D. Buchanan, S.B. Chun, *UCLA-HEP-95-02* (1995)

[11] P.V. Chliapnikov, U.A. Uvarov, *Phys. Lett.* **B345** (1995) 313

[12] G. Marchesini et al., *Comp. PhysĊomm.* **67** (1992) 465

[13] B. Andersson, G. Gustafson, B. Söderberg, *Z. Phys.* **C20** (1983) 317

[14] B. Andersson, G. Gustafson, J. Samuelsson, *Z. Phys.* **C64** (1994) 653

[15] OPAL Collaboration, R. Akers et al., *Z. Phys.* **C63** (1994) 181;
OPAL Collaboration, P.D. Acton et al., *Phys. Lett.* **B291** (1992) 503

[16] DELPHI Collaboration, P. Abreau et al., *CERN-PPE/95-28* (1995)

[17] DELPHI Collaboration, P. Abreau et al., *Phys. Lett.* **B318** (1993) 249

[18] L3 Collaboration, M. Acciari et al., *Phys. Lett.* **B328** (1993) 223

[19] ALEPH Collaboration, D. Buskulic et al., *Z. Phys.* **C64** (1994) 361;
ALEPH Collaboration, D. Buskulic et al., *Z. Phys.* **C66** (1995) 355

[20] K Hamacher, M Weierstall, *DELPHI 95-80 PHYS 515* (1995) ;
R. Hemingway, OPAL Technical Note, TN279

[21] M.G.Bowler, *Z. Phys.* **C11** (1981) 169;
D.A.Morris, *Nucl. Phys.* **B313** (1989) 634

[22] J. Häkkinen, *Z. Phys.* **C75** (1997) 35

[23] C. Peterson et al., *Phys. Rev.* **D27** (1983) 105

[24] B. Andersson, G. Gustafson, T. Sjöstrand, *Z. Phys.* **C6** (1980) 235

[25] OPAL Collaboration, P.D. Acton et al., *Phys. Lett.* **B305** (1993) 415

[26] OPAL Collaboration, R. Akers et al. *Measurement of Λ_c^+ production in Z^0 decays*, preliminary results presented at ICHEP94 Glasgow

A Program for Baryon Production and Its Applications to Baryon Fragmentation in DIS

Paper II

A Program for Baryon Generation and Its Applications to Baryon Fragmentation in DIS

Patrik Edén
Department of Theoretical Physics
Lund University

In an earlier paper, we discuss the "popcorn" model for baryon production in quark and gluon jets, and present an improved model (which we call Modified Popcorn Scenarium, MOPS). In this paper we give a manual to the MC program based on MOPS, and also discuss the application of the model to baryon fragmentation, i.e. fragmentation of strings originally contaning a diquark. Model predictions for baryon production in DIS are compared with data.

2.1 Introduction

In ref [1], a model for baryon production in the hadronization process is presented. The model is called "Modified Popcorn Scenarium" (MOPS), and is a revision of the "popcorn" mechanism [2] for baryon production in the Lund string fragmentation picture [3]. In ref [1], the discussion is focused on baryon production in e^+e^- annihilation. However, the model can also be applied to fragmentation of strings originally containing a diquark. Physical considerations about this extension of the model are discussed in section 2.3, where also some results are presented.

A large part of this paper (section 2.4 and forward) is a manual to a FORTRAN source code file called "MOPS.f", which is an implementation of the the new model and works as a complement to JETSET$\geq$ 7.4 [4]. The program is intended for those who already have some experience of the JETSET Monte Carlo.

2.2 Baryon Production

In the "popcorn" model [2] a diquark is produced in a stepwise manner. In the string it is possible to produce a $\mathrm{q\overline{q}}$ pair of "wrong" colour, which does not split the string in two singlet systems. If instead the original and new quark(antiquark) form an antitriplet(triplet) state, the colour field between the produced quark and antiquark will correspond to a triplet colour field with the same strength as the original field. Then no net force is acting on the produced quark and antiquark and in accordance with the uncertainty principle they can move freely for a time inversely proportional to their energy. If the string breaks within the colour fluctuation region, an effective diquark-antidiquark pair is produced. If several break-ups occur, there will be one (or several) intermediate mesons between the baryon and antibaryon.

As no net force is acting on the colour fluctuation quarks they appear as free particles. Therefore it was in ref [2] expected that the probability to find such a $\mathrm{q\overline{q}}$ pair with transverse mass $\mu_\perp$ at a separation d in space is proportional to $|\Delta_F(d,\mu_\perp)|^2$. The suppression factor for producing effective diquarks and intermediate mesons of a total invariant mass $M_\perp$ in a string with energy density κ is thus estimated by

$$|\Delta_F(d,\mu_\perp)|^2 \sim \exp(-2\mu_\perp M_\perp/\kappa). \tag{2.1}$$

When implementing the model to a MC, the suppression factor Eq (2.1) was originally represented by a set of parameters, governing production rates of different diquarks and the probability for one intermediate meson. The small probability for several "popcorn" mesons was neglected. In ref [1] the model

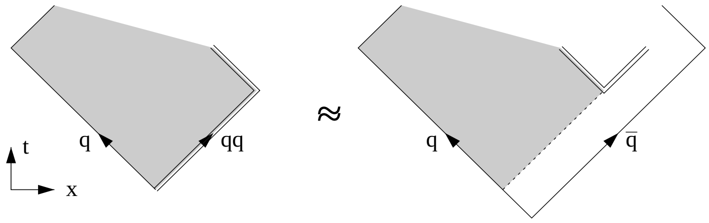

Figure 2.1: *A string with an original diquark can be assumed to have similar properties as a string remainder after an effective diquark break-up.*

was reformulated in such a way that Eq (2.1) could be used explicitly in the MC. The two parameters

$$\beta_{\mathrm{q}} \equiv 2\left\langle \mu_{\perp \mathrm{q}} \right\rangle / \kappa, \quad \text{or} \quad \beta_{\mathrm{u}} \text{ and } \Delta\beta \equiv \beta_{\mathrm{s}} - \beta_{\mathrm{u}}, \tag{2.2}$$

then govern both the diquark and the intermediate meson production. The result is a reduced number of tunable parameters.

We have assumed that the colour fluctuation quarks appear as free, massive particles. This implies that they cannot move along light-cones. Instead there is an area of possible starting points for the colour fluctuation, which is essentially given by the proper time of the production vertex squared. To get the total weight for a colour fluctuation, we must sum over all possible starting points. The result is a relative suppression of diquark vertices at early times, and consequently a softening of baryon momentum spectra, consistent with experimental data.

2.3 Diquark Jet Fragmentation

An algorithm for baron production in a $\mathrm{q}\overline{\mathrm{q}}$ string can be applied to fragmentation of a string originally containing a diquark. This string is then assumed to behave like the remainder of a $\mathrm{q}\overline{\mathrm{q}}$ string after an effective diquark vertex, as symbolically shown in Fig 2.1.

This identification must be made with some care. The general statement that a remainder string behaves like an original string is based on the fact that two string systems separated by a vertex are causally disconnected. In the case of diquark vertices, this is not obviously correct. Due to the popcorn mechanism, the string segments A and B in Fig 2.2 share a common set of possible histories. Choosing among those when fragmenting A will influence the probability for different final states in B.

In the specific case of the model presented in [1], the discussion about different production points for the colour fluctuation pair, giving rise to the

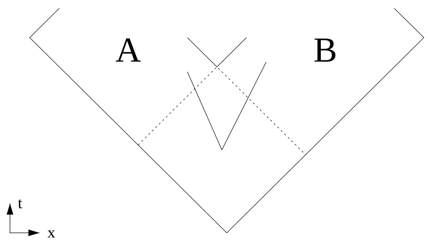

Figure 2.2: *Two string segments A and B, causally connected by a common colour fluctuation quark pair.*

suppression of break-ups at small proper times (small-Γ suppression, where $\Gamma \equiv \kappa^2\tau^2$) is not applicable to fragmentation of original diquarks. Furthermore, in the process (original diquark $\rightarrow$ baryon+$\overline{\mathrm{q}}$) the decuplet suppression should not apply at full strength. This suppression factor stems from the normalization of the overlapping q and $\overline{\mathrm{q}}$ wavefunctions in a newly produced $\mathrm{q}\overline{\mathrm{q}}$ pair [5, 3], but in the process considered here, two out of three valence quarks already exist as an initial condition of the string.

Finally the suppression factor for popcorn mesons (which is exponential in the invariant mass of the meson system) is derived from the assumption of colour fluctuations violating energy conservation and thus being suppressed by the Heisenberg uncertainty principle. When splitting an original diquark into two more independent quarks, the same kind of energy shift does not obviously emerge. We could still expect large separations of the diquark constituents to be suppressed, since the two quarks originate from a common diquark wave function. The shape of this suppression is beyond the scope of our model, but for simplicity we assume the same kind of exponential suppression as in the "true popcorn" case. However, there is little reason to assume that the strength of the suppression must be exactly the same in the different situations. Thus the suppression of leading rank meson production in a diquark jet is governed by a new β parameter, which is independent of the popcorn parameters β_{u} and $\Delta\beta$.

To summarize, when implementing the popcorn algorithm to the case of original diquarks, we have made the following changes:

* The Γ suppression does not apply.
* The decuplet suppression does not apply when qq$\rightarrow$ (rank 1 B)+$\overline{\mathrm{q}}$, but when qq$\rightarrow$ M+...+(higher rank B)+$\overline{\mathrm{q}}$.
* The β parameter used in the exponential popcorn suppression is independent of β_{u} and $\Delta\beta$, which are fitted to e^+e^- baryon production data.

To test the model, we have made simulations of π^+p and K$^+$p collisions

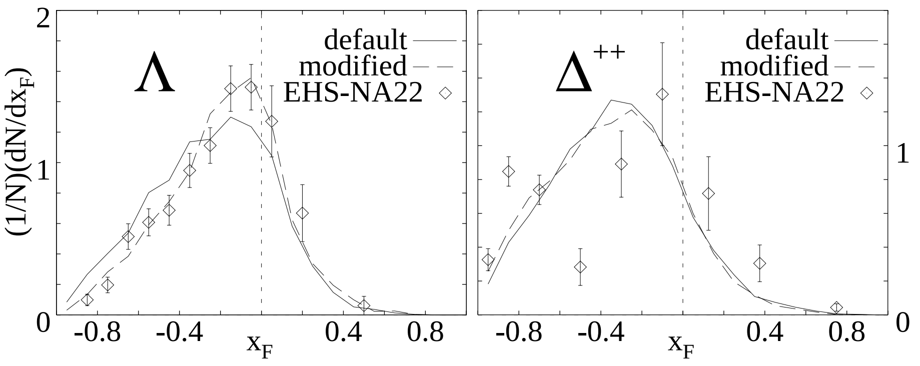

Figure 2.3: *Normalized Feynman-x distribution of* Λ *and* Δ^{++} *in* π^+p *collisions at ∼20GeV cms energy. The meson is moving in the positive direction. Data from [6] are compared to simulations with* Fritiof *7.02 combined with* Jetset *default (solid lines) and modified with* $\beta = 0.6 GeV^{-1}$ *(dashed lines).*

		s/u=0.3		s/u=0.2	
baryon	EHS-NA22	default	mod.	default	mod.
Λ	0.092±0.008	0.115**	0.152***	0.077*	0.108*
Δ^{++}	0.214±0.034	0.155*	0.142**	0.170*	0.148*
Σ^{*+}	0.021±0.009	0.017	0.020	0.013	0.015
$\overline{\Lambda}$	0.061±0.009	0.087**	0.074*	0.078*	0.065

Table 2.1: *Multiplicities of baryons in* K^+p *collisions at* ∼ 20 *GeV cms energy. Data from [6] are compared to simulations with* Fritiof *7.02 combined with* Jetset *default and modified, for two different values of the strangeness suppression parameter. N stars indicates that the simulated result is more than N standard deviations away from experimental data.*

at $\sqrt{s} \sim$ 20GeV, and compared the predictions with the results of ref [6]. In the simulations, we have used Fritiof 7.02 and Jetset 7.4 (default and modified). Before presenting the results, we want to stress that the low energy-scale involved ($\sqrt{s} \sim$ 20GeV $\Rightarrow$ string energies mostly $<$ 10 GeV) makes it dangerous to draw too firm conclusions from iterative Monte Carlo simulation programs.

The results from this preliminary study are briefly (cf. Fig 2.3 and Table 2.1):

- The new model improves fit to Λ x_F spectra.
- No version reproduces the "dip" in the Δ^{++} spectra.

- The new model does not reproduce multiplicities as well as the default version.
- Changing the s/u parameter from 0.3 to 0.2, both versions improve multiplicity predictions, and now the new model is slightly better than default.

The last result is of some interest, since HERA data at much higher energies also indicate support for s/u~ 0.2 in DIS [7].

2.4 The MOPS Program

Installation

All changes of the code are inside the subroutine LUSTRF. The modifications have been tested with JETSET version 7.403. However, the file MOPS.f does not contain the complete JETSET code, but only the modified LUSTRF (and some new subroutines called by it). Thus it should be possible to combine the modifications with different sub-versions of JETSET 7.4 and perhaps later versions. To use the modified program, remove the subroutine LUSTRF from a copy of the JETSET code. Create object files both of this copy of JETSET and of MOPS.f, with the same options you normally use when compiling JETSET, and link your main program together with both these object files. The modified program should then work exactly as JETSET ≥ 7.4 with all default options available and some new options added.

Two precautions must be made:

- The new code uses some of the available positions in the LUDAT1 commonblock.
  If anyone of these has been occupied in your version of JETSET *it might be impossible to use the modifications.*
- Positions in a commonblock that are unused by JETSET default are given the value 0.
  Thus the new switches and variables must be explicitly initiated by the user.

Uncovered physical aspects

This is not an official change of the LUSTRF code. It is not prepared for every possible string configuration. Three known shortcomings are:

- The present implementation seriously underestimates baryon production in closed strings (e.g. Υ decay or closed strings from colour reconnection).
- Tensor meson production inside a colour fluctuation is not implemented.
- Modification not available for “junction strings”, coming from multiple interactions. (This is however a feature not fully implemented in JETSET at present.)

There are no immediate plans of extending the implementation to cover the points above, unless feed-back shows a need to do so.

Diquark probability shift

In the way the new model is implemented, some of the produced baryons are rejected due to Γ suppression. To get a proper amount of final baryons, the program therefore needs a larger $P(\mathrm{qq})/P(\mathrm{q})$ value as input. This could of course be achieved simply by changing PARJ(1). However, the default flavour selection subroutine, LUKFDI, is sometimes called by LUDECY (which handles particle decays). Since the new model is not implemented in LUDECY, a drastic enhancement of PARJ(1) could lead to an overestimate of heavy hadrons decaying into baryon-antibaryon pairs.

Instead of including a modified LUDECY in MOPS.f, the shift of $P(\mathrm{qq})/P(\mathrm{q})$ is implemented as a new parameter, giving a multiplicative factor to PARJ(1) when using the Γ suppression algorithm. This new parameter has however no physical interpretation, and could be excluded by implementing modifications to LUDECY.

2.5 Subroutines

Some new subroutines are called inside LUSTRF, but the user should not need to call them explicitly. Here is however a short description.

SUBROUTINE LUSTRF(IP) : fragments a string as default LUSTRF, with options added to use Γ suppression of baryons (MSTJ(12)$\geq$ 4) and new flavour algorithm (MSTJ(12)=5).

SUBROUTINE POKFDI(KF1,KFQPOP,KF3,KF,PT2,PI5) : generates a new flavour and combines it with an existing flavour to give a hadron, i.e. the same as LUKFDI. POKFDI handles incoming diquarks according to the new popcorn algorithm, switched on by MSTJ(12)=5.

- **KFL1 :** (input) incoming flavour.
- **KFQPOP :** (both) flavour of present colour fluctuation quark. When a popcorn system is started (q $\to$ B + qq), KFQPOP is initiated in POKFDI. If KFQPOP is a diquark flavour, the subroutine will instead form a final baryon, build up by KF1 and KFQPOP.
- **KFL3 :** (output) produced new flavour. Is 0 if KFQPOP is a diquark.
- **KF :** (output) produced hadron.
- **PT2 :** (input) $p_\perp^2$ of hadron to be produced.
- **PI5 :** (output) Transverse mass squared of produced hadron.

SUBROUTINE DIQINI : initiates weights for diquark flavours, baryons and popcorn mesons in the MSTJ(12)=5 popcorn algorithm. Is called if MSTJ(5)=0 and sets MSTJ(5) to 1. *If changing any parameter or switch governing these weights during a run,* MSTJ(5) *must be reset to* 0 *or* DIQINI *called explicitly.*

SUBROUTINE PONMES(IWT) : generates number of mesons to be produced in a popcorn system. If the total system is not accepted, a completely new one is started, and PONMES is called again.

IWT : (input) Switch used to identify original diquark fragmentation (=1) or ordinary popcorn system (=0).

2.6 Parameters and Switches

The modified program uses MSTJ(5), MSTU(121,122) and PARJ(8-10,20,27). *Do not combine the modification with a* JETSET *version in which any of these variables are occupied!*

The flavour weights depend differently on the implemented parameters in different situations, and the calculations needed to extract proper weights from the parameters can be rather lengthy. For efficiency, the program starts a simulation by calculating the large but limited number of weights. The result is stored in PARF(201-517). Strictly speaking, these positions are occupied: In JETSET, the user has an option to define flavour weights in PARF(201-1960). However, since it must be considered nonsense to combine the flavour modification of this program with "home-made" flavour weights, this common-block space is used, and a combination of the new flavour algorithm and the MSTJ(15)>0 option is explicitly forbidden.

Note that the default values (denoted by "(D=...)" below) are completely nonsense! This is due to the fact that the subroutine BLOCK DATA which defines default values might change significantly between different JETSET versions. In order to make it possible to link the modification to different JETSET versions, the BLOCK DATA subroutine is not included in the file MOPS.f. Thus the default values are *not* related to the new model. The preliminary tune presented in [1] was: MSTJ(5)=0, MSTJ(12)=5, PARJ(8)=0.6, PARJ(9)=1.2, PARJ(10)=2.09, PARJ(20)=0.6 (from the preliminary results presented in section 2.3 of this paper) and PARJ(27)=0.19.

MSTU(121) : (Internal) counts popcorn mesons. Each time a popcorn system is started in the new algorithm, the number of mesons to be created is stored in MSTU(121) which then is decreased by 1 for each meson produced. When MSTU(121)=0 and the popcorn system is accepted in spite of suppressions, a baryon is produced and the system completed.

MSTU(122) : (Internal) switch to remember whether a popcorn system started through ($q \to B + qq$) production or a baryon remnant diquark at the string end.

MSTJ(5) : (D=0) switch to calculate different weights related to the parameters of the model. DIQINI is called by LUSTRF if MSTJ(5)=0. Is set to 1 in DIQINI. Reset to 0 or call DIQINI explicitly if you change any parameters governing flavour or popcorn weights during the run.

MSTJ(12) : (D=2; suggestion 5) choice of baryon production model.

= **0-3 :** see manual, default version.

= **4 :** popcorn model (as =2) with Γ suppression.

= **5 :** Γ suppression and new popcorn algorithm, independent of PARJ(3-7,18). Instead depending on PARJ(8-9,27) (Baryon remnant fragmentation also depends on PARJ(20)).

PARJ(8,9) : (D=0.,0.; suggestion 0.6,1.2) give β_{u} and $\Delta\beta$ in GeV^{-1} for the popcorn suppression factor.

PARJ(10) : (D=0.; suggestion 2.1) multiplicative factor to PARJ(1)= $P(\mathrm{qq})/P(\mathrm{q})$, used if MSTJ(12)$\geq$4, compensating for rejected popcorn systems due to Γ suppression. PARJ(10) merely corresponds to a shift of the PARJ(1) value. With the present implementation of particle decays in JETSET, it is however important not to change PARJ(1) far from default. This could affect some decay channels of heavy hadrons in an undesired way.

PARJ(20) : (D=0.; suggestion 0.6) gives β in GeV^{-1} for the case of fragmenting a string spanned by an original diquark.

PARJ(27) : (D=0.; suggestion 0.19) gives the suppression of baryons in the decuplet. PARJ(27) in the new model is exactly the same as PARJ(18) in the default one. The reason for using a new spot in the commonblock is again that a change of the flavour parameters used in LUKFDI affects decay channels of heavy hadrons.

Acknowledgments

The Modified Popcorn Scenarium, including the extension described in section 2.3, was developed together with Gösta Gustafson. In writing the MC program, I have benefited greatly from discussions with Torbjörn Sjöstrand. I want to sincerely thank them both.

References

[1] P. Edén, G. Gustafson, *Z. Phys.* **C75** (1997) 41

[2] B. Andersson, G. Gustafson, T. Sjöstrand, *Phys. Scripta* **32** (1985) 574

[3] B. Andersson, G. Gustafson, G. Ingelman, T. Sjöstrand, *Phys. Rep.* **97** (1983) 31

[4] M. Bengtsson, T. Sjöstrand, *Comp. Phys. Comm.* **39** (1986) 347
T. Sjöstrand, *Comp. Phys. Comm.* **82** (1994) 74

[5] H. Bohr, H.B. Nielsen, *NBI-HE-78-3* (1978)

[6] EHS-NA22 collaboration, I.V. Ajinenko et al., *Z. Phys.* **C44** (1989) 573

[7] ZEUS collaboration, M. Derrick et al., *Z. Phys.* **C68** (1995) 29
H1 collaboration, *EPS-0479, presented at the 1995 EPS-HEP meeting, Brussels, Belgium.*

Using Two-jet Events to Understand Hadronization

Paper III

Using Two-jet Events to Understand Hadronization

Patrik Edén, Gösta Gustafson
Department of Theoretical Physics
Lund University

While the hard phase of the strong interaction is well described by perturbative QCD, the soft hadronization phase is less understood. Benefiting from the high statistics from e^+e^- experiments at the Z^0 resonance, it is possible to impose strong two-jet cuts on the data without loosing the statistical significance. In these events perturbative activity is suppressed and hadronization effects can be more prominent. We show that after proper event cuts a set of observables are sensitive to differences in the hadronization models. These observables can thus be important tools for a more detailed study of the hadronization mechanism.

3.1 Introduction

High energy reactions like $e^+e^- \to$ hadrons are usually described in terms of two phases, an initial hard perturbative phase formulated as a parton cascade followed by a soft non-perturbative hadronization phase, for which phenomenological models are needed. The first phase can be calculated from perturbative QCD, but as exact perturbative results in most cases are available only to second order approximate schemes have to be used. In the large N_c limit planar diagrams dominate [1], and for e^+e^--annihilation, descriptions in terms of parton cascades have been quite successful.

Global features like shape variables (thrust, sphericity, oblateness, major, minor etc.) and inclusive particle spectra in e.g. x_F and $p_\perp$, reflect mainly the parton distribution in the initial perturbative phase. These observables can be well described assuming that the hadron distribution closely follows the distribution of partons (local parton hadron duality, LPHD [2]), provided a locally invariant cut-off is applied to the cascade. One example is the observed peak position of the distribution in the variable $\xi = \ln(1/x_F)$, which for most hadrons agrees with parton level results, using a virtuality cut-off Q_0 which is larger for heavier hadrons. Also in some more phenomenological models, e.g. in the cluster fragmentation model [3] and the UCLA model [4] the hadronization properties are to a large extent determined by the hadron masses.

A more detailed description of the final hadronic state, including e.g. flavour, the baryon to meson ratio, spin and polarization as well as correlations (including Bose-Einstein correlations), depends also on the non-perturbative properties of QCD, including the structure of the vacuum condensate. These features cannot be obtained from perturbative calculations. Although some of them may in the future be accessible e.g. from lattice calculations, at present it is unavoidable that a model attempting to give a detailed description of the hadronization process must contain a significant number of phenomenological parameters.

To gain insight in the properties of QCD in the soft region and the vacuum structure it is essential to isolate the hadronization process from the perturbative cascade. This is however not an easy problem. At the end of the cascade the running α_s becomes relatively large. The result depends on a necessary infrared cut-off and nonplanar diagrams and interference effects may be important. This implies that this phase is more uncertain and therefore difficult to isolate. It is also possible that the separation between the perturbative and non-perturbative regions cannot be well defined. As discussed in ref [5] a change in the perturbative cut-off can to a large extent be compensated by a modification of the hadronization parameters. The transition region between the two domains may also show interesting coherence effects [6].

In this paper we will study ways to isolate high energy systems with little perturbative activity, in which the non-perturbative features ought to be more prominent. With the very high statistics available from the LEP1 experiments, it is possible to impose event cuts which exclude a significant amount of perturbative activity, and still have remaining events numerous enough for detailed studies of hadronization. It is possible to calculate purity and efficiency measures for different event shape cuts. Our result is however that a simultaneous purity and efficiency close to 1 cannot be obtained; there is no cut that can be called optimal. Instead different cuts are suitable for a study of different features of the hadronization process.

The outline of this paper is as follows: In section 3.2 we study a set of different event cuts. In section 3.3 we study some observables which have been proposed for a separation of different hadronization mechanisms. In section 3.4 we discuss a few models with different properties and in section 3.5 their predictions for the considered observables. Conclusions are given in section 3.6.

Much of the discussion in this paper will concern different aspects of transverse momenta. These will be denoted $k_\perp$ for partons and $p_\perp$ for hadrons. We will also discuss a sum of hadron $p_\perp$, which we will call $Q_\perp$.

3.2 Cuts

We will here discuss a set of event shape cuts suitable to extract events with little perturbative activity. The performance of the cuts are investigated using Monte Carlo simulations, where the underlying parton state is known.

For simulated events we will here with "little perturbative activity" mean events where all gluon emissions occur at a $k_\perp$ below some $k_{\perp 0}$. (In the analysis presented below we will take $k_{\perp 0} = 2$ GeV.) The reason for choosing this definition, rather than e.g. a cut on the sum of $E_\perp$ for all gluons, is that one hard gluon gives rise to a distinct three jet structure, which introduces long range correlations in azimuthal angle. Such a gluon also increases the phase space for softer ones, which enhances its effects on the final state.

Through further emissions, the energy of one gluon is distributed among its emission products. As this rather enhances than reduces the importance of the perturbative phase, we require $k_\perp$ to be smaller than $k_{\perp 0}$ for each emission, and not for the final partons at the end of the cascade.

We examine the performance of the cuts in terms of purity and efficiency. Purity is defined as the rate of events where the highest $k_\perp$ for a gluon emission, $k_{\perp\max}$, is below $k_{\perp 0}$. If the purity is low, perturbative gluons may shadow many hadronization effects. Efficiency is defined as the acceptance rate among the desired events with $k_{\perp\max}<k_{\perp 0}$. If the efficiency is low, the sample might be biased, and the interpretation of the results is more difficult. Low efficiency also implies low statistics.

The cuts are applied to hadronic final states from Z^0 decays, in events generated by the ARIADNE and JETSET MC [7, 8]. ARIADNE is an implementation of the colour dipole formalism for a QCD cascade [9]. This cascade is convenient to use in the present analysis, as it is ordered in $k_\perp$, which implies that $k_{\perp\max}$ of the cascade is easily extracted as the $k_\perp$ of the first gluon emission. JETSET is a MC for the Lund string fragmentation model [10], which in general gives a good description of e^+e^- data.

The considered two-jet measures are

- $1-T$ (T=Thrust=$\max_{\overline{n}_T} \frac{\sum |\overline{n}_T \cdot \overline{p}|}{\sum |p|}$).
- M (M=Major=$\max_{\overline{n}_M \perp \overline{n}_T} \frac{\sum |\overline{n}_M \cdot \overline{p}|}{\sum |p|}$).
- $k_{\perp\mathrm{clus}}$= transverse momentum of three-jet configuration found using $k_\perp$-based cluster method (we have chosen the DICLUS algorithm [11]).
- Sphericity S, which measures the sum of $p_\perp^2$ w.r.t. the axis minimizing this sum.
- "Linearized sphericity" L, which is similar to sphericity, but linear in particle momenta.
- Multiplicity.

Sphericity S is determined by the largest eigenvalue $\lambda_{\max}$ to the sphericity tensor

$$S^{\alpha\beta} \equiv \frac{\sum_i p_i^\alpha p_i^\beta}{\sum_i |\mathbf{p}_i|^2}, \tag{3.1}$$

through the definition $S = \frac{3}{2}(1-\lambda_{\max})$. Thus $S \approx 0$ for a two-jet event and $S \approx 1$ for an isotropic event. Sphericity is quadratic in particle momenta, which implies that the value is changed if a particle is split in two collinear ones. A linear correspondence to sphericity, suitable for perturbative calculations [12], is obtained by a modified tensor

$$L^{\alpha\beta} \equiv \frac{\sum_i p_i^\alpha p_i^\beta / |\mathbf{p}_i|}{\sum_i |\mathbf{p}_i|}. \tag{3.2}$$

The quantity $L = \frac{3}{2}(1-\lambda_{\max}^{(L)})$ thus measures the summed $p_\perp^2/|\mathbf{p}|$ w.r.t. the event axis. In this paper we will use the terminology suggested by Sjöstrand, and call this measure linearized sphericity.

The event shape cuts in thrust, sphericity and jet-$k_\perp$ are widely used to obtain two-jet events. Apart from these quantities, we have chosen to investigate two measures which can be expected to be closely related to the maximal $k_\perp$ of the parton cascade. One is major, which is given by the maximal summed $|\mathbf{p}|$ component orthogonal to the thrust axis, and the other is linearized sphericity discussed above. The cut in multiplicity is used partly to ensure that the more

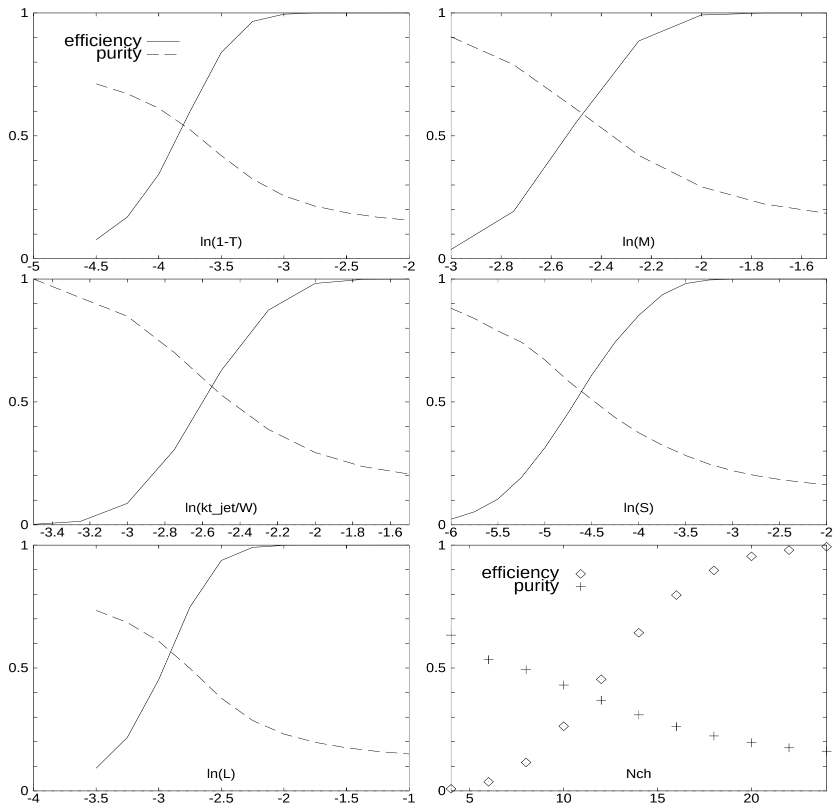

Figure 3.1: *Purity and efficiency for different two-jet cuts.*

carefully designed cuts indeed perform better. Nevertheless it enhances the rate of events with little perturbative activity, as the emitted gluons in general give rise to high multiplicities. One advantage of this cut, which makes it worth consideration, is that $p_\perp$ observables are left relatively unbiased.

Fig 3.1 shows efficiency and purity results for a $k_{\perp 0}$= 2 GeV for the simulated gluon emissions. Most two-jet cuts perform similarly, but it could be noted that the commonly used cut in $1-T$ not obviously is the most successful. For large rapidities of the emitted gluon jet, $1-T$ is approximately $4k_\perp^2/s$ and thus not very restrictive in $k_\perp$. In the central rapidity region, however, $1-T$ behaves as $k_\perp/\sqrt{s}$. For a study in this region, a cut in $1-T$ therefore performs very similarly to the other ones considered in Fig 3.1. The multiplicity cut performs noticeably worse than the others. This is expected, since it is not an cut explicitly in a $p_\perp$ variable.

We end this section by noting that the purity and efficiency measures are not very sensitive to the choice of cut. There is thus no optimal cut in all respects, and as we will see, the preferred cut instead depends on the observable under investigation.

3.3 Observables

In this section we want to study a set of observables which depend on the properties of the hadronization mechanism, but where this dependence is masked by perturbative gluon emission. Thus we will not discuss here the flavour composition of the hadrons, as this appears to be less affected by gluon radiation. (We note, however, that this may not be completely true, as there are experimental indications for a larger procution rate of Λ-particles in Υ decays [13], and also a larger rate of high-energy η-particles in gluon jets [14], than expected from available fragmentation models.)

The observables discussed here are all related to transverse momentum. In many models $p_\perp$ of neighbouring hadrons are anti-correlated to a larger or lesser degree. This anti-correlation is counteracted by jet (or minijet) emission, which gives a positive correlation between hadrons close in rapidity, making the analysis of the soft $p_\perp$ generation very nontrivial.

3.3.1 Inclusive $p_\perp$-distribution

The models discussed in the following sections all have tunable parameters for the soft $p_\perp$ generation. The values of these parameters can be adjusted to reproduce the inclusive distribution of the hadronic $p_\perp$. Thus this distribution acts as a constraint and cannot be used to separate the different models. For this we have to use more complicated observables, e.g. collective variables or correlations.

3.3.2 $\mathbf{p}_\perp$ transfer

One collective variable which can distinguish between different models is the vector sum $\mathbf{Q}_\perp(y)$ of all hadrons with rapidity less than a given rapidity y

$$\mathbf{Q}_\perp(y) \equiv \sum_{y_i<y} \mathbf{p}_{\perp i}, \tag{3.3}$$

which measures the $p_\perp$ transfer over the rapidity y. (This variable has frequently been advocated by E. de Wolf [15].) For a longitudinal phase space model constrained by overall momentum conservation, $Q_\perp$ grows with the number of particles as a random walk. Thus in this model $Q_\perp$ is larger in the central

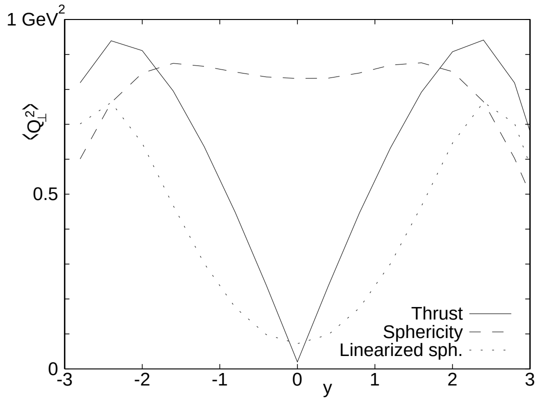

Figure 3.2: *The properties of $\left\langle Q_\perp^2 \right\rangle$ in MC simulated events depend on the choice of axis. The thrust axis, which maximizes longitudinal momentum, by construction gives $Q_\perp = 0$ when $y = 0$. A similar behaviour is seen for Linearized sphericity. The conventional Sphericity axis, minimizing squared transverse momentum, gives the central rapidity plateau expected from the chosen string fragmentation model.*

region and larger in events with high multiplicity. In many fragmentation models, however, the $\mathbf{p}_\perp$ of a hadron is compensated locally in phase space. In such a model, $Q_\perp$ is limited and essentially independent of rapidity and multiplicity.

An essential point when using the $Q_\perp$ variable is the choice of axis. In an experiment the direction of the initial $q\overline{q}$ pair is not known. If the thrust axis is used to define the transverse directions, $Q_\perp(y)$ is kinematically constrained to be equal to zero for $y = 0$. This definition is therefore very unsuitable, if one wants to use the value of $Q_\perp$ in the central region to distinguish between different models.

We have measured $Q_\perp$ w.r.t. different axes in MC generated events, using the JETSET default fragmentation scheme, where $p_\perp$ is compensated essentially by neighbouring particles in rapidity. This implies that we expect a rapidity plateau in $Q_\perp$, though decays of unstable hadrons and the perturbative activity present in the analysed two-jet events introduce corrections to this result. As seen in Fig 3.2, both the thrust axis and the linearized sphericity axis by construction create a significant dip in $Q_\perp$ when $y = 0$. The sphericity axis, on the other hand, reproduces the plateau extremely well. This should not be over-interpreted, for the reasons mentioned above, but it is clear that the sphericity axis is to prefer in a $Q_\perp$ analysis, and it will be used in the results presented below.

The collective quantity $Q_\perp$ is sensitive to correlations between neighbouring

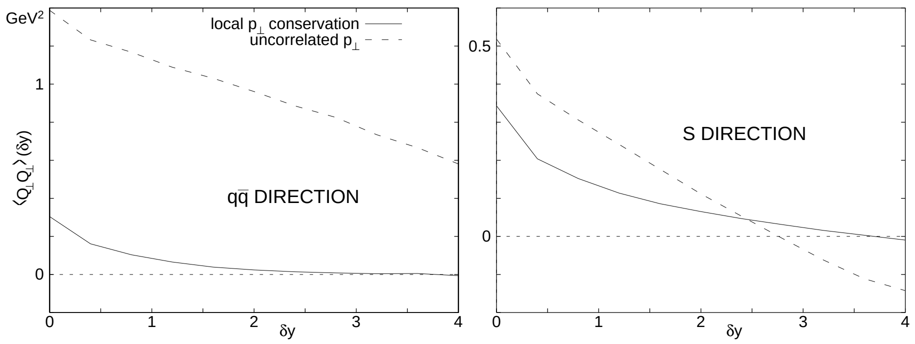

Figure 3.3: *An explicit measurement of the correlation length δy is distorted by the choice of axis. Two very different $p_\perp$ compensation models are compared when measured w.r.t. the original* $\mathrm{q\overline{q}}$ *axis (left) and the sphericity axis (right). To emphasize the effects of axis choice, both the parton cascade and hadron decays have been turned off in the simulations.*

hadrons. It is also possible to study directly the correlation in $p_\perp$ between two hadrons separated by a rapidity interval δy

$$\langle \mathbf{p}_\perp(y_1) \cdot \mathbf{p}_\perp(y_2 = y_1 + \delta y) \rangle \,, \tag{3.4}$$

or the correlation between $\mathbf{Q}_\perp$ for two separated y-values

$$\langle \mathbf{Q}_\perp(y_1) \cdot \mathbf{Q}_\perp(y_2 = y_1 + \delta y) \rangle \,. \tag{3.5}$$

The interpretation of these observables will however be hampered by the systematic effects related to the reconstruction of the event axis. In Fig 3.3 we compare $\langle \mathbf{Q}_\perp \cdot \mathbf{Q}_\perp \rangle (\delta y)$ for two models, one with local $p_\perp$ conservation and one with essentially uncorrelated $p_\perp$. In the MC simulations, we have taken the liberty to turn off both the parton cascade and the hadron decays, in order to more clearly illustrate the effects of axis choice. The plots show the results obtained w.r.t. the original $\mathrm{q\overline{q}}$ axis and the sphericity axis, respectively, and it is clear that the behavior of $\langle \mathbf{Q}_\perp \cdot \mathbf{Q}_\perp \rangle (\delta y)$ is drastically changed. (Equally drastic changes occur if using the thrust axis or linearized sphericity axis.) Due to these effects of axis reconstruction in e^+e^-, a variation of δy does not seem to provide much more information than is available from the observable $\langle Q_\perp^2 \rangle$. This argument does *not* imply that the δy correlation cannot be an interesting observable in deep inelastic scattering and hadron-hadron collisions, where the event axis is better known.

3.3.3 Screwiness

A particular correlation between rapidity and azimuthal angle is determined by a variable called screwiness and introduced in ref [6]. Screwiness is defined by

$$S(\omega) \equiv \frac{1}{\langle N(y_{\mathrm{cut}})\rangle} \left\langle \left| \sum_{|y_i|<y_{\mathrm{cut}}} \exp(i(\omega y_i - \phi_i)) \right|^2 \right\rangle , \tag{3.6}$$

where y_i and ϕ_i is the rapidity and azimuthal angle for particle i, and the sum runs over all central rapidity particles, specified by some y_{cut}. For large ω the sum describes a random walk along unit vectors in the complex plane, and the absolute square of the sum becomes the average multiplicity in the considered interval, $\langle N(y_{\mathrm{cut}})\rangle$. We have normalized $S(\omega)$ by this quantity, which implies that it is 1 for large ω.

The screwiness measure is constructed to give a signal for a helix-like correlation between y and ϕ. A motivation why such a correlation might be expected is presented in ref [6] and shortly described in the following section.

3.4 Models

The most studied hadronization models are based on string dynamics or cluster fragmentation. In the cluster model implemented in the Herwig MC [16] the gluons split into $\mathrm{q\overline{q}}$ pairs at the end of the cascade. A quark is then combined with an adjacent antiquark to form a colourless cluster, which normally decays to two (possibly unstable) hadrons. This approach becomes less realistic and must be modified in events with unusually low gluon radiation. In such events some clusters can get very large masses, and in the Herwig MC these clusters decay in a stringlike fashion. Consequently, if we select events with low gluon activity we cut away those events for which Herwig is meant to work best. For this reason we feel that it would not be meaningful to compare such an event sample with Herwig simulations, and therefore we will instead in the following study some different versions of string hadronization, and for comparison also a model with a $p_\perp$ behaviour similar to a longitudinal phase space.

3.4.1 String fragmentation

In the Lund string model the confining colour field is assumed to behave as a massless relativistic string starting at a quark, passing the gluons in accordance with their order in colour, and ending at an antiquark. Thus the gluons act as transverse excitations or kinks on the string. The string breaks by the production of $\mathrm{q\overline{q}}$ pairs (or occasionally $(\mathrm{qq})(\overline{\mathrm{qq}})$ systems) which combine to hadrons.

For the longitudinal momentum distribution it is assumed that any breakup divides the string in two causally disconnected pieces, which decay further independently of each other. Together with the assumption of a central rapidity plateau this implies a unique result, the symmetric Lund fragmentation model [17, 10]. The result can be generated in an iterative way with a splitting function of the form

$$f(z) \propto \frac{(1-z)^a}{z} \exp(-bM_\perp^2/z), \tag{3.7}$$

where $M_\perp$ is the transverse mass of the generated hadron and z is its fraction of jet energy plus longitudinal momentum.

The iterative procedure specifies an ordering of hadrons called rank. The original quark q_0 combines with an antiquark $\overline{\mathrm{q}}_1$ from the $\mathrm{q}_1\overline{\mathrm{q}}_1$ breakup into the rank one meson. q_1 then forms the rank two meson together with the antiquark $\overline{\mathrm{q}}_2$ from the next breakup, etc. Though the order in rank is not an observable, it is strongly correlated to the order in rapidity.

The string breakup by $\mathrm{q}\overline{\mathrm{q}}$ creation has been treated as a tunneling process [18, 19], in which the transverse momenta should be described by a Gaussian with a width determined by the string tension κ:

$$\frac{\mathrm{d}P}{\mathrm{d}k_\perp^2} \propto \exp(-m_\perp^2/\sigma^2). \tag{3.8}$$

Here $m_\perp^2 = m^2 + k_\perp^2$ is the squared transverse mass of the quark or the antiquark, and from the tunneling mechanism the width should be given by $\sigma^2 = \kappa/\pi$.

An essential property of the string fragmentation is infrared stability, meaning that a soft or collinear gluon has only little influence on the string motion and therefore also on the final hadronic state [1]. This feature makes the result less sensitive to the cutoff for the partonic cascade, and a change in the cutoff can be well compensated by a change in the hadronization parameters when looking at event shapes and inclusive observables for the total event sample [5]. Thus a larger cutoff is compensated by a larger width σ for the hadronization $k_\perp$. Some differences may remain, however, as a gluon tends to give extra $k_\perp$ in the same direction to neighbouring hadrons, while hadronization-$p_\perp$ tends to be in opposite directions, depending on the details in the fragmentation model.

In section 3.3.2 we discussed an observable called $\mathbf{Q}_\perp$, which is sensitive to the properties of $p_\perp$ compensation. We will continue this section by describing different hadronization-$p_\perp$ models, which give slightly different predictions on

[1] To treat situations where a hadron obtains energy and momentum from several small string pieces is however not uniquely specified from the string dynamics. In the models studied below we will use the method developed by Sjöstrand [20] and implemented in the JETSET MC.

$Q_\perp$ and the other observables discussed in section 3.3. In section 3.5 we examine how well these differences can be distinguished in a two-jet event sample.

3.4.2 Jetset default

In the Jetset default version of the string fragmentation model the $\mathrm{q\overline{q}}$ breakups of the string are uncorrelated both in transverse momentum and in flavour. As the quark and the antiquark in a pair have balancing $k_\perp$ the transverse momentum of one hadron is fully compensated by its two neighbours in rank. This implies that $p_\perp$ is conserved very locally in rapidity.

From Eq (3.8) we expect that the width of the $k_\perp$-distribution should be given by $\sqrt{\kappa/\pi} \approx 250$ MeV, but in applications it is treated as a tunable parameter, correlated to the cut-off for the parton cascade. Fits to data give a value around 360 to 400 MeV. Eq (3.8) also introduces an overall suppression of heavy quarks. This implies that the rate of c is completely negligible (the c/u ratio is $\sim 10^{-11}$). To get the rate of s-quarks we would have to know its effective mass. The observed s/u ratio around 1/3 corresponds to the very reasonable value 250 MeV.

Studies of photons at LEP1 indicate a larger tail for high-$p_\perp$ π^0s [21]. The origin of this tail is not clear, but in Jetset default a small component with higher $p_\perp$ is included ($k_\perp$ is multiplied by a factor of 2 for 1% of the vertices).

3.4.3 Partial $p_\perp$ Compensation

The production rate for η and η' cannot be reproduced if neighbouring string breakups are uncorrelated in flavour. Also studies of two-particle correlations observed in hadron–hadron collisions are not well described if the $\mathbf{k}_\perp$ in different breakups are totally uncorrelated [22]. As discussed above, this would imply that the $p_\perp$ of a hadron is fully compensated by its two neighbours in rank. In ref [23] a model is presented in which there are correlations in flavour and $k_\perp$ with some finite correlation length. The model implies a suppression of η and η' production, and also that only a fraction $\gamma < 1$ of the $p_\perp$ of a hadron is compensated by the neighbouring hadrons in rank. Thus $p_\perp$ is compensated within a finite correlation length, but this range is larger than in Jetset default.

In [23] it is shown that this $p_\perp$ compensation assumption can be embedded in an iterative fragmentation scheme. The inclusive $p_\perp$ distribution is then a Gaussian,

$$\mathrm{d}P \propto \exp(-\frac{\alpha}{2\gamma}p_\perp^2)\mathrm{d}^2\mathbf{p}_\perp, \tag{3.9}$$

where α is a tunable parameter. Furthermore, the sum in $\mathbf{p}_\perp$ for the first i particles in rank, $\mathbf{Q}_{\perp i}$, saturates for large i towards the distribution

$$\mathrm{d}P \propto \exp(-\alpha Q_\perp^2)\mathrm{d}^2\mathbf{Q}_\perp. \tag{3.10}$$

We note that for fixed $\langle p_\perp^2 \rangle$ for the hadrons, the collective variable $\langle Q_{\perp i}^2 \rangle$ is smaller for larger γ. This is just the previously stated behaviour for the closely related observable $\langle Q_\perp^2(y) \rangle$, which is small if $p_\perp$ is conserved locally in rapidity.

The JETSET default algorithm is retrieved by setting $\gamma = 1$ and $\alpha = 1/\sigma^2$, where σ is the width in Eq (3.8). In [23], γ is instead assumed to depend on the hadron mass M, and is parametrized as

$$\gamma = \frac{1}{1 + M_0/M}, \tag{3.11}$$

where M_0 is set to 0.9 GeV.

3.4.4 Uncorrelated $p_\perp$

To test whether the data really show a local $p_\perp$ conservation, we also want to study a situation where the hadronic transverse momenta are uncorrelated apart from overall $p_\perp$ conservation. This can be achieved by pushing M_0 to infinity in Eq (3.11), which corresponds to γ being small, but keeping α/γ finite. The MC from [23] is not designed to cope with very large M_0-values. When hadrons are peeled off from both ends of the string usually a large $p_\perp$ is built up for a remaining string piece in the centre. Such events have to be discarded, keeping only those events where by chance this string piece has limited $p_\perp$. In this paper we study only central particles in the accepted events, and thus for our purposes we obtain a fair estimate of the result if in the MC we peel off hadrons from one end only, pushing the junction to the other and outside the region of study.

3.4.5 The UCLA model

A partial $p_\perp$ compensation is also assumed in the UCLA model [4]. In this model it is assumed that not only the longitudinal momentum distribution but also the flavour composition and the distribution in transverse momentum are determined by the symmetric fragmentation function in Eq (3.7). Thus in this model the quark degrees of freedom do not appear explicitly, but only the momenta and flavour of the hadrons. A direct application of Eq (3.7) will however give a too wide $p_\perp$-distribution. In the UCLA approach this problem is solved by assuming a similar kind of finite $p_\perp$ correlations as in the model in section 3.4.3, with $\gamma = 1/2$. Thus as far as transverse momentum goes we expect rather similar results for the UCLA model and the model in [23], and for this reason we content ourselves to study the latter in our investigatons.

3.4.6 Helix String

At the end of a perturbative parton cascade the virtualities become relatively small and the running coupling therefore relatively large. This implies that interference and coherence effects are expected to be important. In ref [6] arguments are presented for correlations between rapidity and azimuthal angle for the emitted gluons, which correspond to a helix-like field at the end of the cascade. This field configuration has also some similarities with a string coupled to a gauge field or a massive relativistic string [24].

A modification to the Lund fragmentation scheme reflecting the helix-like field is presented in [6]. The rapidity distance Δy between two string breakups is correlated with the azimuthal angle $\Delta\phi$ between the transverse direction of the two produced $\mathrm{q\overline{q}}$ pairs. The pitch of the helix is given by an unknown parameter $\Delta y/\Delta\phi = \tau$, allowing for some Gaussian fluctuations around this value. This implies that the observable $S(\omega)$ defined in section 3.3.3 gets a peak at $\omega \approx 1/\tau$. Expected values of τ are around 0.3 to 0.5. The string energy per unit rapidity available to generate $p_\perp$ is given by a parameter m, which implies that a typical magnitude of hadron $p_\perp$ is given by $m\tau$.

3.4.7 Time Dependent $p_\perp$

In order to investigate the sensitivity of the observables we will also study a model with a correlation between transverse momentum and multiplicity which might not be totally inconceivable. The results in Eq (3.8) with a constant width corresponds to a situation with a static flux tube or stringlike colour field. The estimated width of this flux tube is of the order of 1 fm. One can imagine that at very early times the flux is more concentrated. This might correspond to a larger effective string tension, and also from the uncertainty relation one might then imagine that larger transverse momenta are produced in early breakups. If the transverse dimension of the flux tube equals the proper time τ, then we could expect fluctuations in $k_\perp$ of the order $2/\tau$. Expressed in the variable $\Gamma = \kappa^2\tau^2$ this corresponds to a width $\sigma^2 \sim 4\kappa^2/\Gamma$. This becomes very large when $\Gamma \to 0$, and from a string picture we should expect a saturation. To produce large $k_\perp$ sufficient energy must be stored in the string, which therefore must have a minimum length. As discussed in [19] we expect a suppression when $k_\perp > \kappa\tau$, and thus a saturation when $2/\tau \sim \kappa\tau$ or $\Gamma \sim 2\kappa$. These arguments would give the following width for the $k_\perp$-generation

$$\sigma^2 = \begin{cases} \frac{\kappa}{\pi} + \frac{4\kappa^2}{\Gamma}, & \Gamma < 2\kappa \\ \sigma^2_{\max} = \frac{\kappa}{\pi} + 2\kappa, & \Gamma > 2\kappa \end{cases} \tag{3.12}$$

Actually this expression does reproduce the inclusive $p_\perp$ spectrum with hardly any tuning. In our calculations we allowed for an overall normalization factor on σ,

$$\sigma \to \chi\sigma. \tag{3.13}$$

For the standard perturbative cutoff we get $\chi = 1.08$.

A special consequence of the time dependent $k_\perp$ width is a strong correlation between transverse momentum and multiplicity. An early breakup splits the original system in two pieces with relatively small invariant masses. If these masses are called M_1 and M_2 we have approximately

$$M_1^2 M_2^2 \approx \Gamma s, \tag{3.14}$$

where $\sqrt{s}$ is the total mass of the system. It is also easy to show that the ensuing depletion in multiplicity appears in a rapidity of size $\Delta y \sim \ln(\langle\Gamma\rangle/\Gamma)$ around the breakup, where $\langle\Gamma\rangle$ denotes the average value of Γ.

3.5 Results

3.5.1 Hadron $p_\perp$ spectra

We have used average $p_\perp$ and average multiplicity to impose constraints on the free parameters of the considered models. For simplicity, we have left the ARIADNE+JETSET default algorithm unchanged and tuned the other models to reproduce its values. Differences are then searched for in other observables, which will be discussed below.

All models depend on the $k_{\perp\text{cut}}$ of the cascade and the a and b parameters of the symmetric fragmentation function Eq (3.7). To compare different hadronization models, we are interested in using the same description of the perturbative phase for all models, and we have therefore tuned all models keeping the cascade cut-off $k_{\perp\text{cut}}$ constant to the ARIADNE default value. As $k_{\perp\text{cut}}$ is also an hadronization parameter, we will in some examples compare tunes of the same model with different values of $k_{\perp\text{cut}}$.

The a and b parameters influence the multiplicity distribution. For each setup of other parameters, there is in general a narrow but long band of values in the a and b parameter space which reproduces the average multiplicity. The specific a and b values in the tunes are chosen to give a fair agreement also on multiplicity dispersion. The result is presented in Table 3.1.

$p_\perp$ in low multiplicity events

The different models have been tuned to give similar $p_\perp$ distributions in the full event sample. After a two-jet cut, the $p_\perp$ distribution may differ, as the importance of the perturbative phase is then reduced. We will here investigate that possibility. Among the two-jet cuts discussed in section 3.2, the rather

model	parameters						$\langle N\rangle$	$\langle p_\perp\rangle$
	$k_{\perp\mathrm{cut}}$ (GeV)	a	b GeV^{-2}	others				
Default				$\sigma_{k_\perp}$ (GeV)				
	0.6	0.23	0.34	0.405			34.9	0.60
	1.5	0.5	0.4	0.42			35.1	0.59
Partial $p_\perp$				$\frac{1}{\sqrt{\alpha}}$ (GeV)		M_0 (GeV)		
Comp.	0.6	0.23	0.34	0.67		0.9	34.9	0.60
Uncorr. $p_\perp$	0.6	0.23	0.34	1.52		10	34.8	0.59
Helix				τ	σ_τ	m (GeV)		
	0.6	0.23	0.37	0.3	0.2	1.1	35.0	0.59
	0.6	0.23	0.39	0.5	0.3	0.8	34.8	0.60
	0.6	0.23	0.4	0.7	0.35	0.68	34.6	0.60
Time				χ				
Dep. $p_\perp$	0.6	0.23	0.34	1.08			34.7	0.60
	1.5	0.5	0.42	1.18			34.7	0.60

Table 3.1: *The tuned parameter values of the considered models. The tunes are performed w.r.t. average multiplicity $\langle N\rangle$, with π^0 stable, and average $\langle p_\perp\rangle$ within a rapidity interval $|y| < y_{\mathrm{cut}} = 3$. $\langle p_\perp\rangle$ is measured w.r.t. thrust axis and defined as $\frac{1}{n_{\mathrm{ev}}\langle N(y_{\mathrm{cut}})\rangle}\sum_{\mathrm{ev}}\sum_{|y|<y_{\mathrm{cut}}}|p_\perp|$. The top line of the models is the* ARIADNE+JETSET *default tune which has not been changed. The other models are tuned to give similar results. The models and their parameters are discussed in section 3.4.*

blunt cut in multiplicity is then of interest, as it introduces little bias to the $p_\perp$ spectrum.

In section 3.4.7, we discussed a model where the proper time of a $\mathrm{q\overline{q}}$ vertex in the string influences the width of the $k_\perp$ distribution for the $\mathrm{q\overline{q}}$ pair. This model introduces correlations between average $p_\perp$ and multiplicity.

Gluon emissions in general contribute both to $p_\perp$ and multiplicity. For soft gluons the effects are smaller, but if their contribution to $p_\perp$ dominates, it affects the average $p_\perp$ in low-multipicity events. Thus it is of interest to compare correlations in $\langle p_\perp\rangle$ and multiplicity for the same fragmentation model tuned with different cascade cutoffs.

In Fig 3.4 we compare the time dependent $p_\perp$ model discussed in section 3.4.7 and JETSET default fragmentation by studying average $p_\perp$ of particles

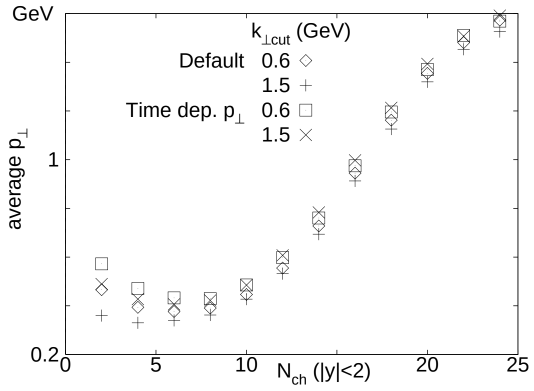

Figure 3.4: *Average $p_\perp$ w.r.t. thrust axis for different charged multiplicities. Statistical errors are well within symbol sizes. The correlation between $p_\perp$ and multiplicity in the time dependent $p_\perp$ model is seen as a higher prediction for average $p_\perp$ in low multiplicity events. For both models $\langle p_\perp \rangle$ is higher in low multiplicity events when the cascade cutoff $k_{\perp \mathrm{cut}}$ is lowered. This indicates that soft gluons in these models give a larger contribution to hadron $p_\perp$ than to hadron multiplicities.*

in the central rapidity region $|y| < 2$, as a function of the charged multiplicity N_{ch} in that region. As expected, average $p_\perp$ at low multiplicities is larger in the time dependent $p_\perp$ model. $p_\perp$ and y are defined w.r.t. the thrust axis, and no two-jet cut in a $p_\perp$ measure is imposed on the event sample.

We note that $\langle p_\perp \rangle$ at low multiplicities is higher for both models if the cascade cutoff is reduced from 1.5 GeV to 0.6 GeV. In the dipole cascade combined with string fragmenation, the soft gluons in this range of $k_\perp$ thus contributes to hadron $p_\perp$ more than to hadron multiplicities.

We have also checked the prediction for the time dependent $p_\perp$ model if the expected saturation of the $\mathrm{q}\overline{\mathrm{q}}$ $k_\perp$ width at very early breakups is neglected. We then get a significantly higher prediction for $\langle p_\perp \rangle$. When $N_{\mathrm{ch}}(|y| < 2) = 2$, it lies between 0.9 and 1.2 GeV, depending on the $k_{\perp \mathrm{cut}}$ for the cascade. The correlation in $p_\perp$ and multiplicity is thus and observable which can be used to confront this kind of unexpected $p_\perp$ generation with experimental data.

3.5.2 $p_\perp$ transfer

The observable $Q_\perp(y)$ discussed in section 3.3.2 measures the $p_\perp$ transfer over the rapidity y and is sensitive to correlations in hadron $p_\perp$. We have investigated $Q_\perp$ for different assumptions about hadron $p_\perp$ conservation. In the

$\langle Q_\perp^2 \rangle$(GeV^2)		default		partial $p_\perp$ compens.	uncorr. $p_\perp$
	$k_{\perp\mathrm{cut}}$ (GeV)	1.5	0.6	0.6	0.6
No cascade		-	0.60	0.71	0.74
With cascade,	all events	12.2	12.3	12.4	12.6
	two-jet events	0.86	0.94	1.02	1.09

Table 3.2: *Average $Q_\perp^2$, measured w.r.t. the sphericity axis in a central rapidity range $|y| < 2$. Results for different assumptions about hadron $p_\perp$ correlation lengts. The differences in the predictions are shadowed by the perturbative cascade, but can be restored by a two-jet cut. Here a cut in sphericity,* $\ln(S) < -4.5$*, has been used.*

default algorithm, $p_\perp$ is compensated by the neighbours in rank, which implies a compensation local in rapidity. In the partial $p_\perp$ compensation model, a fraction $\gamma < 1$ of $p_\perp$ is compensated by closest neighbours. This implies a correlation length for $p_\perp$ of order $1/\gamma$ which is finite, but larger than for Jetset default. We also examine a model where the hadron $p_\perp$ are uncorrelated, apart from global momentum conservation.

In two-jet events, the hadrons can also aquire $p_\perp$ from soft gluons. The compensation of this $p_\perp$ is in general not identical to the one assumed in the fragmentation, and depends on the recoil treatment of the cascade formalism. Thus the assumed $p_\perp$ conservation length may depend on the treatment of recoils in the cascade, and on the cutoff scale, which determines to what extent hadron $p_\perp$ originates from the cascade or the hadronization.

The top row in Table 3.2 shows results without cascade for the three different $p_\perp$ correlation assumptions. $Q_\perp$ clearly grows for less local $p_\perp$ compensation, with a relative difference of 25% between complete $p_\perp$ compensation by neighbours (Jetset default) and uncorrelated $p_\perp$. Adding a cascade allmost wipes out the difference, but after a two-jet cut it is restored to a satisfactory degree. The relative difference between the two extremes with a common cutoff $k_{\perp\mathrm{cut}}$= 0.6 GeV (second and fourth column) is then about 16%. Also partial $p_\perp$ correlation as assumed in [23], similar to the UCLA $p_\perp$ generation model, gives results after a proper two-jet cut which differ significantly from the results of the Jetset default assumption.

A comparison of the first and second column illustrates the difference in $p_\perp$ compensation in the cascade and in the fragmentation. The same $p_\perp$ model, tuned with different cascade cut-offs, give significantly different results on $Q_\perp$. Soft gluon emission in the dipole cascade introduces longer $p_\perp$ correlation lengths than given by default hadronization $p_\perp$, which implies that $Q_\perp$ increases when adding soft gluons in the range 1.5 to 0.6 GeV to the cascade.

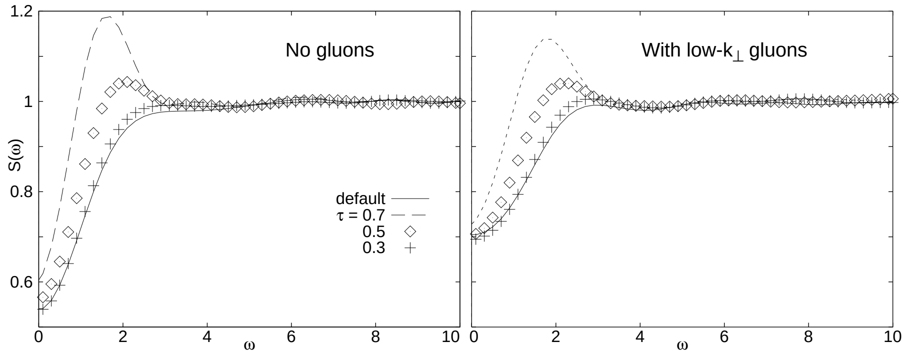

Figure 3.5: *Screwiness without gluons, and with low-$k_\perp$ gluons ($k_\perp$ in the emissions is restricted between 1 and 2 GeV). The central rapidity region $|y| < 2$ is considered. With the assumptions made here about effects from perturbative gluons, the signal survives.*

3.5.3 Screwiness

In [6], MC simulations of $q\overline{q}$ string fragmentation without cascade show a clear signal in $S(\omega)$ in the helix-like fragmentation model for $\tau \sim 0.5$ or larger. To check the influence of relatively soft gluons on the screwiness measure, we have modified JETSET to generate $p_\perp$ according to the helix model. The $p_\perp$ generation is then combined with the JETSET default recipe for passing gluons [20]. This implies that the azimuthal directions on different sides of a gluon kink is not completely uncorrelated, though measured w.r.t. two different directions. The $p_\perp$ component being transverse to both considered directions is preserved when passing a gluon kink.

One could also consider more direct effects, assuming the azimuthal angle of vertices on different string segments to be explicitly uncorrelated, and also allowing the helix to have different orientation on different string segments. The investigation here however focus on the minimal effects of gluons bending the string.

Before looking at screwiness after a full cascade and a two-jet cut, we examine the effects of soft gluons by running a cascade with $k_\perp$ for the emissions constrained between 1 and 2 GeV. As seen in Fig 3.5, the observable $S(\omega)$ is fairly unaffected by these rather soft gluons.

A cascade introduces long-range azimuthal correlations which have large effects on $S(\omega)$. In a three-jet event the thrust direction tends to be aligned with the hardest jet, which implies that the particles of this jet are rather randomly distributed in azimuthal angle ϕ. The softest jet is seen as a set of particles well collimated both in ϕ and y. The particles of the remaining jet

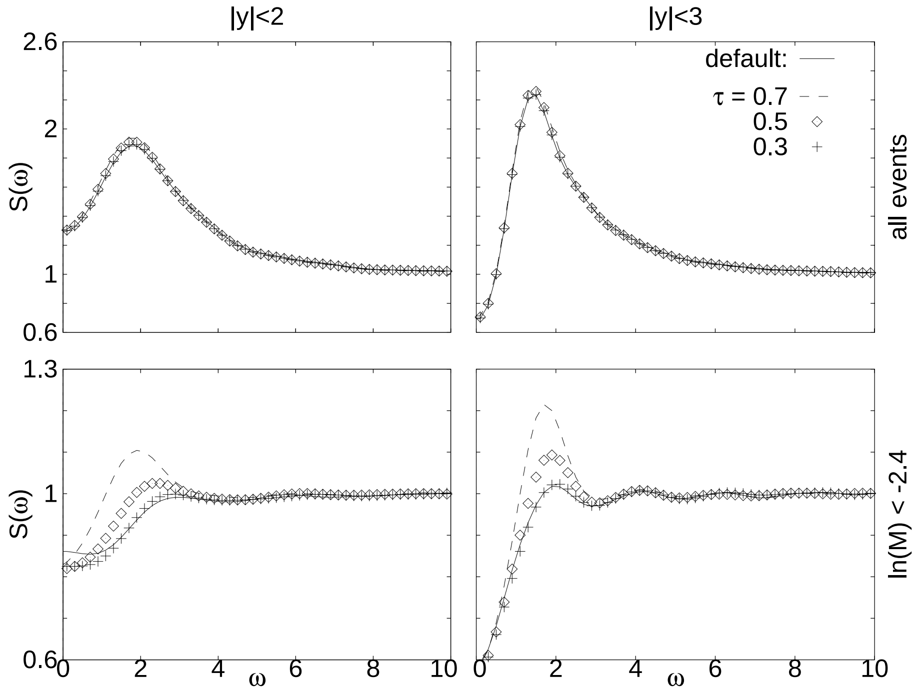

Figure 3.6: *Screwiness after gluon cascade, with and without a two-jet cut. Without any two-jet cuts (upper row), a signal reflecting long-range azimuthal correlations in three-jet structures is seen, independent of fragmentation mechanism. After a two-jet event cut, this signal is removed, and the $S(\omega)$ measure is sensitive to helix-like fragmentation. The results are similar to the ones with only low-$k_\perp$ gluons, and only moderately reduced.*

are more spread out towards large rapidities and have and azimuthal direction opposite to the softest jet. In this typical three-jet configuration, particles of the hardest jet merely introduces noise to $S(\omega)$, while the two softer jets tend to enhance $S(\omega)$ when $\omega \sim \pi/y_{\mathrm{cut}}$, where y_{cut} is the largest considered rapidity in the analysis. Thus we get a signal which is independent of fragmentation mechanism, but is sensitive to the magnitude of the considered central rapidity range. This behaviour is seen in the upper plots of Fig 3.6.

After event cuts (lower plots in Fig 3.6), the result is very similar to those with low-$k_\perp$ gluons in Fig 3.5 and give a clear signal for helix-like string fragmentation if $\tau \sim 0.5$ or larger. In [6], different ways to enhance the signal also for lower values of τ were investigated. The analysis was performed on $\mathrm{q\overline{q}}$ strings without cascade, and it was shown that a lower limit on average $p_\perp$

could be used to distinguish default string fragmentation and helix fragmentation with τ down to 0.3. A lower cut in $p_\perp$ is slightly in conflict with a two-jet cut, but it is possible that a similar approach can be used to enhance the signal in two-jet events obtained from real data.

3.6 Conclusions

High energy reactions like $e^+e^- \rightarrow$ hadrons are usually described in terms of two phases, an initial perturbative phase, formulated as a parton cascade, followed by a soft hadronization phase described by a phenomenological model. It is however not only the description of the soft phase which depends on model assumptions. This is also the case for the perturbative phase towards the end of the cascade, where α_s is large and some kind of cut-off is necessary. The transition region may also exhibit interesting interference or coherence effects, one example being the helix-like field configuration proposed in [6].

In many cases the effects of gluon emission overshadow the features of the hadronization phase. To investigate the hadronization mechanism it is therefore interesting to study whether suitable events cuts can help separating the two phases and give observables sensitive mainly to one of them.

We have examined different strong two-jet cuts to suppress the perturbative activity. It is possible to define efficiency and purity measures for the different cuts. MC simulations show, however, that no cut can be called optimal. Instead the preferred cut depends on the observable under investigation.

As the flavour composition of the final state in most models is less sensitive to the parton cascade, we concentrate here on observables related to transverse momentum. Different assumptions can be made concerning recoil effects and the locality of $p_\perp$ conservation. In most models it is possible to tune the inclusive $p_\perp$ spectrum, and to distinguish the models it is then necessary to study different forms of correlations. The vectorial sum of $\mathbf{p}_\perp$ for all particles with rapidities smaller than some value y, here called $\mathbf{Q}_\perp$, is an observable which is sensitive to the $p_\perp$ correlation length. If $p_\perp$ is locally conserved, average $Q_\perp$ is similar to average $p_\perp$. On the other hand, if only global constraints restrict $p_\perp$, the collective measure $Q_\perp$ gets significantly larger than $p_\perp$.

After a two-jet cut, we find the $Q_\perp$ measure to be sensitive to assumptions about $p_\perp$ compensation in the hadronization phase. It is also sensitive to the value of the cascade cut-off, since the recoil treatment in the cascade in general give longer $p_\perp$ correlation lengths than assumed in the fragmentation.

Another observable which is shown to be sensitive to the cascade cut-off is average $p_\perp$ in low multiplicity events. Though multiplicity in general is not considered a two-jet cut, it suppresses high-$k_\perp$ perturbative emissions, which typically give rise to large multiplicities. Gluon emissions with moderate $k_\perp$ however contribute more to hadronic $p_\perp$ than to hadronic multiplicity, which implies that the correlation between $p_\perp$ and multiplicity is sensitive to the cascade cut-off.

In [6] it is argued that coherence effects in the transition region may give rise to a helix-like colour field, with a correlation beteen rapidity and azimuthal angle. Perturbative gluon emissions mask this correlation to a large extent, but we have found that after a strong two-jet cut, a signal in the proposed observable “screwiness” is present for some possible helix configurations.

The very high statistics now available from experiments at the Z^0 resonance implies that strong two-jet cuts are possible on the data without loosing the statistical significance. Our results show that such cuts can indeed in many cases discriminate between different hadronization models and thus be a tool for a more detailed study of the hadronization mechanism.

References

[1] D. Amati, R. Petronzio, G. Veneziano, *Nucl. Phys.* **B140** (1978) 54; *ibid.* **B146** (1978) 29

[2] Ya.I. Asimov, Yu.L. Dokshitser, V.A. Khoze, S.I. Troyan, *Z. Phys.* **C27** (1985) 65

[3] B.R. Webber, *Nucl. Phys.* **B238** (1984) 492

[4] C.D. Buchanan, S.B. Chun, *Phys. Rev. Lett.* **59** (1987) 1997;
C.D. Buchanan, S.B. Chun, *Phys. Rep.* **292** (1998) 239

[5] B. Andersson, G. Gustafson, A. Nilsson, C. Sjögren, *Z. Phys.* **C49** (1991) 79

[6] B. Andersson, G. Gustafson, J. Häkkinen, M. Ringnér, P. Sutton, *JHEP* **09** (1998) 014

[7] L. Lönnblad, *Comp. Phys. Comm.* **71** (1992) 15

[8] M. Bengtsson, T. Sjöstrand, *Comp. Phys. Comm.* **39** (1986) 347;
T. Sjöstrand, *Comp. Phys. Comm.* **82** (1994) 74

[9] G. Gustafson, *Phys. Lett.* **B175** (1986) 453;
G. Gustafson, U. Pettersson, *Nucl. Phys.* **B306** (1988) 746;
B. Andersson, G. Gustafson, L. Lönnblad, *Nucl. Phys.* **B339** (1990) 393

[10] B. Andersson, G. Gustafson, G. Ingelman, T. Sjöstrand, *Phys. Rep.* **97** (1983) 31

[11] L. Lönnblad, *Z. Phys.* **C58** (1993) 471

[12] G. Parisi, *Phys. Lett.* **B74** (1978) 65;
J.F. Donoghue, F.E. Low, S.Y. Pi, *Phys. Rev.* **D20** (1979) 2759

[13] W. Hofmann, *Ann. Rev. Nucl. Part. Sci.* **38** (1988) 279

[14] L3 Collaboration, M. Acciarri et al., *Phys. Lett.* **B371** (1996) 126

[15] E.A. de Wolf, private communications.

[16] G. Marchesini, B.R. Webber, M.H. Seymour, G. Abbiendi, L. Stanco, I.G. Knowles, *Comp. Phys. Comm.* **67** (1992) 465

[17] B. Andersson, G. Gustafson, B. Söderberg, *Z. Phys.* **C20** (1983) 317

[18] H. Bohr, H.B. Nielsen, *NBI-HE-78-3* (1978)

[19] B. Andersson, G. Gustafson, T. Sjöstrand, *Z. Phys.* **C6** (1980) 235

[20] T. Sjöstrand, *Nucl. Phys.* **B248** (1984) 469

[21] ALEPH Collaboration, D. Buskulic et al., *Z. Phys.* **C57** (1993) 17;
L3 Collaboration, O. Adriani et al., *Phys. Lett.* **B292** (1992) 472

[22] E.A. de Wolf, Contrib. to *Proc. XXII Symp. on Multiparticle Dynamics*, Santiago de Compostela 1992, ed. A. Pajares, World Scientific

[23] B. Andersson, G. Gustafson, J. Samuelsson, *Z. Phys.* **C64** (1994) 653

[24] N.K. Nielsen, *Nucl. Phys.* **B167** (1980) 249

Investigations of Quark Fragmentation Universality

Paper IV

Investigations of Quark Fragmentation Universality

Patrik Edén
Department of Theoretical Physics
Lund University

Abstract:
We propose event cuts in deep inelastic scattering, suitable for an examination of quark fragmentation universality. We compare the current hemisphere of the Breit frame with hemispheres in e^+e^- annihilation events, using Monte Carlo simulations. The agreement between the two processes is improved after the suggested event cuts. A method to study the scale evolution in quark hemispheres using data from fixed energy e^+e^- experiments is presented. This makes it possible to use the high statistics from LEP1 also at scales below the Z^0 mass. We also discuss observables which are sensitive to the dynamics of regions closer to the remnant. The observables probes the relatively clean region on the current side of the hardest emission in the event, and can be used to distinguish between different assumptions about remnant effects and mechanisms for the parton evolution.

4.1 Introduction

In deep inelastic scattering (DIS), the current hemisphere of the Breit frame is expected to be very similar to one hemisphere in an e^+e^- experiment. This expectation relies on the fundamental assumption of quark fragmentation universality. However, a set of features in DIS introduce corrections to this assumption.

QCD radiation can give rise to high-$p_\perp$ emissions, where $p_\perp \sim Q$ or higher. These emissions have no correspondance in an e^+e^- event, where the kinematical constraint for gluon emission is $p_\perp \leq \sqrt{s}/2$. A high-$p_\perp$ emission in DIS significantly changes the kinematical properties of the struck quark, and a high-$p_\perp$ event sometimes manifests itself with a completely empty current region [1]. If the rate of such events is getting non-negligeble, they may introduce an uncertainty to the interpretation of the data. Furthermore, problems arise even if the current region is not empty, but merely depopulated. It is therefore of interest to find a way to exclude high-$p_\perp$ events using another signal than an empty current Breit hemisphere. One candidate method is to reconstruct the highest $p_\perp$-scale of the event using jets, and we will in this paper discuss that approach.

The flavour composition in e^+e^- and DIS is not exactly the same. When excluding high-$p_\perp$ events from the DIS analysis, the boson-gluon fusion channel for heavy quark production is supressed. This implies a lower heavy quark rate in the studied DIS sample, as compared to e^+e^- data at corresponding energies. A uds enriched e^+e^- data sample with high statistics is available from the Z^0 peak. We will in this paper discuss a method to study properties of e^+e^- quark hemispheres at different scales, using data from the fixed energy Z^0 experiments.

At very low squared momentum transfer, when Q^2 is of the same order as the squared ρ-meson mass m_ρ^2, the vector meson component of the photon affects the current region properties. We will restrict the discussion to $Q^2 > 4\text{GeV}^2 \sim 8m_\rho^2$. In this kinematical range the vector meson component of the probe is suppressed, and it will not be discussed further in this paper.

Comparisons of DIS and e^+e^- data support quark fragmentation universality [2]. Some differences are however observed, especially at low Q^2. These can in general be qualitatively explained from the features discussed above, but data on e.g. strangeness rates in DIS are less well understood [3].

In this paper, we investigate how the similarity between e^+e^- and current Breit hemispheres can be improved with proper event cuts. The effects of event cuts are examined with MC simulations. We also discuss observables which are sensitive to the dynamics of regions closer to the remnant, where the theoretical situation is not so clear, due to e.g. the uncertainties from the BFKL Pomeron and from remnant effects. The observables discussed here are defined to probe the current side of the hardest emission in the event. This is a relatively clean region with a reduced dependence on soft remnant properties, as compared to the forward target region. This facilitates the interpretation of the results, which also can be compared to corresponding analyses in e^+e^- experiments. We show that the proposed observables can distinguish between different existing models.

The outline of this paper is as follows. In section 4.2 we discuss suitable jet algorithms in a search for high-$p_\perp$ events. In section 4.3, the current region properties after different event cuts are studied and compared to e^+e^- results. In section 4.4 we discuss a method to obtain experimental e^+e^- data whith a controlled rate of heavy flavours. In section 4.5 we propose observables which are sensitive to the dynamics of regions closer to the remnant. Finally, the results of this paper are summarized in section 4.6.

4.2 Jet Algorithms

In DIS events, high-$p_\perp$ emissions can break the quark fragmentation universality. In this section we discuss jet cluster algorithms suitable for a reconstruction of the highest $p_\perp$-scale of an event. The result may depend on the choice of jet finding algorithm used, and we will here discuss the properties of a set of possible algorithms.

Since the aim of the jet clustering is to find the highest $p_\perp$, it is natural to use $k_\perp$-type cluster algorithms. Our approach will be to combine jets in the order specified by a $k_\perp$ distance, until only three remain (including the remnant jet). The event is accepted if the $p_\perp$ specified by the final three jets is lower than $Q/2$. This cut is in analogy to the kinematical constraint for gluon emissions in e^+e^-, which is $p_{\perp\mathrm{g}} \leq E_\mathrm{g} \leq \sqrt{s}/2$.

Historically, $k_\perp$ algorithms were first designed for e^+e^- physics. A set of different algorithms exist [4]. In DIS, extra requirements are in general imposed on the cluster algorithm, since jet observables in DIS are dependent on structure functions. In a comparison with analytical calculations, a jet algorithm where the properties factorizes into perturbatively calculable coefficients convoluted with the structure functions is preferred. This implies that the remnant jet cannot always be treated on equal footing with the other jets. A $k_\perp$ algorithm designed to fulfill jet requirements in DIS is presented in [5]. However, in the present study we are merely interested in jets with relatively high $p_\perp$, and the infrared properties of the used algorithm are less important. Furthermore, we do not intend to investigate jet cross sections or the jets themselves, but merely to exclude high-$p_\perp$ events. In the accepted sample, the analysis is performed on the current Breit hemisphere, which is defined independently of any jets. We have therefore chosen to use the simpler e^+e^- $k_\perp$ algorithms.

To estimate the reliability of the results obtained using jets, we have used three different algorithms, Luclus [6], Durham [7] and Diclus [8], applied in the hadronic CMS system. All these algorithms start off with the final state particles as initial clusters. These clusters are then iteratively merged in an order specified by a distance of $k_\perp$-type, until all remaining distances are larger than a resolution parameter, or until a specified number of clusters remain.

In the HERA experiments, particles which in the lab frame have a large pseudo-rapidity w.r.t. the proton direction are not detected. In our analysis, we have chosen to exclude all particles with pseudo-rapidity larger than 3.8, to take this into account. For clustering purposes, an initial cluster is introduced along the proton direction, carrying the missing longitudinal momentum. (To exclude the possibility that the obtained results are merely a consequence of the undetected target region, we have also performed analyses where all particles are used in the clustering. The result is that the effects presented in the paper would be even more prominent, if having access to a full coverage detector.)

In the DURHAM algorithm, the distance between the clusters i and j is defined as

$$d_{ij}^{(D)2} = 4\min(E_i^2, E_j^2)\sin^2(\theta_{ij}/2). \tag{4.1}$$

The cluster pair with smallest distance value are combined into one new cluster, with a four-momentum given by the sum of its constituents. For small angles θ_{ij}, the DURHAM distance d_{ij} is the transverse energy of the softer particle with respect to the other. The factor $2\sin(\theta_{ij}/2)$, used instead of $\sin(\theta_{ij})$, prevents unreasonable merging of oppositely moving clusters.

The LUCLUS algorithm is very similar, but uses the distance

$$d_{ij}^{(L)2} = 4\frac{|\mathbf{p}_i|^2|\mathbf{p}_j|^2}{(|\mathbf{p}_i| + |\mathbf{p}_j|)^2}\sin^2(\theta_{ij}/2). \tag{4.2}$$

Apart from the difference between $|\mathbf{p}|$ and E, the DURHAM factor $\min(E_i, E_j)$ corresponds in the LUCLUS measure to $E_iE_j/(E_i + E_j)$. This implies that $d_{ij}^{(L)}$ always is somewhat smaller than $d_{ij}^{(D)}$. To the LUCLUS algorithm, a reassignment scheme is added, where all particles are moved to the closest existing cluster after each merging. At the very end of the algorithm, the reassignment procedure is iterated til convergence. This scheme prevents particles to, through successive mergings, end up in a jet moving in a very different direction.

A cluster algorithm can be viewed as a reconstruction of a parton cascade backwards. The two described algorithms combines two clusters into one, like an inverse parton emission. In the DICLUS algorithm, supplied with the ARIADNE MC [9], three clusters are merged into two. This corresponds to an inverse dipole emission. The distance measure used is

$$\left[d_{i(jk)}^{(A)}\right]^2 = \frac{\left[s_{ij} - (m_i + m_j)^2\right]\left[s_{ik} - (m_i + m_k)^2\right]}{s_{ijk}}. \tag{4.3}$$

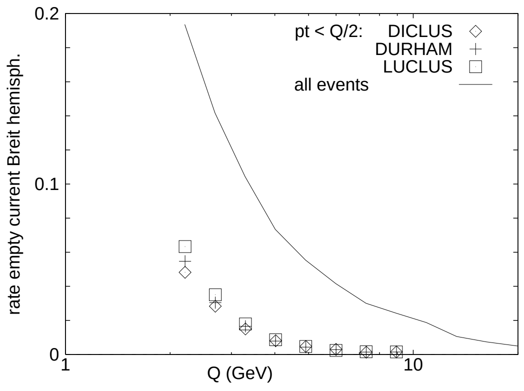

Figure 4.1: *The rate of empty current Breit hemispheres. Results from MC simulations. The solid line shows the rate when considering all generated DIS events. The symbols show the result when events with a jet-$p_\perp > Q/2$ are excluded, using three different $k_\perp$ clustering algorithms. The rate is significantly reduced after the cut in jet-$p_\perp$.*

Here s_{ij} and s_{ijk} are the squared masses of the clusters indicated by the indices. This distance is a Lorentz invariant $p_\perp^2$-measure for parton i with respect to a dipole built up by j and k. In the merging, the cluster i is absorbed into j and k. The momentum of i is distributed in accordance with the recoil treatment in the dipole cascade [9].

In the present analysis, three clusters are constructed using one of the presented algorithms. These final clusters are called jets, and the smallest remaining d_{ij} specifies the $p_\perp$ of the event.

The three chosen algorithms are all of $k_\perp$–type, and hence similar in many respects. For quasi-collinear, massless clusters, the three distance measures are very similar. There are however also noticeable differences. Differences in the distance measures occur at large angles and for heavy clusters, the reassignment procedure in LUCLUS is not used by the other algorithms, and the merging of three clusters into two is a unique feature of the DICLUS algorithm. In the following, we will investigate results using all three algorithms, and we will consider results which are insensitive to the specific choice of algorithm as reliable.

4.3 Current Breit Hemisphere Properties

To examine if a cut in jet-$p_\perp$ is suitable to isolate a sample where universality is expected to hold, we will here study results for the current Breit hemisphere in MC generated events at HERA energies. The results are compared to e^+e^- MC results.

We simulate the electro-weak interaction in DIS using the LEPTO MC [10]. In both the e^+e^- and DIS simulations, we use the Colour Dipole Model [11], implemented in ARIADNE [9], to describe the parton cascade. The Lund string fragmentation model [12], implemented in JETSET [6] is then used to describe hadronization. The chosen MC programs give a generally good description of data in DIS an e^+e^-.

Effects of the $p_\perp$-cut

In Fig 4.1, the rate of events in DIS with empty current Breit hemispheres is shown to be significantly reduced after a $p_\perp < Q/2$ cut, for all jet finding algorithms. As discussed in section 4.2, the LUCLUS distance measure is less restrictive than the DURHAM one, and this is seen as a slightly higher rate of empty events. The rate is however significantly reduced with all three algorithms.

Though the phase space for the current Breit hemisphere is very similar to an e^+e^- hemisphere, there are differences in the regions nearby, which affect the average energies. Consider two hemispheres in the rest frame of an e^+e^- annihilation event. In general, they have different masses and hence different energies. In other words, a high-$p_\perp$ emission in one hemisphere reduces the energy of the other, due to energy–momentum conservation.

As for an e^+e^- hemisphere, the energy of the current Breit hemisphere at fixed Q^2 is expected to deviate from $Q/2$. The energy depends on emissions in this hemisphere and in the nearby phase space of the opposite hemisphere. The latter is in DIS very large, but after our suggested event cuts, it is reduced by the condition $p_\perp < Q/2$. The corresponding kinematical constraint in e^+e^- is however $|\mathbf{p}| < Q/2$, which is more restrictive. Thus the region for high-$p_\perp$ emissions which can reduce the energy of the considered hemisphere is larger in DIS than in e^+e^-. The emission density at this relatively high $p_\perp$ is suppressed, but not zero. Without reaching for a quantitative prediction, we may conclude that we expect the mean energy and multiplicity of the current Breit hemisphere to satisfy

$$\langle E_{\mathrm{CBH}} \rangle < \frac{Q}{2}, \quad \langle N_{\mathrm{CBH}} \rangle < \frac{1}{2} N_{ee}(Q^2), \tag{4.4}$$

where $N_{ee}(Q^2)$ is the average multiplicity in an e^+e^- experiment with invariant mass Q^2.

If $2\langle E_{\mathrm{CBH}} \rangle / Q$ would be much smaller than 1, the similarity between the current Breit hemisphere and an unbiased e^+e^- hemisphere is poor, and it is not likely that reliable conclusions from a comparison can be drawn. On the other hand, if $2\langle E_{\mathrm{CBH}} \rangle / Q \approx 1$, the current Breit hemisphere sample may be

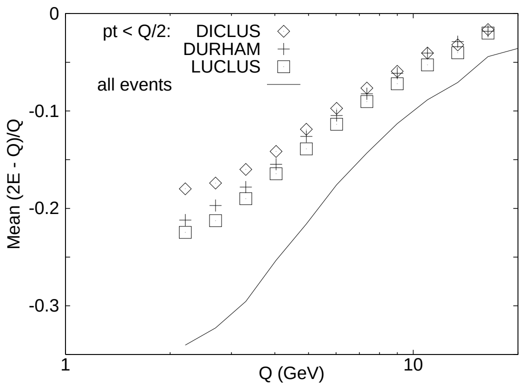

Figure 4.2: *The relative difference between average energy and $Q/2$ in the current Breit hemisphere. The relative shift in the MC simulations is significantly reduced after a $p_\perp < Q/2$ cut.*

closely related to an unbiased e^+e^- hemisphere. In Fig 4.2, the relative energy shift $2\langle E_{\text{CBH}}\rangle/Q - 1$ is shown to be sizeable for the unrestricted event sample, but significantly reduced after imposing a $p_\perp < Q/2$ cut .

Flavour Compositions

In a comparison between e^+e^- and DIS, also the flavour composition in the different experiments need to be considered. In e^+e^- the rate of heavy flavours varies with energy. On the Z^0 pole it is determined by the couplings to the Z^0, while at lower energies it is determined by the quark electric charges. In DIS events at HERA energies, photon exchange is dominating over Z^0 exchange. However, here the flavour composition also depends on soft physics. The rate of charm in the proton structure function (intrinsic charm) is suppressed by the heavy c mass.

A cut in $p_\perp$ suppresses the boson-gluon fusion channel for charm production in DIS. This implies that the c rate in the low-$p_\perp$ sample is reduced. Using MC simulations, we have found charm to be suppressed approximately by a factor 2 in a $p_\perp < Q/2$ event sample, with all cluster algorithms. A problem for the interpretation of this result is the fact that the MC simulation program significantly underestimates the rate of charm events. In the MC this is about 10%, while data indicate a much larger value around 25% [13]. However, a similar suppression ought to be expected also for real data. If boson-gluon fusion is a more important source of charm in Nature than assumed in the MC model, the suppression may be even stronger. It would then be appropriate to compare with uds enriched e^+e^- data. How to obtain such data at different

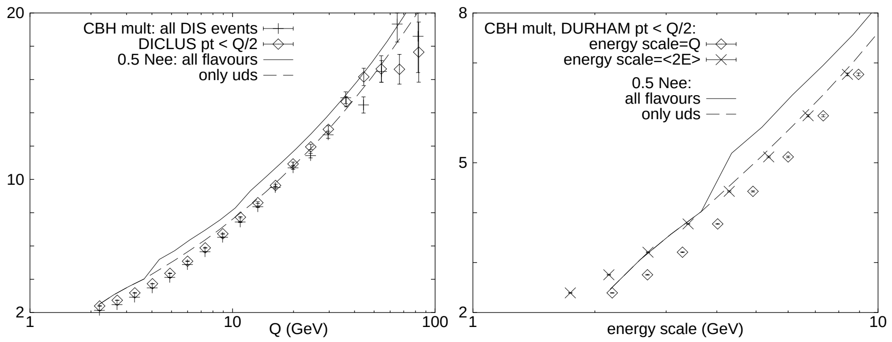

Figure 4.3: *MC simulations of multiplicities in e^+e^- and the current Breit hemisphere (CBH).* **LEFT:** *e^+e^- results with squared mass $s = Q^2$, allowing for all flavours (solid line) and only uds (dashed line), compared to CBH multiplicities using all events (crosses) and a jet-$p_\perp < Q/2$ sample (diamonds). Both the exclusion of high-$p_\perp$ DIS events and heavy flavour e^+e^- events improves the agreement between the multiplicities.* **RIGHT:** *For low energy scales, the agreement is further improved if comparing the CBH multiplicity with e^+e^- data with squared mass $s = 4\langle E_{\mathrm{CBH}}\rangle^2$.*

energies will be discussed in section 4.4.

Monte Carlo results for average multiplicities are presented in the left plot of Fig 4.3. The results for the low-$p_\perp$ DIS sample are essentially equivalent for the three considered jet algorithms, and only the Diclus result is shown. In this MC generated event sample, heavy quark rates are well below 10%, and it is therefore better compared to a MC e^+e^- sample with only uds. The agreement between the low-$p_\perp$ and the e^+e^- uds sample is better than between the unrestricted event samples also shown in Fig 4.3.

Energy Scale Corrections

As discussed previously in this section, high-$p_\perp$ emissions close in rapidity to the considered hemisphere implies a reduction of the average energy in the current Breit hemisphere, $\langle E_{\mathrm{CBH}}\rangle$, to a value slightly smaller than $Q/2$. It is then natural to compare the current Breit hemisphere multiplicities with e^+e^- data at a squared mass $s = 4\langle E_{\mathrm{CBH}}\rangle^2$. The agreement between e^+e^- and Breit frame multiplicities is then significantly improved, as shown in the right plot of Fig 4.3. Only the Durham result is presented, but the other results are very similar.

When compensating for small systematic differences by changing scale to the average energy, many effects – known as well as unknown – may be corrected for. However, after correcting for expected differences in this way, unexpected features which break quark fragmentation universality can still be searched for in observables less blunt than the mean multiplicity, like strangeness rates, energy spectra and higher multiplicity moments.

Comparing the left and right plot in Fig 4.3, we see that the high-$p_\perp$ cut has a relatively small influence on the average multiplicity, as compared to the energy scale shift. However, in Fig 4.1 we note that the rate of empty current Breit hemisphere events, which are excluded from the analysis more by necessity than by theoretical understanding, are reduced with the high-$p_\perp$ cut. This is also the case for the energy shift, as seen in Fig 4.2. Thus we find that a cut in jet-$p_\perp$ is a powerful step towards an event sample where quark fragmentation universality is expected to hold.

4.4 Scale Evolutions in Fixed Energy e^+e^- Annihilation

A large sample of uds enriched events are available from LEP1 at $\sqrt{s} = 90$GeV. This is not the case for other energies corresponding to the HERA kinematical range. In this section we discuss how the scale evolution of e^+e^- uds hemispheres can be examined, using data from a fixed energy e^+e^- experiment.

In search for an algorithm which enables such a study, it is useful to recollect the Breit frame analysis discussed previously in this paper. In that analysis three jets are found with a $k_\perp$ algorithm in the hadronic center of mass frame. In events were the $p_\perp$ of the event is smaller than $Q/2$, the current Breit hemisphere is investigated. This region corresponds to a cone in the hadronic center of mass frame, defined by a constraint on the rapidity measured in the current direction,

$$y > \frac{1}{2}\ln(W^2/Q^2), \tag{4.5}$$

where W^2 is the squared mass of the hadronic system.

We will now consider a very similar algorithm for e^+e^-. In an e^+e^- experiment at squared mass s, we consider an artificial scale $Q^2_{\max} < s$. Three jets are reconstructed with a $k_\perp$ cluster algorithm, and events where $p_\perp > Q_{\max}/2$ are excluded. In the accepted event sample, $Q_{\max}/2$ can be identified with the maximal allowed virtuality for a parton in the event. Thus the multiplicity depend on two scales, energy and virtuality. For $Q^2_{\max} = s$, the two scales coincide and we have an unbiased event sample.

We study the multiplicity for particles where the rapidity, measured in the thrust direction, satisfies

$$|y| > \frac{1}{2}\ln(s/Q^2_{\max}). \tag{4.6}$$

In e^+e^-, where no proton remnant is present, both the positive and negative rapidity cone is considered. These cones in the thrust direction correspond to e^+e^- hemispheres with squared invariant mass $Q^2_{\rm max}$, and their evolution with this scale can thus be studied in a fixed energy experiment. (For a more detailed discussion, see e.g. [14].)

The "thrust-cone" method presented here is designed to be as similar as possible to the Breit frame analysis. In both e^+e^- and DIS, jets reconstructed in the hadronic rest frame are used to exclude high-$p_\perp$ events. In the accepted events, the analysis is performed in rapidity cones defined by Eq (4.5) and Eq (4.6), respectively. These cones correspond in some other Lorentz frame to unbiased hemispheres, where the maximal allowed transverse momentum coincides with the hemisphere energy. (In DIS, the boost to the relevant Lorentz frame, the Breit frame, is performed explicitly.)

Two differences are present due to the absence of a t-channel probe in e^+e^-. The scale Q^2 and the direction which defines the rapidity cones are determined by the probe in DIS. In e^+e^-, the scale $Q^2_{\rm max}$ is chosen freely and the rapidity is measured along the thrust direction.

The upper limit on $p^2_\perp$ in a jet corresponds to the maximal allowed virtuality for the parton initiating the jet. Jet definitions suitable for a systematic study of the dependence upon the two separate scales, energy and virtuality, are presented in [14], and will be further discussed in the section 4.5 of this paper. In the comparison of e^+e^- results with data from the current Breit hemisphere in DIS, we are however mainly interested in quark jets where the two scales coincide. It is then sufficient to study the scale evolution using the relatively simple thrust-cone method.

In Fig 4.4 the multiplicity evolution of an e^+e^- uds sample is compared to results including all flavours and results obtained by the thrust-cone algorithm in a fixed energy uds sample. The thrust-cone multiplicities are plotted as a function of the average energy scales obtained in the cones. These scales are somewhat smaller than the chosen $Q_{\rm max}/2$, and the deviations are of order 5 to 10%.

In rare cases where an emitted gluon gives the hardest jet, the thrust will be directed along the gluon momentum. Thus the average multiplicity in the thrust-cone analysis will get some contribution from gluon jets, which have a larger multiplicity. This results in a systematic overestimation of the multiplicity, as shown in Fig 4.4.

The aim of the thrust-cone algorithm is to reproduce the scale evolution of a e^+e^- uds sample better than a sample including all flavours. As seen in Fig 4.4, this is achieved for moderate $Q_{\rm max}$, between 4 and 8 GeV. This corresponds to current Breit hemispheres in DIS with Q^2 between 15 and 60 GeV^2, which is an important range at the HERA experiments.

For $Q_{\rm max}$ larger than 8 GeV, where large $p_\perp$ gluon jets are not excluded, the

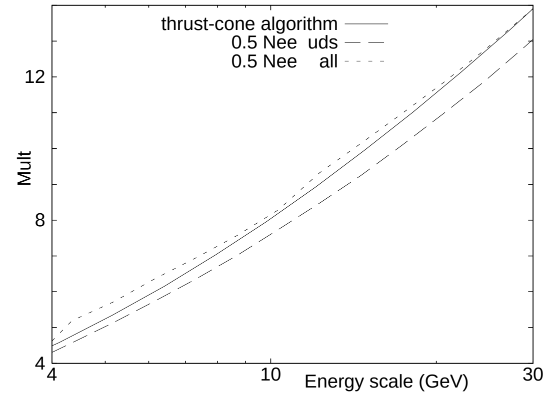

Figure 4.4: *Multiplicities in MC simulated e^+e^- events including all allowed flavours (dotted line) are higher than for light quarks events (dashed line). The multiplicity obtained by the thrust-cone algorithm in a uds sample at the* Z^0 *pole (solid line) are in better agreement with the uds result for moderate scales between 4 and 8 GeV. This corresponds to current Breit hemispheres in DIS with Q^2 between 15 and 60* GeV^2. *For larger scales the thrust-cone results differ from the uds sample in a similar way as the full flavour results.*

effect of gluon "pollution" is of the same order as the effect of the heavy quarks. However, we note that Fig 4.4 shows results from MC simulations. In a realistic experimental analysis, the thrust-cone results applied on uds events at the Z^0 peak will benefit from very large statistics compared to experiments at lower energies, and also from the fact that the scale evolution can be studied over a large range with the same detector. To conclude this section, our investigation indicates that it would be interesting to compare DIS data not only to full e^+e^- results at different s, but also with thrust-cone results in uds samples from the Z^0 experiments.

4.5 Approaching the Proton Remnant

Compared to the current Breit hemisphere, the target region in the Breit frame is theoretically much less understood. It is difficult to determine the basic dynamics (e.g. the importance of the BFKL mechanism) using only inclusive observables, like $E_\perp$-flow. In the far forward direction of the target region, results depend to a large extent on non-trivial soft properties of the remnant. This region is also more difficult to study in many experiments. E.g. at HERA, many particles are lost in the beam pipe.

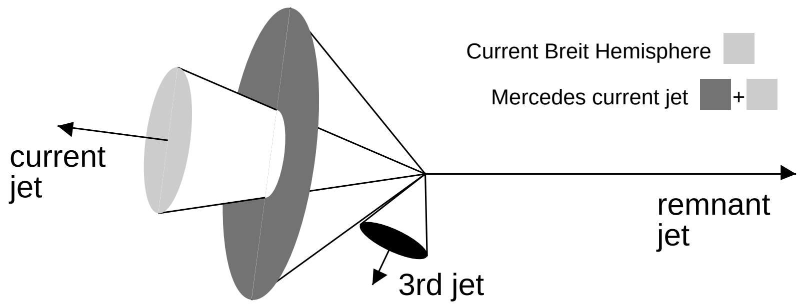

Figure 4.5: *The current Breit hemisphere roughly corresponds to a cone around the current jet in the hadronic center of mass frame (light-gray cone). With the Mercedes algorithm, a current jet region defined to cover the rapidity range up to a resolved high-$p_\perp$ jet is studied (both gray cones). In the figure the third jet lies outside the current Breit hemisphere region and the Mercedes current jet will in this example include central rapidities in the target hemisphere of the Breit frame.*

In this section we discuss two observables which examine the current and central rapidity ranges, but which nevertheless are sensitive to soft remnant effects and the dynamics of the evolution. The first observable is actually the same one that has been discussed throughout the paper, i.e. the multiplicity in the current Breit hemisphere. We will however here focus on results for very high Q^2. The rapidity distance to the remnant is then reduced, and as we will see, different models for remnant effects predict different results in this observable.

We will also propose a method to gradually extend the investigated phase space region, from the current Breit hemisphere, to also include central rapidity regions of the target hemisphere. Compared to the forward target region, this region is less dependent on soft remnant effects, but the basic mechanism for radiation is not very well known and depends to some extent on rather subtle coherence effects (cf. the "Feynman–Gribov puzzle" discussed in [15]).

We will use a jet definition, "the Mercedes algorithm" [14], with which we can construct quark jets with well-defined rapidity regions both in DIS and e^+e^-. This algorithm can be used to examine current jets in DIS, where the considered rapidity range is large enough to reach into the target hemisphere of the Breit frame, and the result can be compared to similarly defined jets in e^+e^-.

The Mercedes algorithm in DIS is applied to three-jet configurations, with a current jet, a remnant jet and a third jet. Around the current jet a cone-like region is studied, which covers rapidities up to the third resolved jet. If this is found outside the region which defines the current Breit hemisphere, as illustrated in Fig 4.5, the Mercedes current jet will probe central rapidities in the target hemisphere of the Breit frame. It will however only cover rapidities on the current side of the highest $p_\perp$ emission. This is a comparatively clean region in which relatively few dynamical mechanisms are important, as compared to more forward regions of the target hemisphere.

We will in this section start to present the Mercedes algorithm, applied e^+e^- and DIS, respectively. The scale dependences and expected properties of the Mercedes jets are then discussed. After a presentation of some different models in DIS, we finally show that Mercedes jet results, and also the current Breit hemisphere results at high Q^2, can be used to distinguish between these.

4.5.1 The Mercedes Algorithm

The starting point of the Mercedes algorithm is a three-jet configuration in e^+e^-, obtained by a $k_\perp$ cluster algorithm in the center of mass frame. The $p_\perp$ of the e^+e^- event is specified as the smallest cluster $k_\perp$-distance between the remaining jets. This implies that no emissions within the jets have higher transverse momentum, and $p_\perp^2$ can thus be identified with the maximal virtuality of a parton initiating a jet in the event.

The jets are analysed after a boost to the symmetric "Mercedes" frame, where all jet angles are $\theta' = 120°$. As the jet definition is not Lorentz invariant, such a Lorentz transformation can transfer soft particles from one jet to another. Thus the mass of a jet is not invariant. Instead the jet direction can be interpreted as the direction of a massless parton initiating the jet, which implies that it transforms as a light-like vector. (The DICLUS algorithm is a Lorentz-invariant cluster algorithm, which thus is an exception to this discussion. However, particles are not assigned to any specific jet in this algorithm, and the produced jets are explicitly massless.)

In the Mercedes frame the boundaries between the jets are determined by the bisectors between them. In [14] it is shown that when the gluon is significantly softer than the quarks, the rapidity ranges (at a lower cut-off scale Λ) for the quark jets are given by

$$y_{\mathrm{q}} \approx \frac{1}{2}\ln\left(\frac{4p_\perp^2}{\Lambda^2}\right) + \ln\left(\frac{1}{2(1-x_{\mathrm{q}})}\right). \tag{4.7}$$

The first term on the right-hand side of Eq (4.7) is the rapidity range in the forward region of the jet where $2y > \ln(s/4p_\perp^2)$, which corresponds to an unbiased hemisphere of an event with squared invariant mass equal to $4p_\perp^2$ (cf. Eq (4.6)). The second term is the extra rapidity range included in the Mercedes quark jet. In this range the maximal allowed transverse momentum is $p_\perp$.

Thus the jet properties depend on two independent scales. The virtuality scale $p_\perp$ determines the size of the first range and the maximal allowed transverse momentum in the second, while the energy sets the size of the second range. This is not a unique feature of the Mercedes jet, all jets can in general be subdivided into two regions in a similar way, and thus depend on two scales. When looking at a forward cone, so that the second term vanishes, the two scales coincide. The cone then corresponds to an unbiased e^+e^- hemisphere. In the region corresponding to the second term in Eq (4.7), where the maximal transverse momentum is constant, the emission density in an e^+e^- jet is essentially flat in rapidity. This implies that the multiplicity in the jet is expected to grow linearly with the allowed rapidity range, for fixed virtualities.

When applying the Mercedes algorithm to DIS events, we will use the Durham $k_\perp$ cluster algorithm in the hadronic center of mass frame, in order to resemble the corresponding e^+e^- analysis. Three jets are reconstructed, and the smallest remaining $k_\perp$-distance between these specifies the $p_\perp$ of the event. The current jet is tagged as the one with smallest polar angle to the probe direction, and is analyzed in the Mercedes frame. The considered rapidity range for the current jet is then given by Eq (4.7), with x_q being the scaled energy $2E_\mathrm{q}/W$ of the outgoing struck quark in the hadronic center of mass frame.

The Mercedes current jet can reach into the target region of the Breit frame. The rapidity range for the current Breit hemisphere (the light-gray cone in Fig 4.5) is $\ln(Q/\Lambda)$. Eq (4.7) implies that the Mercedes current jet in DIS will cover a region which extends into the target hemisphere of the Breit frame (the dark-gray cone in Fig 4.5) when $p_\perp > Q(1 - x_\mathrm{q})$.

As for the e^+e^- case, the properties of the Mercedes current jet in DIS depends both on its energy and its virtuality. It may, however, also depend on the DIS scales x and Q^2. These scale dependences can be investigated for a set of observables. E.g., the Mercedes jet properties in events where $p_\perp > Q$ could be used to investigate the mechanisms behind resolved photon events [16]. It is also possible to investigate different rapidity intervals in the Mercedes current jet separately.

Here we will investigate whether the Mercedes jet can be used to distinguish between different models in DIS. It is then sufficient to study the simplest possible observable, the average multiplicity in the whole jet. We will compare the rapidity range dependence of the average multiplicity in the DIS current jet and e^+e^- quark jets, keeping the virtuality scale fixed. We note that when Q is smaller than $p_\perp$, a significant Q^2 dependence could be expected for the current jet in DIS. For the jets in the two experiments to be similar, we therefore exclude DIS events where $p_\perp > Q/2$. In the remaining event sample, we study the inclusive results, integrated over Q^2 and x.

4.5.2 Models

To demonstrate that the proposed observable can distinguish between different production mechanisms, we study some different models and see that they indeed give different results. We have chosen two versions of the LEPTO MC [10], based on a DGLAP parton evolution, and two versions of the ARIADNE MC [9], implementing the soft radiation model [17] with boson-gluon fusion included. All the chosen models uses the Lund string fragmentation to describe hadronization. The models however differ in the treatment of parton evolution and proton remnant effects.

In the LEPTO MC, a parton shower based on the DGLAP evolution equation is implemented. This implies that parton emissions are strongly ordered in rapidity and transverse momentum. A ladder diagram describing a DIS event specifies a colour ordering for the emissions, which due to colour coherence also specifies the order in rapidity. For large Q^2, the leading order contribution to the cross section is given by diagrams where the transverse momenta are strongly ordered, so that the parton closest in rapidity to the remnant has the smallest $p_\perp$, and the parton closest to the quark interacting with the probe the largest. It is diagrams with this ordering in transverse momentum that are considered in the DGLAP evolution.

A model for soft colour interaction [18] (SCI) is supplied in the LEPTO MC. In this model, the proton remnant may interact with the perturbatively produced partons by exchanging soft colour quanta. These have negligible effect on the parton momenta, but alter the colour flow of the parton configuration. This implies that a $q\overline{q}$ pair produced in a boson-gluon fusion event may change its colour state from an octet to a singlet. This introduces a rapidity gap in the colour flow from the current to the remnant. In cluster and string fragmentation models the colour topology determines the phase space for hadron production, and thus the same rapidity gap manifests itself in the hadronic final state. This is a way to model diffractive DIS events, alternative to the Pomeron approach.

Another possible consequence of SCI is that the colour flow is enlarged, thus producing more hadrons. This increases the $E_\perp$-flow in a way which is consistent with data [18].

In the default version of the ARIADNE MC, the radiation in DIS is expressed in terms of a dipole spanned from the struck quark to the remnant. The emitted partons are not necessarily ordered in $k_\perp$ and rapidity as in the DGLAP case, but the fact that the remnant is an extended object, and not point-like, gives rise to a suppression of high-$p_\perp$ emissions in the remnant direction. Though this model is rather different from the DGLAP formalism, the radiation from the struck quark in the current region is treated similarly in the two Monte Carlos.

The suppression of high-$p_\perp$ emissions, in the way it is modeled in ARIADNE, may reach into the current Breit hemisphere when Q^2 is very high. It could

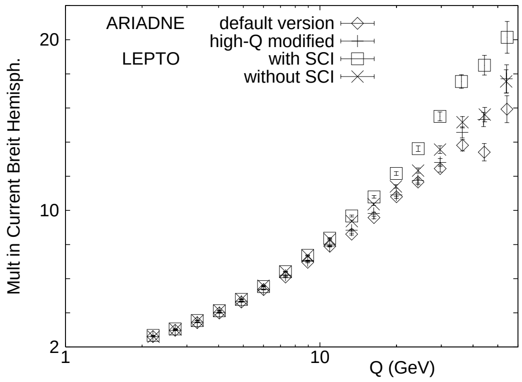

Figure 4.6: *Different model predictions for the multiplicity in the current Breit hemisphere. In the* ARIADNE *default version the remnant suppression of high-$p_\perp$ emissions can reach into the current Breit hemisphere in events with high Q^2. This implies a lower multiplicity. In the* LEPTO *MC with soft colour interaction, where the hadronization phase space in terms of a colour string can be enlarged, the multiplicities lie above the others.*

however be argued that the suppression in this case is overestimated, since the maximal allowed virtuality for the struck quark then is lower than Q^2. A modification has therefore been developed, where the unsuppressed phase space is enlarged in high Q^2 events, to always include the expected region for final state emissions from the struck quark [19].

4.5.3 Results

We will here study the prediction of different MC simulation models on two observables, the multiplicity in the current Breit hemisphere at high Q^2 and the current jet multiplicity obtained by the Mercedes algorithm.

In Fig 4.6, the prediction for the multiplicities in the current Breit hemisphere are shown, using different models. At very high Q^2, the rapidity distance to the remnant is reduced, and different assumptions about remnant effects give different predictions .

The differences can be understood from the remnant treatments of the models. The ARIADNE default version, where the remnant suppression of high-$p_\perp$ emissions can reach into the current Breit hemisphere for very large Q, predicts a lower multiplicity than the other models. The prediction from LEPTO with soft colour interactions (SCI) lies above the others. SCI can give rise both to rapidity gaps and an extended colour flow, which increases the hadron

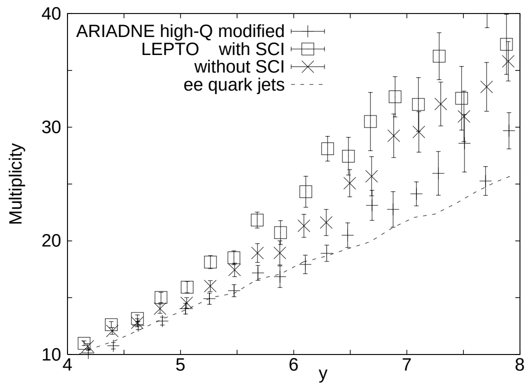

Figure 4.7: *MC results on the multiplicity in DIS current jets and e^+e^- quark jets using the Mercedes algorithm, as a function of the rapidity range in Eq (4.7). The transverse momentum scale is constrained to 3 GeV $< p_\perp <$ 3.6 GeV.*

multiplicity. The results here indicates that the latter effect dominates in the current rapidity region.

The Lepto MC without SCI and the high-Q modified Ariadne MC differ mainly in the evolution of the parton distributions. In Lepto the evolution is based on the DGLAP equation, while the Ariadne MC implements a soft radiation model based on colour dipoles. The properties of the current Breit hemisphere are expected to be essentially independent of the form of the parton distribution evolution. The two MC results are similar at very high Q^2, in agreement with this expectation.

The MC result for an e^+e^- uds sample (not shown) agrees well with the high-Q modified Ariadne and Lepto without SCI. Whether this agreement between e^+e^- and DIS results with similar flavour compositions holds also for experimental data is however not fully investigated yet. The differences between the results in Fig 4.6 show that the high-Q^2 Breit frame analysis can be used to discriminate between different models.

Fig 4.7 shows the Mercedes algorithm multiplicity of the current jet in DIS and quark jets in e^+e^-, as a function of the available rapidity range y. The transverse momentum is constrained to the range 3GeV$< p_\perp <$3.6GeV and DIS events with $Q/2 < p_\perp$ are excluded from the analysis. We have investigated the results for a rather low $p_\perp$, in order to make the analysis complementary to the high-Q^2 analysis shown in Fig 4.6. The multiplicity of the e^+e^- jets rise fairly linearly with y, as expected. For low values of y the examined region lies within the current Breit hemisphere, and the DIS results are similar to the

e^+e^- result.

Ideally, all jets correspond to a perturbative gluon emission, with similar $p_\perp$. However, "junk jets" may be formed, where hadrons which happen to be close in phase space are merged into a resolved jet, even though no corresponding gluon was emitted. These "junk jets" are more easily formed when the multiplicity is high. Thus their presence in the considered event sample increases the average multiplicity. If the probability to emit gluons giving rise to "proper" jets is reduced, the fraction of junk jet events in the accepted sample increases, and their effect on the result gets more prominent. The results for Mercedes jets with large rapidity ranges are based on events where one jet is found in the target region. There the probability for gluon emission is smaller than in a corresponding region in e^+e^-, and in Fig 4.7 the junk jet contribution is seen as a larger multiplicity for DIS Mercedes jets with large rapidity ranges.

The probability for jet-generating gluons in the target region differ in the considered DIS models, being lower for the DGLAP based Lepto MC than the dipole based Ariadne MC. Thus the high-Q modified Ariadne MC and the Lepto MC without SCI, which give very similar results in the high-Q^2 Breit frame analysis of Fig 4.6, differ in the Mercedes algorithm results in Fig 4.7. This result suggests that properties of the parton evolution, such as $p_\perp$ ordering, can be examined using the Mercedes algorithm for jet analyses.

4.6 Summary

The assumption of quark fragmentation universality implies that the current Breit hemisphere in DIS is expected to be very similar to a hemisphere in e^+e^- annihilation. However, the experimental situations are different, and several corrections to universality are present. We have here proposed event cuts to improve the expected validity of quark fragmentation universality. DIS events with high-$p_\perp$ emissions, which have no correspondence in e^+e^- events, are excluded, where the $p_\perp$-scale is reconstructed using jet cluster algorithms.

The effects of the cuts have been investigated using MC simulations, and the agreement between e^+e^- and Breit frame results is shown to improve. The results after a cut in jet $p_\perp$ may depend on the choice of cluster algorithm. We have investigated three different types of $k_\perp$ cluster schemes, and find our results to be algorithm independent.

In the accepted low-$p_\perp$ DIS sample, heavy quarks are suppressed. This motivates a comparison with uds enriched e^+e^- data, which are available from the experiments at the Z^0 pole, but not at lower energies. We have here presented a method, the "thrust-cone algorithm", to study scale evolutions of e^+e^- quark hemispheres, using data from fixed energy experiments. With this algorithm, uds enriched data with high statistics from the LEP1 experiments can be compared to results for the current Breit hemisphere, over a large range of energies.

At high Q^2, the rapidity distance from the current Breit hemisphere to the remnant end is reduced. By comparing results from different MC programs, we find that the multiplicity in the current Breit hemisphere at very high Q^2 can be used to distinguish between different assumptions of remnant effects.

We also propose an observable which more directly investigates the properties of the target region. A current jet is defined with the “Mercedes” algorithm [14]. The Mercedes current jet probes central rapidity regions in the Breit frame, but always stays on the current side of the highest $p_\perp$ emission of the event. This is a comparatively clean region, as compared to the forward target region. A corresponding jet definition can be studied in e^+e^- experiments, which enables a comparison between the processes, and could facilitate the interpretation of the results. The properties of the Mercedes current jet is shown to be sensitive both to remnant effects and mechanisms behind the parton evolution, and can be used to discriminate between different existing models.

Acknowledgments

I want to thank Leif Lönnblad and Gösta Gustafson for their significant contributions to this investigation.

This work was supported in part by the EU Fourth Framework Programme ‘Training and Mobility of Researchers’, Network ‘Quantum Chromodynamics and the Deep Structure of Elementary Particles’, contract FMRX-CT98-0194 (DG 12 - MIHT).

References

[1] K.H. Streng, T.F. Walsh, P.M. Zerwas, *Z. Phys.* **C2** (1979) 237

[2] ZEUS collaboration, *Z. Phys.* **C67** (1995) 93;
ZEUS collaboration, *Phys. Lett.* **B414** (1997) 428;
H1 collaboration, *Nucl. Phys.* **B504** (1997) 3

[3] ZEUS preliminary results, contributed paper 809, ICHEP’98, Vancouver

[4] Yu.L. Dokshitser, G.D. Leder, S. Moretti and B.R. Webber, *JHEP* **08** (1997) 001;
For a review, see L. Lönnblad, S. Moretti, T. Sjöstrand, *JHEP* **08** (1998) 001

[5] S. Catani, Yu.L. Dokshitser, B.R. Webber, *Phys. Lett.* **B285** (1992) 291

[6] M. Bengtsson, T. Sjöstrand, *Comp. Phys. Comm.* **39** (1986) 347; T. Sjöstrand, *Comp. Phys. Comm.* **82** (1994) 74

[7] S. Catani, Yu.L. Dokshitser, M. Olsson, G. Turnock and B.R. Webber, *Phys. Lett.* **B269** (1991) 432

[8] L. Lönnblad, *Z. Phys.* **C58** (1993) 471

[9] L. Lönnblad, *Comp. Phys. Comm.* **71** (1992) 15

[10] G. Ingelman, A. Edin, J. Rathsman, *Comp.Phys.Comm.* **101** (1997) 108

[11] G. Gustafson, *Phys. Lett.* **B175** (1986) 453; G. Gustafson, U. Pettersson, *Nucl. Phys.* **B306** (1988) 746; B. Andersson, G. Gustafson, L. Lönnblad, *Nucl. Phys.* **B339** (1990) 393

[12] B. Andersson, G. Gustafson, G. Ingelman, T. Sjöstrand, *Phys. Rep.* **97** (1983) 31

[13] H1 Collaboration, *Z.Phys* **C72** (1996) 593 H1 preliminary results, contributed paper 540, ICHEP'98, Vancouver; ZEUS preliminary results, contributed paper 768, ICHEP'98, Vancouver

[14] P. Edén, G. Gustafson, *JHEP* **09** (1998) 015

[15] Yu.L. Dokshitser, V.A. Khoze, A.H. Mueller and S.I. Troyan, Basics of Perturbative QCD, (*Editions Frontières, Gif-sur-Yvette, 1991*), p. 107-109

[16] H. Jung, L. Jönsson, H. Kuster, DESY preprint 98-051, hep-ph/9805396 v2

[17] B. Andersson, G. Gustafson, L. Lönnblad, U. Pettersson, *Z. Phys.* **C43** (1989) 625

[18] G. Ingelman, A. Edin, J. Rathsman, *Phys. Lett.* **B366** (1996) 371

[19] L. Lönnblad, private communications, version of ARIADNE to appear in future release.

Energy and Virtuality Scale Dependence in Quark and Gluon Jets

Paper V

Energy and Virtuality Scale Dependence in Quark and Gluon Jets

Patrik Edén, Gösta Gustafson
Department of Theoretical Physics
Lund University

We discuss some important issues concerning multiplicities in quark and gluon jets in e^+e^- annihilation. In QCD the properties of a jet in general depends on two scales, the energy and virtuality of the jet. Frequently theoretical predictions apply to a situation where these scales coincide, while for experimental data they are often different. Thus an analysis to extract e.g. the asymptotic multiplicity ratio $C_\mathrm{F}/C_\mathrm{A}$ between quark and gluon jets, needs a carefully specified jet definition, together with a calculation of nonleading corrections to the multiplicity evolution.

We propose methods to systematically study the separate dependence upon the two scales in experimental data and compare the results with theory. We present jet finding algorithms which correspond well to the theoretically considered jets. We also show that recoil effects add corrections to the modified leading log approximation which are quantitatively important, though formally suppressed at high energies.

5.1 Introduction

QCD predictions on the scale dependence of multiplicities in high energy $q\overline{q}$ systems are experimentally well confirmed [1]. A similar multiplicity behaviour is to be expected from high energy gluon jets, the major difference being the different colour charges of gluons and quarks. In this paper we want to address a set of problems which have to be carefully treated for a quantitative analysis of jet properties:

- At experimentally accessible energies subleading effects are quantitatively important.
- The jet properties depend in general on two scales, the energy of the jet and its virtuality, specified by the largest possible transverse momentum of one of its subjets. Theoretical calculations frequently refer to a situation where the two scales coincide, while in experimental analyses the two scales are often different.
- In contrast to the topology of an event, which is mostly determined by a few energetic particles, the multiplicities in jets are sensitive to how the softer particles are associated to different jets.

As will be discussed in this paper, the multiplicity of hadrons depends not only on the properties of the perturbative parton cascade, but also on the soft hadronization process. The assumption of Local Parton Hadron Duality (LPHD) [2] implies a direct relation between the number of hadrons and the number of partons, provided a proper, locally invariant, cut-off is imposed on the parton cascade. The asymptotic behaviour of the multiplicity in jets was calculated in the leading log approximation in [3]. In the modified leading log approximation (MLLA), subleading terms in the evolution equations of relative magnitude $1/\sqrt{\ln s}$ are included [4, 5]. With arguments based on "preconfinement" [6] and LPHD we demonstrate in this paper that an important correction factor is expected due to recoil effects. Although formally suppressed by a factor $1/\ln s$, this effect is quantitatively large and has an essential impact on the ratio between quark and gluon jets at accessible energies.

Many jet finding algorithms have been presented for the study of e^+e^- annihilation events [7]. Several of these have been successfully used in comparisons between data and theory for properties like the distribution in the number of jets, and how this varies with the resolution scale. We want to stress that our problem is a different one, as described in the third point above, and it will be important to specifically consider the treatment of soft particles in the analysis.

The angular ordering effect in QCD [8] implies that soft particles at large angles are emitted coherently from harder particles which they cannot resolve. Strictly speaking, these soft particles do not belong to any specific jet, and the colour factor for the emission is determined by the colour state of the combined unresolved partons. In ref [9] a method (the "CAMBRIDGE" algorithm) is proposed to associate the above-mentioned soft particles with the quark (or antiquark) jet, leaving to the gluon jet only those particles directly associated with the emitted gluon and the gluon colour charge. In this paper we study this question further and propose some modified cluster algorithms.

If we study two-jet events obtained in e^+e^- annihilation using a jet finding algorithm with a distance measure of $k_\perp$-type, the jet properties (e.g. the hadron multiplicity) depend not only on the jet energy but also on the $k_\perp$-cut used. For minimum bias events, one hemisphere corresponds to a quark jet where these two scales are the same (an "unbiased quark jet"). Similarly the multiplicity of an unbiased gluon jet corresponds to one half of an imagined gg system stemming from a point source. In section 5.5 we will discuss how this quantity is related to a gluon jet in a $\mathrm{q\overline{q}g}$ event. We will also present methods by which both of the jet scales can be systematically examined, as well as methods designed to define unbiased jets, where the two scales coincide.

Some experimental results of relevance for this paper have already been presented. In [10, 11], the hemisphere opposite to two quasi-collinear heavy quark jets in e^+e^- events is analyzed. This corresponds well to an unbiased gluon jet, with $E_\mathrm{g} \approx \sqrt{s}/2$. In [12] the energy scale dependence of quark and gluon jets is studied. There a fixed resolution scale is used in the cluster algorithm, which implies that the virtuality scale is held constant. In this paper, we discuss how to systematically study both scales in a jet. We also present methods to construct unbiased quark and gluon jets in a general three-jet topology, which enables a study of the scale evolution of unbiased jets.

In our analysis we will for convenience work in the Colour Dipole Model (CDM) [13], which provides a geometric picture which is easily interpreted. The outline of this paper is as follows: In section 5.2 we discuss preconfinement and LPHD. In section 5.3 we discuss the CDM and the multiplicity distributions, including corrections relevant to the MLLA approximation, as presented in [14]. In section 5.4 we discuss recoil corrections to the multiplicity evolution. In section 5.5 and 5.6 we discuss the two different scale dependences of multiplicities in jets and present cluster algorithms designed to extract these from data. In section 5.7 we present results obtained by MC simulations. The results are discussed in section 5.8.

5.2 Preconfinement and Local Parton Hadron Duality

It is essential to realize that the hadronic multiplicity cannot be determined from perturbative QCD alone. From perturbative QCD it is possible to cal-

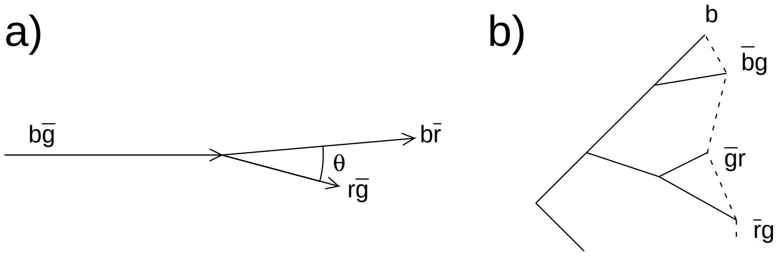

Figure 5.1: **a)** *After a $g \to gg$ emission with a small angle θ, there is a screening of the new colour charges* (r$\bar{r}$ *in the picture). This implies that they give no net contribution to the emissions of soft gluons at polar angles larger that θ (the angular ordering effect). Their contribution to the emission at smaller angles corresponds to normal dipole emission in the* r$\bar{r}$ *back-to-back frame.* **b)** *After a gluon cascade, further emissions of soft gluons corresponds to a set of independently emitting dipoles.*

culate the parton multiplicity within a given phase space region. As the parton multiplicity diverges for collinear and soft emissions, some kind of cut-off is needed in order to find a quantity which is correlated to the hadronic multiplicity. The nature of this cut-off depends on the properties of the soft hadronization mechanism, and is therefore not calculable within perturbative theory.

The parton cascades are dominated by planar diagrams [15] (to leading log level in an axial gauge). This implies that every colour charge after a cascade has a well defined partner anti-charge. As shown by Amati and Veneziano [6], the final parton state can be subdivided in colour singlet clusters, whose masses stay limited also when the total energy becomes very large. In [16], Marchesini, Trentadue and Veneziano showed that these "preconfinement" clusters are limited not only in momentum space but also in real space-time. At least in the large N_c limit it is then natural to assume that the clusters hadronize independently from the rest of the system. This means that the nonperturbative confinement mechanism is *local* in the sense that it combines partons which are directly colour connected and that it acts only locally also in momentum space.

This idea is further developed in the notion of Local Parton Hadron Duality (LPHD), proposed by the Leningrad group [2]. Here a direct relation is assumed between partons and hadrons, which is *local* in phase space, which means that the dominant features of hadron distributions can be obtained from the parton cascades with an appropriate cut-off which is locally invariant.

A very essential feature of the QCD cascade is "soft gluon interference" and "angular ordering" [8]. Study e.g. a b$\bar{g}$ gluon emitting a r$\bar{g}$ gluon thereby changing its own colour to b$\bar{r}$ in a Lorentz frame where θ is small (see Fig 5.1a).

In this case the red and antired charges screen each other in such a way that they do not give any emissions in directions with polar angles larger than θ, the angle of the first emission. For these larger angles the two gluons emit softer gluons coherently as a single $\mathrm{b\overline{g}}$ gluon, while for smaller angles the two gluons emit essentially independently. (For emission angles close to θ there is some azimuthal asymmetry.) This implies that in a frame where the red and antired charges move back-to-back, their contribution to the emission of softer gluons is just the normal emission from a separating charge-anticharge pair.

The soft gluon interference (angular ordering) and a local cut-off are incorporated in the Marchesini-Webber formalism for the parton cascade [17]. This formalism is implemented in the HERWIG Monte Carlo [18, 19]. In [18] it is also shown that a locally invariant cut-off in the parton virtuality is essentially equivalent to a cut-off in transverse momentum relative to the emitting parent parton, if this is measured in a Lorentz frame where the parton energies are large and the angles small. The HERWIG MC also contains a cluster fragmentation model with local properties. In this model the gluons are at the cut-off level split into $\mathrm{q\overline{q}}$ pairs, which are combined to colourless clusters, which finally decay into hadrons.

A cut-off in $k_\perp$ measured in the fast-moving (small angle) frame is approximately equivalent to a cut-off with the same $k_{\perp\mathrm{cut}}$ in the rest frame of the emitting charge-anticharge pair. In this "dipole rest frame" the emission is proportional to $\frac{\mathrm{d}k_\perp}{k_\perp}\mathrm{d}y$, which for a given $k_\perp$ means a smooth rapidity distribution within the kinematically allowed region

$$|y| < \frac{1}{2}\ln(\hat{s}/k_\perp^2), \tag{5.1}$$

where $\hat{s}$ is the squared mass of the dipole. This phase space corresponds in the fastmoving frame just to the region allowed by angular ordering. We see e.g. that for given $k_\perp$, the rapidity range in the two jets is given by (for small angles θ)

$$\begin{aligned}\Delta y_1 + \Delta y_2 &= \Big[\ln(2p_1/k_\perp) - \ln(\cot\theta/2)\Big] + \Big[\ln(2p_2/k_\perp) - \ln(\cot\theta/2)\Big] \approx \\ &\approx \ln(2p_1p_2(1-\cos\theta)/k_\perp^2) = \ln(\hat{s}/k_\perp^2),\end{aligned} \tag{5.2}$$

i.e. exactly the same result as in the dipole rest frame. Thus in a gluonic cascade as in Fig 5.1b the emission of softer gluons corresponds to a set of independent "dipole emissions". A locally invariant cut-off is obtained by a $k_{\perp\mathrm{cut}}$ in the individual dipole rest frames. This is the basis of the Lund Colour Dipole Model [13], which is discussed in more detail in the following section.

The local feature of the hadronization mechanism is also inherent in the Lund string fragmentation model [20]. Here the hadrons which originate from the colour field stretched between a colour charge and its associated anticharge is independent of what happens further away in the system, with a correlation length corresponding to a few hadron masses [21]. In ref [22] a measure, called λ, is proposed, which in the string fragmentation model is strongly correlated to the hadron multiplicity. With a local cut-off for the cascade, the λ-measure is also strongly correlated to the parton multiplicity [23]. We note that in both cluster and string fragmentation there is a connection between a colour charge and its associated anticharge. Thus, although the parton and hadron distributions are strongly correlated, they are not exactly identical.

The colour coherence and the local properties of the hadronization process are fundamental features of the models implemented in the MC simulation programs HERWIG [19], ARIADNE [24] and JETSET/PYTHIA [25]. The great phenomenological success for these programs in describing experimental data, in particular for e^+e^--annihilation, is a strong support for the local features of the hadronization mechanisms expressed in preconfinement and LPHD. We note also that the independent jet fragmentation model, which does not have this feature, has not been able to describe the data in a satisfactory way.

In spite of the phenomenological success mentioned above, there are still fundamental open questions concerning the hadronization mechanism. In the large N_c limit there is a unique way to connect the partons as in Fig 5.1b. This is, however, not the case when $N_\mathrm{c} = 3$. If two gluons have identical colours the confinement mechanism may connect partons which are not directly connected in the cascade generated by the simulation program. These "colour reconnection" effects are suppressed by $1/N_\mathrm{c}^2$, and some possible consequences are discussed in [26, 27, 28]. No effects have, however, been observed so far in experimental data [11]. Closely related to this problem is the possibility of colour reconnection between partons from the decay of different W:s in a W^+W^- pair at LEP2 [28, 29]. This is of special interest as it might affect the W mass determination, but also here no statistically significant effects have yet been found, e.g. in form of different decay multiplicity or modified Bose-Einstein correlations [30].

In perturbation theory it is possible to calculate the *parton* multiplicity within a given region of phase space. The conclusion of this section is that this is not the whole story if we want to calculate the multiplicity of *hadrons*. The hadronization effects of a parton containing e.g. a red colour charge depends upon where in phase space its partner antired charge is located, and this dependence is determined by the soft hadronization mechanism. An effective cut-off depends on the local properties of a jet and cannot be determined as a fixed phase space region valid for the whole jet. In [31] Gaffney and Mueller calculate the ratio of the parton multiplicity in quark and gluon jets within a fixed narrow cone, including correction terms of order $\alpha_\mathrm{s}(Q^2)$ (or $\mathcal{O}(1/\ln Q^2)$). In section 5.4 we show that, assuming a local hadronization mechanism based on preconfinement and LPHD, we expect a further correction term which, although suppressed by a factor $1/\ln Q^2$, is numerically important.

5.3 The Colour Dipole Model

5.3.1 The Dipole Cascade

A high energy $\mathrm{q\overline{q}}$ system radiates gluons with the distribution

$$\mathrm{d}n = C_{\mathrm{F}} \frac{\alpha_{\mathrm{s}}}{2\pi} \mathrm{d}x_1 \mathrm{d}x_3 \frac{x_1^2 + x_3^2}{(1-x_1)(1-x_3)}, \tag{5.3}$$

where x_1 and x_3 are the scaled quark and antiquark momenta, and $C_{\mathrm{F}} = \frac{1}{2}N_{\mathrm{c}}(1 - 1/N_{\mathrm{c}}^2)$. With the definitions

$$\begin{aligned}
\alpha_0 &= \frac{6}{11 - 2N_{\mathrm{f}}/N_{\mathrm{c}}}, & \alpha_{\mathrm{q}} &= \alpha_0 \left(1 - \frac{1}{N_{\mathrm{c}}^2}\right), \\
k_\perp^2 &= s(1-x_1)(1-x_3), & y &= \frac{1}{2}\ln\left(\frac{1-x_3}{1-x_1}\right), \\
\kappa &= \ln(k_\perp^2/\Lambda^2), & \frac{N_{\mathrm{c}}\alpha_{\mathrm{s}}(k_\perp^2)}{2\pi} &= \frac{\alpha_0}{\kappa},
\end{aligned} \tag{5.4}$$

this distribution can be written

$$\mathrm{d}n = \frac{\alpha_{\mathrm{q}}}{\kappa} \mathrm{d}\kappa \mathrm{d}y \frac{x_1^2 + x_3^2}{2} \approx \frac{\alpha_{\mathrm{q}}}{\kappa} \mathrm{d}\kappa \mathrm{d}y, \tag{5.5}$$

where the last approximation holds for soft gluons.

The kinematical constraint $k_\perp < \sqrt{s}/(2\cosh y) \approx \sqrt{s}\exp(-|y|)$ implies that $\kappa + 2|y| < L$, where L is given by

$$L = \ln(s/\Lambda^2). \tag{5.6}$$

Thus the allowed phase space for gluon emission is approximately a triangular region in the κ, y-plane, cf. Fig 5.2a. After the emission of a gluon at κ_1, y_1, the distribution for emissions of softer gluons corresponds to two independently emitting dipoles, one between the quark and the gluon, the other between the gluon and the antiquark. The available rapidity range for a gluon at $\kappa_2 < \kappa_1$ is then $\ln(s_{\mathrm{qg}}/k_{\perp 2}^2) + \ln(s_{\mathrm{g\overline{q}}}/k_{\perp 2}^2) = L + \kappa_1 - 2\kappa_2$. Thus the phase space for further emissions can be represented by a folded surface as in Fig 5.2b. This can be generalized for several emissions and a multi-gluon event corresponds to a picture with many folds and sub-folds as in Fig 5.2c.

In this language an initial gg system corresponds to two dipoles. If the gluons are e.g. $\mathrm{r\overline{g}}$ and $\mathrm{g\overline{r}}$, we have a $\mathrm{r\overline{r}}$ and a $\mathrm{g\overline{g}}$ dipole as illustrated in Fig 5.3a. If one of these dipoles emits a gluon, the emission of softer gluons corresponds

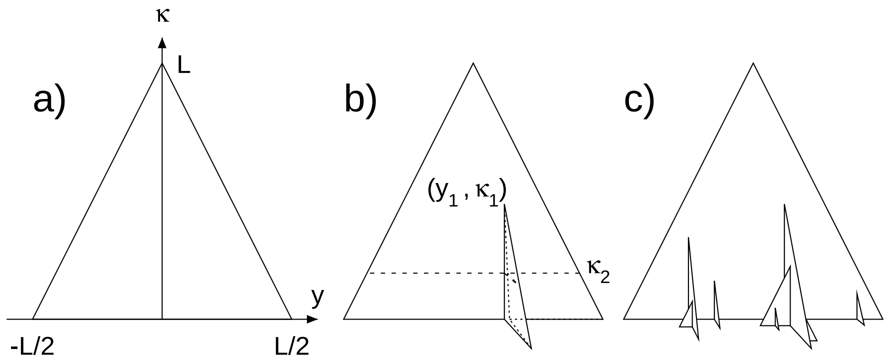

Figure 5.2: **a)** *The phase space for a gluon emitted from a* q$\overline{\text{q}}$ *dipole is a triangular region in the (y,κ)-plane (*$\kappa = \ln k_\perp^2/\Lambda^2$*,* $L = \ln s/\Lambda^2$*).* **b)** *After one emission at* (y_1, κ_1)*, the phase space for a second (softer) gluon is represented by this folded surface.* **c)** *Each emitted gluon increases the phase space for softer gluons. The total gluonic phase space corresponds to this multifaceted surface. The hadron multiplicity measure,* $\lambda(L)$*, is given by the length of the baseline.*

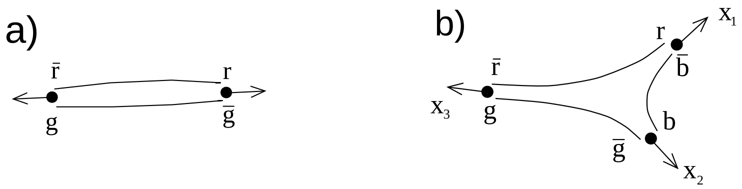

Figure 5.3: **a)** *An original two-gluon system corresponds to two colour dipoles.* **b)** *After one emission, the emission of softer gluons (with lower* $k_\perp$*) corresponds to three dipoles.*

to three dipoles, as illustrated in Fig 5.3b, and after n emissions we get a closed chain of $n+2$ dipoles. The phase space of an original gg system corresponds to two triangular regions as in Fig 5.2a, glued together along the outer diagonal lines.

The emission from a dipole stretched between two gluons is however not exactly the same as from a dipole stretched between a quark and an antiquark. For a gg dipole the emission can in analogy to Eq (5.3) be described by the distribution [13]

$$\mathrm{d}n = \frac{N_\mathrm{c}}{2}\frac{\alpha_\mathrm{s}}{2\pi}\mathrm{d}x_1\mathrm{d}x_3\frac{x_1^3 + x_3^3}{(1-x_1)(1-x_3)}. \tag{5.7}$$

For soft and collinear emissions this goes over into the standard g→gg splitting

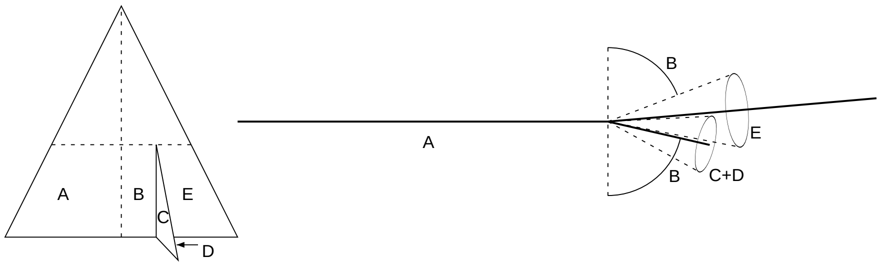

Figure 5.4: *After one gluon emission, the different regions in the folded κ-y phase space approximately corresponds to the angular regions shown in the right figure. The angular directions in which the gluon and (anti)quark emits coherently approximately corresponds to region B, and the emission density there is proportional to C_F. Corrections to these region identifications are discussed in section 5.6.2.*

function [13]. For soft emissions we have $x_1^3 + x_3^3 \approx 2$, which implies

$$\mathrm{d}n \approx \frac{\alpha_0}{\kappa}\mathrm{d}\kappa\mathrm{d}y. \tag{5.8}$$

This result agrees with the soft emission from a $q\overline{q}$ dipole in Eq (5.3) apart from the colour suppressed difference between α_q and α_0, i.e. between C_F and $N_c/2$.

After the first emission in a $q\overline{q}$ dipole, the different phase space regions for further emissions can be associated to different angular regions. Region A of Fig 5.4 roughly corresponds to emissions with negative rapidity in the overall CMS-frame, and region B to particles with positive rapidity and a larger angle to the $q\overline{q}$ direction than the first gluon. Emissions from region E have larger rapidity (smaller angle) than the first gluon. This is also the case for region $C + D$, with the rapidity measured in the gluon direction. The first emitted gluon and the (anti)quark will radiate coherently with the colour charge of the parent (anti)quark in region B. This argument can be generalized to a situation with several gluon emissions. For a cascade strongly ordered in $k_\perp$, this implies that the colour factor is C_F in the original $q\overline{q}$ phase space triangle and $N_c/2$ on all extra folds. The identification of regions presented in Fig 5.4 is however only approximately true and we will in section 5.6.2 study the corrections and their consequences in more detail.

5.3.2 Multiplicity Distributions

Assuming LPHD, the hadron multiplicity N^h is closely related with the parton multiplicity n^p. We will here briefly describe how the parton distribution $P(n =$

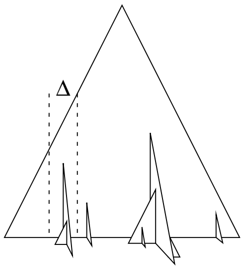

Figure 5.5: *The distribution P can be subdivided into distributions for different rapidity intervals Δ.*

$n^p, L = \ln(s)$) is derived in the dipole formulation [13], in order to more easily discuss the effects of recoil corrections in the next section. To find the parton distribution $P(n, L)$, we first look at the distribution $P_\Delta(n)$ in a small rapidity interval Δ, cf. Fig 5.5. The Laplace transform

$$\mathcal{P}_\Delta(\gamma) \equiv \sum_n \exp(-\gamma n) P_\Delta(n) \tag{5.9}$$

has the property $\mathcal{P}_{\Delta_1+\Delta_2} = \mathcal{P}_{\Delta_1}\mathcal{P}_{\Delta_2}$. Thus

$$\ln\mathcal{P}(\gamma, L) = \sum_i \ln\mathcal{P}_{\Delta_i}(\gamma). \tag{5.10}$$

$P_\Delta(n)$ depends both on the width and the height of the interval Δ. We denote the phase space height at rapidity y by $l(|y|)$ and define

$$R(\gamma, l) \equiv \lim_{\Delta\to 0} \frac{\ln\mathcal{P}_\Delta(\gamma)}{\Delta}. \tag{5.11}$$

Eq (5.10) can then be written

$$\ln\mathcal{P}(\gamma, L) = \int_{-y_{\max}}^{y_{\max}} \mathrm{d}y R(\gamma, l(|y|)) = 2\int_{\kappa_c}^{L} \mathrm{d}l R(\gamma, l) \left|\frac{\mathrm{d}y}{\mathrm{d}l}\right|. \tag{5.12}$$

In [22], it is shown that R also is related to $\mathcal{P}$ by

$$\frac{\mathrm{d}}{\mathrm{d}L} R^{(i)}(\gamma, L) = \frac{\alpha_i}{L}\left[\mathcal{P}^{(\mathrm{g})}(\gamma, L) - 1\right], \quad i = \mathrm{q}, \mathrm{g}, \quad \alpha_{\mathrm{g}} = \alpha_0. \tag{5.13}$$

The boundary condition at some cut-off scale κ_c for the cascade

$$P_\Delta^{(i)}(n, \kappa_c) = \delta_{n0} \quad \Rightarrow \quad R^{(i)}(\gamma, \kappa_c) = 0, \tag{5.14}$$

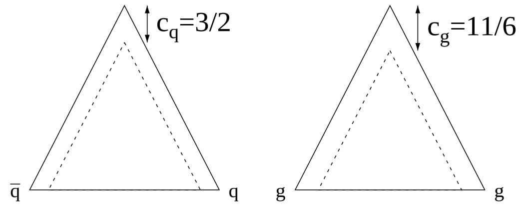

Figure 5.6: *The hyperbolic shape of the true phase space limits and the inequality* $x_1^3 + x_3^3 < x_1^2 + x_3^2 < 2$ *are both neglected in the leading order result. This can be corrected for by cutting off a strip at the triangle edges, thus reducing the available phase space. The different heights of the strips reflects the difference between* $x_1^3 + x_3^3$ *and* $x_1^2 + x_3^2$*, appearing in the emission density for a gg– and* $\mathrm{q\overline{q}}$ *dipole, respectively. The different magnitudes of phase space reductions implies* $\overline{n^{(\mathrm{q})}}(L) \sim \overline{n^{(\mathrm{g})}}(L + c_{\mathrm{g}} - c_{\mathrm{q}})$.

then implies

$$R^{(\mathrm{g})}(\gamma, L) = \frac{\alpha_0}{\alpha_{\mathrm{q}}} R^{(\mathrm{q})}(\gamma, L). \tag{5.15}$$

Combining Eq (5.12) and Eq (5.13) gives the following differential equation for $\mathcal{P}$, valid in the LLA:

$$\frac{\mathrm{d}^2}{\mathrm{d}L^2} \ln \mathcal{P}^{(i)}(\gamma, L) = \frac{\alpha_i}{L} \left[\mathcal{P}^{(\mathrm{g})}(\gamma, L) - 1 \right]. \tag{5.16}$$

5.3.3 MLLA Corrections

Since the approximate triangular (κ, y) region is somewhat larger than the true hyperbolic shape of the phase space, and the inequality $x_1^3 + x_3^3 < x_1^2 + x_3^2 < 2$ was neglected, the emission density is overestimated in LLA (especially in a gg-dipole). In the Modified Leading Logarithmic approximation (MLLA) [4], corrections of relative order $1/\sqrt{L}$ are included. In [14] it is shown, that evolution equations correct to relative order $1/\sqrt{L}$ are obtained if we maintain the approximation $x_1^3 + x_3^3 \approx x_1^2 + x_3^2 \approx 2$ and instead reduce the available phase space by cutting out a strip at the edges, as illustrated in Fig 5.6. The height of the strip is

$$c_{\mathrm{q}} = 3/2, \quad c_{\mathrm{g}} = 11/6, \tag{5.17}$$

for a $\mathrm{q\overline{q}}$- and gg-dipole, respectively. The constant phase space reduction modifies $|\mathrm{d}y/\mathrm{d}l|$ to

$$2\,|\mathrm{d}y/\mathrm{d}l|^{(i)} = \Theta(L - c_i - l), \tag{5.18}$$

which implies

$$\frac{\mathrm{d}}{\mathrm{d}L}\ln\mathcal{P}^{(i)}(\gamma, L) = \alpha_i R^{(i)}(\gamma, L - c_i), \tag{5.19}$$

$$\frac{\mathrm{d}^2}{\mathrm{d}L^2}\ln\mathcal{P}^{(i)}(\gamma, L) = \frac{\alpha_i}{L - c_i}\left[\mathcal{P}^{(\mathrm{g})}(\gamma, L - c_i) - 1\right]. \tag{5.20}$$

For the gluon case, the equations are modified by the possibility of $\mathrm{g}\to\mathrm{q}\overline{\mathrm{q}}$ splittings [14]. We do not reproduce the algebraic details here, but refer to refs [4, 13]. Extracting moments in γ of Eq (5.20) leads to differential equations for $\overline{n^{(\mathrm{g})}}$ and $\overline{n^{(\mathrm{q})}}$. Their asymptotic behaviours are

$$\overline{n^{(\mathrm{q})}} \approx (\alpha_\mathrm{q}/\alpha_0)\overline{n^{(\mathrm{g})}} \sim L^\rho \exp(2\sqrt{\alpha_0 L}), \tag{5.21}$$

where

$$\rho = \frac{1}{4} - (2N_\mathrm{f}/N_\mathrm{c}^3 + 11)\frac{\alpha_0}{12} \tag{5.22}$$

in MLLA. Thus the introduction of $1/\sqrt{L}$-suppressed terms in the evolution equations changes the asymptotic behaviour of $\overline{n^{(\mathrm{i})}}$.

The contribution to ρ from the $\mathrm{g}\to\mathrm{q}\overline{\mathrm{q}}$ process is the term $2N_\mathrm{f}/N_\mathrm{c}^3$ in the parenthesis, which is clearly a small contribution compared to the other term 11. The contribution from this process to the ratio $N_\mathrm{q}/N_\mathrm{g}$ is also very small. Using numerical calculations we have found that it only modifies the ratio by less than 2% for all energies above 4 GeV. For this reason we will neglect the splitting process in the analytical calculations presented below. However, when we compare our analytic results with MC simulations, the latter will include also the $\mathrm{g}\to\mathrm{q}\overline{\mathrm{q}}$ process.

Neglecting the $\mathrm{g}\to\mathrm{q}\overline{\mathrm{q}}$ process for these reasons, we find from Eq (5.20) for the ratio $N_\mathrm{q}/N_\mathrm{g}$ the MLLA result

$$\frac{\alpha_0}{\alpha_\mathrm{q}}\overline{n^{(\mathrm{q})}}(L) \approx \overline{n^{(\mathrm{g})}}(L + c_\mathrm{g} - c_\mathrm{q}), \tag{5.23}$$

which essentially is a $1/\sqrt{L}$ correction approaching the LLA result Eq (5.21) for large L.

We also want to point out that the distribution in the multiplicity measure λ, mentioned in section 5.3.2, satisfy exactly the same evolution equations as the distribution in n. Therefore the asymptotic increase is also the same. The boundary conditions at threshold are however different, which implies some deviations at lower energies.

5.3.4 Virtuality Scale Dependence

If we consider a two-jet event sample, picked from $\mathrm{q}\overline{\mathrm{q}}$ events using some jet resolution scale $k_{\perp r}$, the mean multiplicity of the sample will be related to

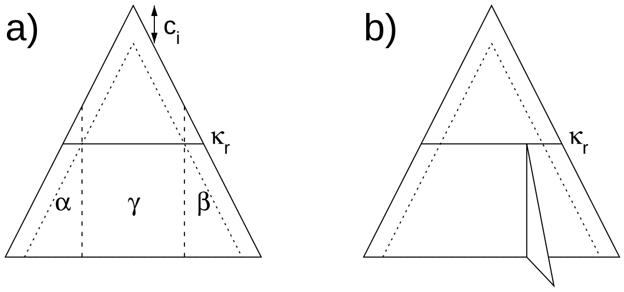

Figure 5.7: **a)** *A two-scale dependent multiplicity can be studied in two-jet* $\mathrm{q}\overline{\mathrm{q}}$ *events, using a resolution* $\kappa_r \neq L$. *The multiplicity is related to the phase space below the cut-off line at* κ_r. *The parton multiplicity is given by* $\overline{n^{(\mathrm{i})}}_{\alpha+\beta} = \overline{n^{(\mathrm{i})}}(\kappa_r + c_i)$, *and* $\overline{n^{(\mathrm{i})}}_\gamma = (L - \kappa_r - c_i)\frac{\mathrm{d}}{\mathrm{d}\kappa_r}\overline{n^{(\mathrm{i})}}(\kappa_r + c_i)$. **b)** *If the hardest gluon jet is found at* κ_r, *the phase space which determines the multiplicity is given by the same region* $\alpha + \beta + \gamma$, *plus a fold. The multiplicity on this fold is given by* $\overline{n^{(\mathrm{g})}}(\kappa_r)$.

phase space area below $\kappa_r \equiv 2\ln(k_{\perp r}/\Lambda)$. As shown in Fig 5.7, this implies

$$\overline{n^{(\mathrm{q})}}(L, \kappa < \kappa_r) \equiv \overline{n^{(\mathrm{q})}}(\kappa_r + c_\mathrm{q}) + (L - \kappa_r - c_\mathrm{q})\left.\frac{\mathrm{d}}{\mathrm{d}l}\overline{n^{(\mathrm{q})}}(l + c_\mathrm{q})\right|_{l=\kappa_r}. \tag{5.24}$$

Here the first term on the right hand side corresponds to the region $\alpha + \beta$ in Fig 5.7a, while the second term corresponds to the region γ. Thus the mean hadron multiplicity, N^h, in $\mathrm{q}\overline{\mathrm{q}}$ events where no jet is resolved above κ_r is given by

$$N^h_{\mathrm{qq}}(L, \kappa < \kappa_r) = N^h_{\mathrm{qq}}(\kappa_r + c_\mathrm{q}) + (L - \kappa_r - c_\mathrm{q})\frac{\mathrm{d}}{\mathrm{d}\kappa_r}N^h_{\mathrm{qq}}(\kappa_r + c_\mathrm{q}). \tag{5.25}$$

Events where the hardest gluon jet is found at κ_r corresponds to the phase space below the horizontal line in Fig 5.7b. The hard gluon jet gives the contribution $\frac{1}{2}N^h_{\mathrm{gg}}(\kappa_r)$ and therefore

$$N^h_{\mathrm{qq}}(L, \kappa = \kappa_r) = N^h_{\mathrm{qq}}(L, \kappa < \kappa_r) + \frac{1}{2}N^h_{\mathrm{gg}}(\kappa_r). \tag{5.26}$$

We note that while the κ_r dependence is fairly complicated, the L dependence is simply linear.

5.4 Recoil Effects and Boundary Conditions

The ratio of the *parton* multiplicities in quark and gluon jets within a narrow cone was calculated including corrections to order α_s, i.e. of order $1/L$, in ref [31] (cf. also ref [32]). The result is that the $\mathcal{O}(1/L)$ corrections are very small, only a few percent for energies above 30 GeV.

In a parton cascade, Λ cannot be associated to a specific renormalization scheme, but must be treated as a free parameter. Changing Λ introduces terms of relative suppression $1/L$ in the evolution equations Eq (5.20). Within the language of parton cascades, it is therefore non-trivial to systematically find a complete set of $1/L$ suppressed correction terms to many observables. We note however that the $1/L$ terms induced by changing Λ are similar for the multiplicity in quark and gluon jets. Therefore these terms cancel to a large extent for the ratio $N_\mathrm{q}/N_\mathrm{g}$. This is in agreement with the result in ref [31], that the correction term of order α_s to the ratio $N_\mathrm{q}/N_\mathrm{g}$ is small and scheme independent.

As discussed in detail in section 5.2, the observable hadrons are not directly determined by the partons within a fixed phase space region. The hadrons originating from a particular parton colour charge depend also on the location in phase space of its corresponding anticharge. This implies that the necessary cut-off in the parton cascade should depend upon the location in phase space of an associated colour anticharge. Such a dependence appears naturally in the dipole cascade formalism with a $k_\perp$-cut in the dipole restframe. Therefore the result can be sensitive to recoil effects experienced by the emitting parent partons. Assuming the local properties of the hadronization mechanism discussed in section 2, we will in the next subsection derive a correction term to the ratio $N_\mathrm{q}/N_\mathrm{g}$. Although formally of order $1/L$, this recoil effect is numerically large, and important for comparisons between theory and experimental results.

In section 5.7, we compare our results with data from OPAL [11] for jets with energy $M_Z/2$. In section 5.6 we also discuss how to analyze LEP data at the Z pole in order to obtain the ratio $N_\mathrm{q}/N_\mathrm{g}$ for a range of jet energies.

5.4.1 Recoil Effects

As discussed in section 5.3.3 we will neglect the effect caused by the $\mathrm{g}\rightarrow\mathrm{q}\overline{\mathrm{q}}$ process. Numerical calculations have shown that this process, which is both colour suppressed and kinematically suppressed, only has a negligible influence on the result. In principle the splitting process could be included at the expense of more complicated expressions, which would make the result less transparent.

Let us study the emission from an original gg-system. As discussed in section 5.3.1 this emission corresponds to two dipoles (a $\mathrm{r}\overline{\mathrm{r}}$ and a $\mathrm{g}\overline{\mathrm{g}}$ dipole in Fig 5.3a), and the phase space can be represented by two parallel triangular regions. If one gluon is emitted (e.g. from the $\mathrm{g}\overline{\mathrm{g}}$ dipole), the ensuing 3g state emits further soft gluons as three dipoles, as indicated in Fig 5.3b. As discussed in section 5.2, the emission from the separation between the b charge in the emitted gluon (2) and the $\overline{\mathrm{b}}$ charge in the emitting (recoiling) gluon (1) is determined by the invariant mass s_{12}. The Landau-Pomeranchuk formation time for an emitted quantum is determined by the $k_\perp$ of the emission. Thus there is a time ordering, such that a softer gluon (a gluon with smaller $k_\perp$) is emitted after the establishment of the configuration in Fig 5.3b. We must then expect that the weight of the $\mathrm{r\bar{r}}$ and $\mathrm{g\bar{g}}$ dipoles in Fig 5.3b are determined by the corresponding dipole masses. The squared mass of the "spectator" $\mathrm{r\bar{r}}$ dipole is reduced from its initial value s to $s_{13} = (1-x_2)s$, which thus reduces the phase space for emissions from this dipole. We note that this recoil effect is very different for a $\mathrm{q\bar{q}}$ system, where the weight of the corresponding dipole is negative, and suppressed by a factor $1/N_c^2$. Therefore recoils will affect the ratio between quark and gluon jets, and we will now estimate the size of this effect.

The density of gluons with squared transverse momentum $k_\perp^2 = s(1-x_1)(1-x_3)$ emitted by e.g. the $\mathrm{g\bar{g}}$ dipole in Fig 5.3a is given by Eq (5.7). This initial emission reduces the emission of softer gluons with $k_\perp'^2 < k_\perp^2$ in the partner $\mathrm{r\bar{r}}$ dipole, so that the rapidity range is reduced from $\Delta y = \ln s/k_\perp'^2$ to $\Delta y = \ln s_{13}/k_\perp'^2 = \ln s/k_\perp'^2 + \ln(1-x_2)$. On average the reduction δy caused by gluons within an interval $\mathrm{d}\ln k_\perp^2 \equiv \mathrm{d}\kappa$ is then

$$\begin{aligned} \delta y &= -\frac{\alpha_0}{\kappa}\mathrm{d}\kappa \int \frac{\mathrm{d}x_1 \mathrm{d}x_3 (x_1^3 + x_3^3)}{2(1-x_1)(1-x_3)} \ln(1-x_2)\delta(\kappa - \ln[s(1-x_1)(1-x_3)]) \equiv \\ &\equiv \frac{\alpha_0}{\kappa}\mathrm{d}\kappa \cdot I(L-\kappa), \quad (L = \ln s). \end{aligned} \tag{5.27}$$

For a strongly ordered cascade we have $L \gg \kappa$, and in this limit we find

$$I = 2\left(\frac{\pi^2}{6} - \frac{49}{72}\right) \equiv c_\mathrm{r}, \quad L - \kappa \gg 1. \tag{5.28}$$

Deviations from this limiting value give corrections which are suppressed at high energies. We have however also checked that the value in Eq (5.28) is a very good approximation in the whole relevant part of phase space. Typical values of $L-\kappa$ become smaller for smaller L–values, i.e. smaller dipole energies, due to the increase of α_s. Within the MLLA approximation we find that for $L \sim 6$ the average value of κ becomes ≈ 2, i.e. $k_\perp \approx e\Lambda$, which is very close to the standard cutoff in the Ariadne cascade MC. Thus typical values of $L-\kappa$ are always larger than 4, and for these values I deviates from the value in Eq (5.28) by less than 10%.

Half of the effect in Eq (5.27) corresponds to positive rapidities, in which case the recoil is taken essentially by the gluon (1) in Fig 5.3b, while in the other half the recoil is taken by gluon (3). The emissions in the $\mathrm{r\bar{r}}$ dipole in Fig 5.3a has however a similar effect on the $\mathrm{g\bar{g}}$ system, and the net result on one of the gluon jets is thus given by Eq (5.27).

Once one gluon is emitted two smaller dipoles are formed (between the pairs 3-2 and 2-1 in Fig 5.3b) emitting softer gluons, which give similar reductions of the "spectator dipole" phase space. Further down the emission cascade the original $g\overline{g}$ dipole in Fig 5.3a corresponds to a chain of dipoles. Emissions in the two end links of this chain give recoil effects on the spectator system originating from the $r\overline{r}$ dipole in Fig 5.3a. Consequently we obtain a recoil effect described by Eq (5.27) for *all* values of κ, not only those which correspond to the first emission. Summing up the effects from all emissions above a given value $l = \ln k_\perp^2/\Lambda^2$, and replacing I with its limiting value c_r, gives the total phase space reduction

$$\delta y_\mathrm{tot}(l) = \int_l^{L-c_\mathrm{g}} \mathrm{d}\kappa \frac{\alpha_0}{\kappa} c_\mathrm{r} = \alpha_0 c_\mathrm{r} \ln \frac{L-c_\mathrm{g}}{l}. \tag{5.29}$$

The upper limit is given by the kinematical limit in the MLLA approximation, $L - c_\mathrm{g}$. Thus the effective rapidity range becomes

$$\Delta y_\mathrm{eff}(l) = L - l - c_\mathrm{g} - \alpha_0 c_\mathrm{r} \ln \frac{L-c_\mathrm{g}}{l}, \tag{5.30}$$

where c_g is the MLLA correction and the last term is the recoil effect. We note in particular that the recoil term goes to zero at the kinematical limit $l = L - c_\mathrm{g}$, as it should. From Eq (5.30) we find

$$\left| \frac{\mathrm{d}\Delta y_\mathrm{eff}(l)}{\mathrm{d}l} \right| = 1 - \frac{\alpha_0 c_\mathrm{r}}{l}, \tag{5.31}$$

which should be inserted in into Eq (5.12) (with $2y$ replaced by Δy_eff). Doing so, and taking the MLLA modification in Eq (5.18) into account, we find instead of Eq (5.19)

$$\frac{\mathrm{d}}{\mathrm{d}L} \ln \mathcal{P}^{(\mathrm{g})}(\gamma, L) = \left(1 - \frac{\alpha_0 c_\mathrm{r}}{L - c_\mathrm{g}}\right) R^{(\mathrm{g})}(\gamma, L - c_\mathrm{g}). \tag{5.32}$$

We note in particular that the result in Eq (5.31) is independent of L and that the correction in Eq (5.29) goes to zero in the kinematical limit. These two features imply that the structure of the evolution equation is unchanged when going from Eq (5.19) to Eq (5.32).

For an initial $q\overline{q}$ system the emission from a quark colour charge is lower than one half of a gluon charge, $C_\mathrm{F} = \frac{N_\mathrm{c}}{2}(1 - 1/N_\mathrm{c}^2)$. For the radiation from a $q\overline{q}g$ system, this can be expressed as a *negative* contribution with relative weight $-1/N_\mathrm{c}^2$ from a dipole stretched between the quark and antiquark, corresponding to the $r\overline{r}$ dipole in Fig 5.3b for the purely gluonic case. If we assume that we can treat this negative dipole in the same way, we would get the following result for a quark jet

$$\frac{\mathrm{d}}{\mathrm{d}L} \ln \mathcal{P}^{(\mathrm{q})}(\gamma, L) = \left(1 + \frac{\alpha_0 c_\mathrm{r}^{(\mathrm{q})}}{L - c_\mathrm{q}}\right) R^{(\mathrm{q})}(\gamma, L - c_\mathrm{q}), \tag{5.33}$$

$$c_{\mathrm{r}}^{(\mathrm{q})} \equiv -\frac{1}{N_{\mathrm{c}}^2}\int_0^1 \mathrm{d}x \frac{1+(1-x)^2}{x}\ln(1-x) = \frac{2}{N_{\mathrm{c}}^2}\left(\frac{\pi^2}{6}-\frac{5}{8}\right). \tag{5.34}$$

Combining Eqs (5.32), (5.33) and (5.15) now leads to

$$\begin{aligned}\frac{\mathrm{d}}{\mathrm{d}L}\ln\mathcal{P}^{(\mathrm{g})}(\gamma, L+c_{\mathrm{g}}-c_{\mathrm{q}}) &= \frac{\alpha_0}{\alpha_{\mathrm{q}}}\frac{1-\alpha_0 c_{\mathrm{r}}^{(\mathrm{g})}/(L-c_{\mathrm{q}})}{1+\alpha_0 c_{\mathrm{r}}^{(\mathrm{q})}/(L-c_{\mathrm{q}})}\frac{\mathrm{d}}{\mathrm{d}L}\ln\mathcal{P}^{(\mathrm{q})}(\gamma, L) \approx \\ &\approx \frac{\alpha_0}{\alpha_{\mathrm{q}}}\left(1-\frac{\alpha_0 c_{\mathrm{r}}}{L}\right)\frac{\mathrm{d}}{\mathrm{d}L}\ln\mathcal{P}^{(\mathrm{q})}(\gamma, L),\end{aligned} \tag{5.35}$$

where c_{r} now is modified by approximately 10%, to

$$c_{\mathrm{r}} \equiv c_{\mathrm{r}}^{(\mathrm{g})} + c_{\mathrm{r}}^{(\mathrm{q})} = \frac{10}{27}\pi^2 - \frac{3}{2} \tag{5.36}$$

The negative dipole in the $\mathrm{q\overline{q}g}$ system is caused by interference effects due to identical colour charges. As discussed in section 2, these interference effects are also connected to the possibility of "colour reconnection" in the hadronization process. As these problems are still not solved, we regard the recoil effect for the quark jet as uncertain. Since this contribution is only 10% of the total effect this is however not a serious problem here.

Taking the first moment in the Laplace transform variable γ, we find the relation Eq (5.35) between $\frac{\mathrm{d}}{\mathrm{d}L}\overline{n^{(\mathrm{g})}}$ and $\frac{\mathrm{d}}{\mathrm{d}L}\overline{n^{(\mathrm{q})}}$ as well. Remembering that $\overline{n^{(\mathrm{g})}}$ refers to a gluon jet while $\overline{n^{(\mathrm{q})}}$ refers to a $\mathrm{q\overline{q}}$ system, the relations between multiplicities in two-parton systems should be given by

$$\frac{\mathrm{d}}{\mathrm{d}L}N_{\mathrm{gg}}^h(L+c_{\mathrm{g}}-c_{\mathrm{q}}) = \frac{N_{\mathrm{c}}}{C_{\mathrm{F}}}\left(1-\frac{\alpha_0 c_{\mathrm{r}}}{L}\right)\frac{\mathrm{d}}{\mathrm{d}L}N_{\mathrm{qq}}^h(L). \tag{5.37}$$

5.4.2 Boundary Conditions for Hadron Multiplicities

The relation Eq (5.37) has to be supplemented by appropriate boundary conditions. Extrapolating Eq (5.37) down to too small values of L would imply that the hadron multiplicity in a $\mathrm{q\overline{q}}$ system would be significantly larger than that in a gg system. At low values of L, the hadron multiplicity is largely determined by the hadronic phase space and thus by the total available energy. This implies that at some threshold value L_0, we expect to have the relation

$$N_{\mathrm{gg}}^h(L_0) \approx N_{\mathrm{qq}}^h(L_0) \equiv N_0, \tag{5.38}$$

Here L_0, though larger than κ_{c}, should correspond to an energy of only a few GeV.

The precise value of L_0 strongly depends on non-perturbative QCD effects. At low energies, the fact that a $\mathrm{q\overline{q}}$ string contains two quarks while a gg string does not, may influence the ratio $N^h_{\rm qq}/N^h_{\rm gg}$. Thus the value of L_0 is sensitive to details in the fragmentation of low energy $\rm q\overline{q}$ and gg systems, while N_0 to a large extent depends on how the primarily produced hadrons decay. In principle L_0 ought to be determined by experimental data from charmonium and bottonium decays. In our analysis, we have instead determined L_0 and N_0 from Monte Carlo simulations of the Lund String Fragmentation model, using the JETSET 7.4 computer program [25]. We then get $L_0 \sim 5.7$, corresponding to an energy $E_0 = \Lambda \exp(L_0/2) \sim 4$GeV for $\Lambda = 0.22$GeV. Given $N^h_{\rm qq}$ and L_0 from MC simulations, $N^h_{\rm gg}$ can be derived by numerical integration of the right hand side of Eq (5.37). The dependence on the threshold behaviour can however be avoided if one studies how the multiplicity varies with increasing energy. This possibility is further discussed in section 5.7.

5.5 Scale Dependences in Jets

In the following discussion we will use the notation of [5] and [14], i.e. $N^h_{\rm g}$ and $N^h_{\rm q}$ denote multiplicities in jets, while $N^h_{\rm gg}$ and $N^h_{\rm qq}$ refer to multiplicities in two-parton systems. We have already introduced L and κ as logarithmic energy– and virtuality scales for two-parton systems. The multiplicity in a jet j with energy E_j will be studied as a function of the logarithmic jet energy scale

$$L_j \equiv \ln\left((2E_j)^2/\Lambda^2\right). \tag{5.39}$$

The jet energy is multiplied by a factor 2 for two "cosmetic" reasons: Then the scales coincide for a gluon jet when the simple condition

$$L_j = \kappa \tag{5.40}$$

is fulfilled. (I.e. the relevant energy scale of this gluon jet is $E_{\rm g} = k_\perp/2$, which is the MLLA result presented in [33, 5].) Furthermore, the multiplicity in a one-scale dependent jet is simply given by

$$N^h_{\rm p}(L_j) = \frac{1}{2}N^h_{\rm pp}(L_j), \quad {\rm p} = {\rm q},{\rm g}. \tag{5.41}$$

In general, the multiplicity of a jet depends on *two* scales, energy and virtuality. Reducing the maximal allowed transverse momentum within a jet reduces the multiplicity, even if the energy remains constant (cf. Fig 5.8).

As discussed in section 5.3.4, the virtuality scale dependence of the multiplicity in quark jets can be easily studied in two-jet $\rm q\overline{q}$ events varying the resolution scale. To compare quark and gluon jets we can use a three-jet event sample. The multiplicity in the jets will also in this sample depend both on the jet energy and the resolution scale $k_{\perp r}$. Keeping $k_{\perp r}$ fixed, the energy scale dependence can be studied [12]. However, the restriction implied by a fixed $k_{\perp r}$

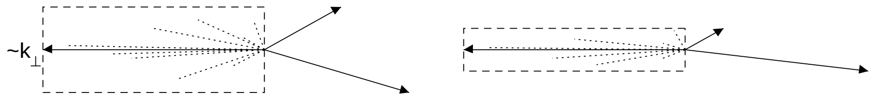

Figure 5.8: *The transverse resolution scale $k_\perp$ between the softer jets in a three-jet event also specifies the maximal allowed transverse momentum of unresolved particles within the jets. The multiplicity of the jets thus depends both on the jet energy and on $k_\perp$.*

is rarely considered in theoretical predictions. Rather, most calculations apply to the very forward region of jets [5, 31]. There coherence effects are negligible, and energy-momentum conservation restricts $k_\perp$ of emissions to such an extent that $k_{\perp r}$ introduces no new bias. We will here examine the possibility to study unbiased jets at moderate energies, using the broadest possible cones to define the contents of the jets.

To find the jets of an event, cluster algorithms are used. In general, these contain a definition of a distance measure d between the jets, combine the two closest jets into one, and continues until all distances are above some resolution scale d_{cut}. In CDM and other approaches [19], the transverse momentum specifies the resolution. Thus it is appropriate to use a $k_\perp$-type of distance measure, as e.g. in the DURHAM [34], LUCLUS [25] or DICLUS [24] algorithms. We will use an approach, where jets are combined in the order given by the chosen algorithm until only three remain. The topology of the jets then specifies the transverse momentum, $k_\perp$, of the event (cf. Fig 5.8). This approach enables the definition of unbiased jets, whose evolution with $k_\perp$ can be studied, while the energy scale dependence can be examined in an event sample with fixed $k_\perp$.

To construct unbiased jets, we note that a cone-like surface used to define the forward contents of a jet corresponds to a perpendicular plane in some other frame. In this frame the jet resembles one hemisphere of a full event, and if the energy and virtuality scales in this frame are equal, the jet is unbiased. We will refer to this observation as the "One-Scale Criterion" (OSC), since the mean multiplicity of the jet in this case indeed only depends on one scale – the energy of the corresponding full event.

5.6 Jet Algorithms

Soft gluon coherence can be approximated by an angular ordering (AO) constraint [8]. The multiplicity in a jet defined by AO will thus depend on one colour factor only. According to LLA, the jet will also be unbiased and depend on one single transverse energy scale, *provided* no extra cut-off in transverse momentum is imposed by a fixed jet resolution scale. We will present results from two algorithms based on this AO observation: The CAMBRIDGE algorithm presented in [9], and a previously undiscussed "Mercedes" algorithm, where the multiplicities of the jets are defined in the symmetric "Mercedes" Lorentz frame of the event. The main reason for studying both is to look for similarities, which point at general properties in the AO approximation.

Corrections to the AO algorithms can be found by using the OSC explicitly. We will here discuss one such algorithm, which has similarities with the CAMBRIDGE algorithm, called the "Cone Exclusion" algorithm, and one corrected "Boost" algorithm where the jets are analyzed in a frame similar to the Mercedes one. The two OSC algorithms give the same gluon jets, but the definition of quark jets differ. With the Cone Exclusion algorithm all three jets are unbiased, while the Boost algorithm constructs quark jets with well-defined but different energy and virtuality scales. Thus the Boost algorithm is suitable for a study of the separate dependence of the two scales, while the Cone Exclusion algorithm is suitable for a comparison of quark jets vs. gluon jets.

5.6.1 Angular Ordering Algorithms

The Cambridge Algorithm

The CAMBRIDGE algorithm is designed to construct gluon jets uncontaminated by coherently emitted particles. Thus the gluon jet properties depend only on the transverse momentum to the nearest harder jet, and on the gluon colour factor N_c. More specifically, the DURHAM $k_\perp$-distance

$$d_{ij} \equiv 2\frac{\min\{E_i^2, E_j^2\}}{E_{\rm vis}^2}(1-\cos\theta_{ij}) \tag{5.42}$$

is used to resolve jets, but the particles and sub-jets are merged in inverse angular order (those closest in angle are combined first). Once a soft jet is resolved, it is "frozen out", i.e. it gets no extra multiplicity contribution. Thus the contents of the soft jet is confined to a cone given by the smallest angle to any harder jet. This implies that the treatment of a gluon jet depends on wether its energy is higher or smaller than the quark jet energy. The CAMBRIDGE algorithm is therefore suitable for gluon jet analyses primarily when the hardest gluon jet is significantly softer than the quark jets.

In the CAMBRIDGE algorithm, $d_{\rm cut}$ not only determines when the clustering stops, but also at what stage different jets are frozen out. Producing a fixed number of jets is therefore not a completely trivial task. If we put $d_{\rm cut}$ artificially large and pursue the clustering down to three jets, no freezing will occur. This would then correspond to a strict angular ordered clustering, similar to a cone algorithm. Fixing the number of jets is therefore better achieved by changing d_{cut} in every event to a value which produces three jets. This procedure faces two problems: There may not be any d_{cut} giving three jets, and when there is a large range of d_{cut} values giving three jets, the multiplicities in the jets could depend on the choice of d_{cut}. However, both of these situations occur very rarely (at percentage level), and reliable conclusions may therefore be drawn from events clustered by the CAMBRIDGE algorithm, varying d_{cut} to fix the number of jets to three.

The Mercedes Algorithm

In conventional cluster algorithms the bisectors between jets roughly separate the contents of them. In the specific case of a completely symmetric three-jet event, commonly referred to as a Mercedes event, such a jet definition will satisfy angular ordering [5]. The kinematical constraint implies a fixed scale, but the scale evolution can still be studied by boosting a general three-jet event to its Mercedes frame. Since particles are in general shuffled from one jet to another under a Lorentz transformation, the mass of a jet is not invariant. Instead the *direction* of a jet, corresponding to a parton in the cascade, approximately transforms as a light-like vector. Using a $k_\perp$-based algorithm to find the jets, the Mercedes algorithm constructs gluon jets similar to those in the CAMBRIDGE algorithm.

5.6.2 OSC Algorithms

The Cone Exclusion Algorithm

The "Cone Exclusion" (CE) method combines $k_\perp$- and angular distances in a way that has similarities with the CAMBRIDGE algorithm. After the construction of three jets using a $k_\perp$-distance, a cone-like region is defined around the gluon jet. Only particles assigned to the jet that lie inside the region are then contributing to the multiplicity. Note that in spite of the name "Cone Exclusion", the method is using a $k_\perp$-based cluster scheme to find the jets. The "Cones" are used to assign soft particles to the correct jet.

With this method it is simpler to fix the number of jets to three than in the CAMBRIDGE algorithm, and it provides a better treatment of hard gluon jets. It is however specifically designed for studies of multiplicities in jets in three-jet events, and does not share the benefits of the CAMBRIDGE algorithm as compared to other $k_\perp$-algorithms in other respects. E.g., the CAMBRIDGE algorithm is designed to avoid the formation of "junk jets" (when soft particles from different jets which happen to be close in phase space are combined and may be resolved as a jet if the resolution scale d_{cut} is small). Since we in this analysis always pursue the clustering until only three jets remain, these "junk jets" will in general be absorbed into "proper jets", and we are therefore not

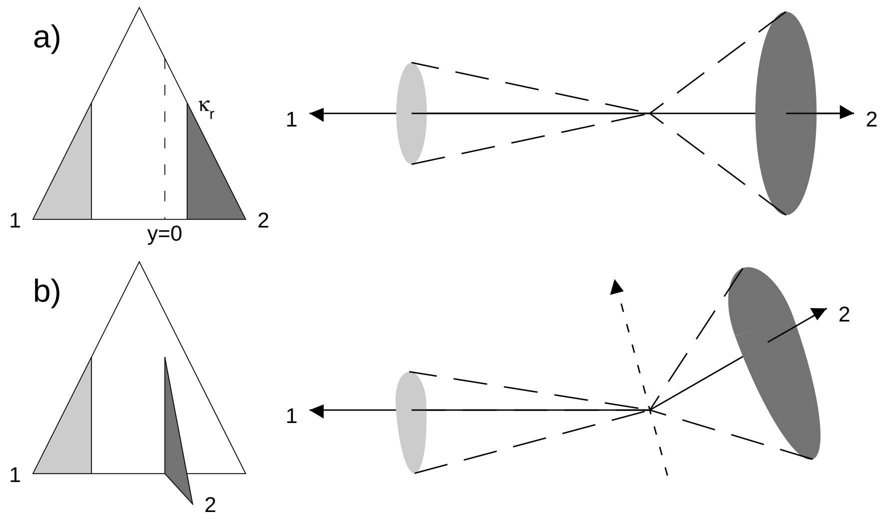

Figure 5.9: **a)** *If the partons of a dipole are going apart back-to-back, particles from the triangular region of height κ_r in the direction of jet j all have a rapidity $y > \ln(2E_j/\Lambda) - \kappa_r/2$, which implies $\cot(\theta_j/2) > 2E_j/k_{\perp r}$. This holds also if the dipole is not in its CMS.* **b)** *If the dipole is in a general frame, the triangular phase space areas corresponds to two "egg-shaped" regions which after a boost along the bisector to the back-to-back frame become the cones of (a), i.e. which satisfy $\cot(\theta'_j/2) > 2E'_j/k_{\perp r}$, where θ'_j and E'_j are measured in the collinear frame.*

very sensitive to this problem addressed by the CAMBRIDGE algorithm.

To find the proper cones to use, we will start our discussion with two-jets events obtained with some resolution $k_{\perp r}$. We look at the events in a frame where the original partons are going out back-to-back, though not necessarily in the overall CMS. In the κ, y phase space picture (with folds), an unbiased jet corresponds to a triangular region. When the partons of a dipole are moving apart back-to-back, the relation $4E_1E_2 = s$ implies

$$L = \ln(\frac{2E_1}{\Lambda}) + \ln(\frac{2E_2}{\Lambda}) = \frac{1}{2}(L_1 + L_2), \tag{5.43}$$

where L_1 and L_2 are the logarithmic jet energy scales in this frame. A particle p stemming from a triangular region of height $\kappa_r = 2\ln(k_{\perp r}/\Lambda)$ in the direction of e.g. jet 2 has an angle $\theta_{\mathrm{p}2}$ to the jet given by (cf. Fig 5.9a)

$$\frac{1}{2}\ln\left(\cot^2\frac{\theta_{\mathrm{p}2}}{2}\right) = y > \frac{L_2 - \kappa_r}{2} = \ln\left(\frac{2E_2}{k_{\perp r}}\right). \tag{5.44}$$

An equivalent expression for this constraint is

$$\ln(s_{\mathrm{p1}}) - \ln(s_{\mathrm{p2}}) > \ln(s_{12}) - \ln(k_{\perp r}^2). \tag{5.45}$$

We now turn to three-jet events, where $k_\perp^2 = s(1-x_1)(1-x_3)$ specifies the resolution. Then all quantities in the constraint in Eq (5.45) are Lorentz invariant, and it can immediately be applied to the three jets in the CMS. For the qg dipole, the constraints are then

$$\frac{x_{\mathrm{g}} \sin^2(\theta_{\mathrm{pg}}/2)}{x_{\mathrm{q}} \sin^2(\theta_{\mathrm{pq}}/2)} < 1 - x_{\mathrm{q}} \tag{5.46}$$

for the gluon jet and

$$\frac{x_{\mathrm{q}} \sin^2(\theta_{\mathrm{pq}}/2)}{x_{\mathrm{g}} \sin^2(\theta_{\mathrm{pg}}/2)} < 1 - x_{\mathrm{q}} \tag{5.47}$$

for the quark jet. Here θ_{pq} (θ_{pg}) denote as before the angles between the hadron p and the jet direction q (g). The relations for the $\overline{\mathrm{q}}$g dipole are similar.

For the q (or $\overline{\mathrm{q}}$) jet, Eq (5.47) specifies an "egg-shaped" region, which after a boost along the bisector of the dipole to a back-to-back frame becomes a cone satisfying Eq (5.44) (cf. Fig 5.9). The gluon jet is however attached to two dipoles, and CE thus specifies two different regions. In the directions being accepted by one dipole but not the other, most particles emerge from the "wrong" dipole and should not contribute to the multiplicity of the gluon jet. We have required particles belonging to the gluon jet to satisfy both possible restrictions from Eq (5.46).

To summarize, the Cone Exclusion algorithm works as follows: Three jets are constructed, using a $k_\perp$-based cluster algorithm. A particle assigned to the gluon jet will then contribute to the multiplicity only if it satisfies Eq (5.46). The quark jets are treated similarly, using Eq (5.47). Thus the multiplicity in the forward region of every jet – corresponding to an unbiased jet – is studied, while soft central particles are simply ignored.

The Boost Algorithm

The OSC can also be used to improve the AO-based Lorentz transformation to the Mercedes frame. Consider a three-jet event boosted to a Lorentz frame where the angles are

$$\theta'_{\overline{\mathrm{q}}\mathrm{g}} = \theta'_{\mathrm{qg}} \equiv \theta', \tag{5.48}$$

and the partons carry energies E'_i. Let the bisectors define the planes between different jet regions. For the gluon, the logarithmic back-to-back jet energy scale from both dipoles is then

$$L_{\mathrm{g}} = 2\ln\left(\frac{2E'_{\mathrm{g}}}{\Lambda} \sin\frac{\theta'}{2}\right), \tag{5.49}$$

which coincides with the virtuality scale when $L_{\mathrm{g}} = \kappa$. This implies

$$x'^{\,2}_{\mathrm{g}} \sin^2(\theta'/2) = (1-x_{\mathrm{q}})(1-x_{\overline{\mathrm{q}}}), \quad x'_i \equiv \frac{2E'_i}{\sqrt{s}}. \tag{5.50}$$

The search for cone-like boundaries which define an unbiased gluon jet has thus been reformulated to a search for a specific Lorentz frame where the jet regions are easily identified.

After a bit of algebra, one finds the general relation

$$x'^{\,2}_{\mathrm{g}} \sin^2(\theta'/2) = (1-x_{\mathrm{q}})(1-x_{\overline{\mathrm{q}}})\frac{4}{1-x_{\mathrm{g}}}\cos^2(\theta'/2). \tag{5.51}$$

Thus the requirement Eq (5.50) is satisfied when

$$\cos^2(\theta'/2) = \frac{1-x_{\mathrm{g}}}{4}. \tag{5.52}$$

In the soft gluon limit, the wanted Lorentz frame coincides with the Mercedes frame, with $\theta' = 120°$, but larger gluon energies give larger angles θ'. We also note that the energy scale for the quark jet in this frame is

$$x'^{\,2}_{\mathrm{q}} \sin^2(\theta'/2) = \frac{1-x_{\overline{\mathrm{q}}}}{1-x_{\mathrm{q}}}, \tag{5.53}$$

and similarly for the $\overline{\mathrm{q}}$ jet.

The *gluon* jet defined in this way is actually equivalent to the one defined by the CE algorithm. If we combine Eq (5.50) and (5.53) into $x'_{\mathrm{g}}/x'_{\mathrm{q}} = 1 - x_{\mathrm{q}}$ and exploit the Lorentz invariance of the left hand side of Eq (5.46), we note that the CE condition for the gluon jet in Eq (5.46) can be rewritten as $\sin^2(\theta'_{\mathrm{pg}}/2) < \sin^2(\theta'_{\mathrm{pq}}/2)$, which is just the bisector condition in the Boost algorithm. The treatment of massive particles, whose masses have been neglected in the discussion, differ however in the two algorithms. Using both is a simple test of the sensitivity on particle masses.

The definition of quark jets differ in the two OSC algorithms. From Eq (5.53) we see that the quark jets in the Boost algorithm correspond to regions $A+B$ and E in Fig 5.4. Thus the Boost algorithm provides means to study the two-scale dependent multiplicity for different jet energy scales in a fixed energy experiment, while the CE algorithm is better to use for the study of one-scale dependent multiplicities.

To summarize, the Boost algorithm is as follows: Find three jets using a $k_\perp$-based cluster algorithm. Boost the event to the frame where the jet directions, assumed to be massless, satisfies Eq (5.48) and Eq (5.52). Let the jet boundaries be given by the bisectors to the other jets in this new frame and re-assign particles to the jets accordingly.

5.7 Results

We have tested the analytic form for the ratio $N^h_{\mathrm{qq}}/N^h_{\mathrm{gg}}$ in Eq (5.37) by comparing with multiplicity results from MC simulations and preliminary data [11]. Using MC simulations, we also examine the presented jet algorithms by comparing the multiplicities obtained in jets with the multiplicity of complete events at corresponding energies.

The CDM is available as a Monte Carlo simulation program, Ariadne [24]. There distribution factors such as $x_1^2 + x_3^2$ are taken into account and energy conservation is obeyed. Thus Monte Carlo simulations can show whether corrections other than presented above are needed to understand the model predictions on the scale evolution.

As discussed in section 5.4, a $\mathrm{q\overline{q}g}$ system can be regarded as three dipoles, where the $\mathrm{q\overline{q}}$ dipole is colour suppressed and has a negative weight. Alternatively, the system can be described by two dipoles, qg and $\mathrm{g\overline{q}}$, where the colour factor transforms from C_{F} in the q ($\mathrm{\overline{q}}$) end to $N_{\mathrm{c}}/2$ in the gluon direction. However, dipoles with negative or non-uniform colour factors are ill suited for MC implementation. In the standard Ariadne Monte Carlo, the solution is to neglect most terms of order N_{c}^{-2}, using the colour factor $N_c/2$ in all gg– and qg dipoles. In [27], a modification to the MC correcting for this approximation is presented. There non-uniform colour factors in dipoles are implemented, in a way reflecting the discussion around Fig 5.4, where the emission density is assumed to be proportional to C_{F} in all of the original $\mathrm{q\overline{q}}$ phase space triangle, while $N_{\mathrm{c}}/2$ applies to all extra phase space folds after gluon emissions.

At moderate energies, the mean multiplicity is mostly determined by the hardest gluon. The emission of this gluon in the $\mathrm{q\overline{q}}$ dipole is correctly given by C_{F} in both MC versions. Thus, results from the two MC approaches are expected to deviate only at larger energies, showing a relative discrepancy of at most $1/N_{\mathrm{c}}^2$.

A ggg configuration is well described by three dipoles, all with positive emission density, determined by $N_{\mathrm{c}}/2$. This picture is implemented in default Ariadne, which is used to obtain the simulation results from gg-systems presented below.

In the simulations we have used the default tune of Ariadne 4.08, with $\Lambda = 0.22$GeV. The parton configurations obtained in the cascade simulation are hadronized using the Jetset Monte Carlo [25], which is an implementation of the Lund String Fragmentation model.

5.7.1 The Multiplicity Ratio $N^h_{\mathrm{qq}}/N^h_{\mathrm{gg}}$

From MC results we find the threshold energy where the multiplicity in quark and gluon jets are the same, to be given by $L_0 \sim 5.7$. This corresponds to a CMS energy of ~ 4GeV. L_0 also specifies $N_0 \equiv N^h_{\mathrm{qq}}(L_0)$.

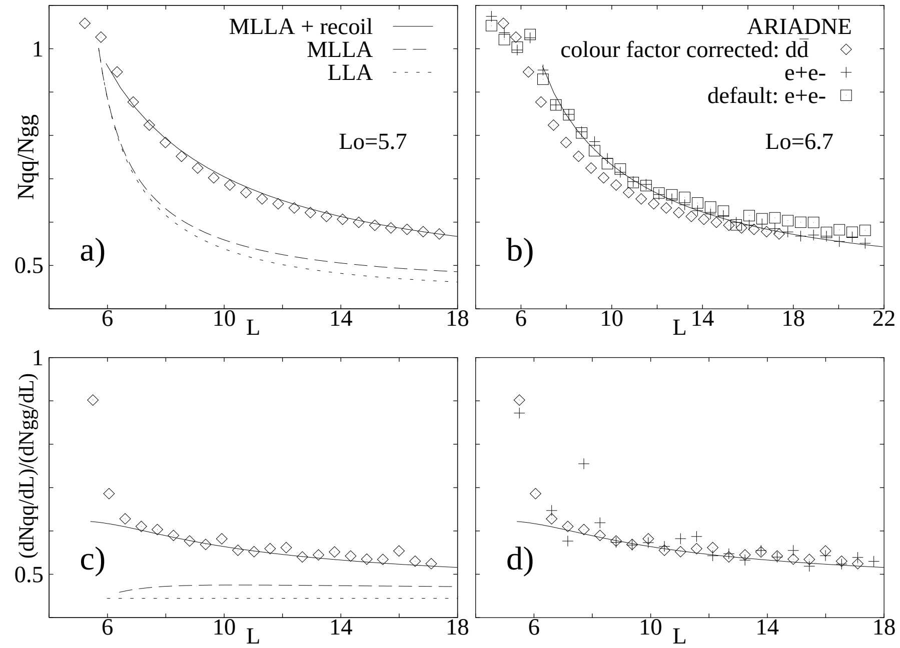

Figure 5.10: *Multiplicities ratios of* $\mathrm{q\overline{q}}$ *and* gg *systems, based on all stable particles.* $\mathrm{q\overline{q}}$ *samples are based on pure* $\mathrm{d\overline{d}}$ *events (diamonds) and* e^+e^- *annihilation, using* Ariadne *default (boxes) and the modification of [27] (crosses). The statistical errors for the MC results are within symbol sizes. We find that* $N^h_{\mathrm{qq}} = N^h_{\mathrm{gg}}$ *at* $L_0 = 5.7$. **a)** *Comparison with the prediction of Eq (5.37), using values of* N_0, L_0 *and* $N^h_{\mathrm{qq}}(L)$ *obtained from the MC. If neglecting the recoil correction (dashed line) and also the scale shift* $c_{\mathrm{g}} - c_{\mathrm{q}}$ *(dotted line), the prediction is far from MC. Thus recoil corrections of order* $1/L$ *are essential, even at* $\sqrt{s} \sim 5\,TeV$. **b)** *For* $\mathrm{e^+e^-}$ *events,* $\mathrm{c\overline{c}}$ *and* $\mathrm{b\overline{b}}$ *threshold effects are seen as a peak at* $L \sim 6$ *and a shoulder starting at* $L \sim 8$. *The relation determined by Eq (5.37) fits well with* $L_0 = 6.7$. *The difference between default and modified MC are important at* $L \sim 20$, *but negligible at* Z_0 *energies and below.* **c)** *The* $\frac{\mathrm{d}}{\mathrm{d}L}N(L)$ *ratio approaches the asymptotic value* $C_{\mathrm{F}}/N_{\mathrm{c}}$ *faster, but subleading corrections cannot be neglected.* **d)** *The ratio of multiplicity derivatives* $\frac{\mathrm{d}}{\mathrm{d}L}N(L)$ *is very similar for* $\mathrm{d\overline{d}}$ *and* e^+e^- *simulations and thus independent of* L_0, *as expected from Eq (5.37).*

In Fig 5.10a, the simulated ratio of $N^h_{\mathrm{qq}}/N^h_{\mathrm{gg}}$ is compared to the prediction of Eq (5.37), using values of N_0, L_0 and $N^h_{\mathrm{qq}}(L)$ obtained from the MC. If the $1/L$ recoil correction in Eq (5.37) is neglected the result differs significantly, even at $L \sim 20$, i.e. at $\sqrt{s} \sim 5$TeV. The prediction is further modified if the MLLA correction of order $1/\sqrt{L}$ in Eq (5.21) is neglected.

Fig 5.10b shows the different multiplicity ratios obtained in simulations of e^+e^- annihilation and pure $\mathrm{d\overline{d}}$ events. At energies slightly above a heavy quark thresh-hold, the mean multiplicity gets a significant contribution from isotropically decaying heavy hadrons. This is seen as a peak at $L \sim 6$ ($\sqrt{s} \sim 2m_D$) and a little shoulder starting at $L \sim 8$ ($\sqrt{s} \sim 2m_B$). The details of these threshold effects are beyond the scope of this paper. Instead we note that Eq (5.37) still fits well with $L_0 \sim 6.7$ ($\sqrt{s} \sim 6.3$GeV). In Fig 5.10b it is also shown that the corrections to N^h_{qq} from the Monte Carlo modification of [27], which more consequently implements the difference between C_{F} and $N_{\mathrm{c}}/2$ after the first gluon emission, are important at very high L, but negligible at Z_0 energies ($L = 12$) and below.

The ratio between the derivatives $\frac{\mathrm{d}}{\mathrm{d}L}N(L)$ is presented in Fig 5.10c. This ratio is expected to approach the asymptotic value $C_{\mathrm{F}}/N_{\mathrm{c}}$ more rapidly, which is also confirmed by data [12]. This is also born out in our analysis, and we note a good agreement between MC and the analytic form in Eq (5.37). According to this relation, the ratio of multiplicity derivatives $\frac{\mathrm{d}}{\mathrm{d}L}N(L)$ is expected to be independent of L_0. Fig 5.10d shows the similar results of $\mathrm{d\overline{d}}$ and e^+e^- simulations, confirming this expectation.

In [11], the OPAL collaboration has studied the $N^h_{\mathrm{gg}}/N^h_{\mathrm{qq}}$ ratio via quark and gluon hemispheres with energies $E = M_Z/2$ ($L = 12$). Their preliminary result

$$\frac{N^h_{\mathrm{gg}}}{N^h_{\mathrm{qq}}}(L = 12) = 1.509 \pm 0.022(stat) \pm 0.046(syst) \tag{5.54}$$

is in excellent agreement with our result including recoil effects in Fig 5.10b,

$$\frac{N^h_{\mathrm{qq}}}{N^h_{\mathrm{gg}}}(L = 12) = 0.67 = \frac{1}{1.5}. \tag{5.55}$$

In [11], OPAL also present preliminary data for the ratio of multiplicities in the central rapidity region,

$$\frac{N^h_{\mathrm{gg}}}{N^h_{\mathrm{qq}}}(L = 12, |y| < 2) = 1.815 \pm 0.038(stat) \pm 0.062(syst). \tag{5.56}$$

For a reasonably small central rapidity range Δy, the multiplicity $N(L, \Delta y)$ corresponds well to $\Delta y \frac{\mathrm{d}}{\mathrm{d}L}N(L)$. It is therefore interesting to compare this result with the analytical expression for the ratio of multiplicity derivatives, which is more independent of the boundary conditions at L_0. From Fig 5.10c, we find

$$\frac{\frac{\mathrm{d}}{\mathrm{d}L}N^h_{\mathrm{qq}}}{\frac{\mathrm{d}}{\mathrm{d}L}N^h_{\mathrm{gg}}}(L = 12) = 0.547 = \frac{1}{1.83}, \tag{5.57}$$

with recoil effects included. The MLLA prediction without recoil effects is smaller than 1/2.

Thus we conclude that MLLA calculations complemented with the recoil effect discussed in this paper are in very good agreement with the preliminary experimental data from OPAL. The recoil effect gives a sizeable correction which implies that the asymptotic value $C_{\mathrm{F}}/N_{\mathrm{c}}$ is far beyond reach in accelerator experiments.

5.7.2 Determination of Multiplicities in Jets

The quantity N_{gg}^{h} in the previous subsection is the multiplicity in a gg event which is hard to realize and study directly in experiments. In section 5.6, different jet algorithms designed to investigate this quantity in normal three-jet events are presented. We have tested their performance by simulating events at Z_0 energies. The events are clustered into three jets and the multiplicities in the jets from different algorithms are studied as a function of κ and y. The results for the jets are compared with the full-event results presented above.

All generated events are considered in the MC analysis. Neutrinos are excluded from the event, all other neutral particles are treated as massless while all charged particles are treated as pions. The obtained visible system in each event is boosted to its CMS before the analysis.

To tag the gluon jet, we note that the algorithms are applicable to a general jet topology. It is therefore possible to study events where one jet is much softer than the other two, when it is a good approximation to assume the softest jet to be the gluon jet. This makes the analysis simple and independent of sophisticated tagging methods. The gluon jet is softest in the phase space region $\kappa + 2|y| < L - \ln(4)$. In our "soft tag" analysis, we have restricted the phase space to $\kappa + 2|y| < L - 2\ln(4)$, in order to avoid events with two similar soft jets. The restriction still allows us to study scales up to $k_{\perp} \sim 20\mathrm{GeV}$.

In an experimental situation, harder gluon jets can be identified using heavy quark information, why it is of interest to test the performance of the presented algorithms in a larger part of phase space. We have therefore also performed an analysis where the gluon jet is tagged using information available in the MC simulation, which however is experimentally non-observable. In this "angle tag" procedure, the jets are identified with the partons in such a way that the sum of jet-parton angles are minimized.

Multiplicities in Gluon Jets

In Fig 5.11a, the multiplicity of the gluon jet obtained by different algorithms is presented as a function of κ. For each κ, results for several values of y are plotted. The gluon jet was identified with the "angle tag" method. The Angular Ordering algorithms (Cambridge and Mercedes) have similar behaviours.

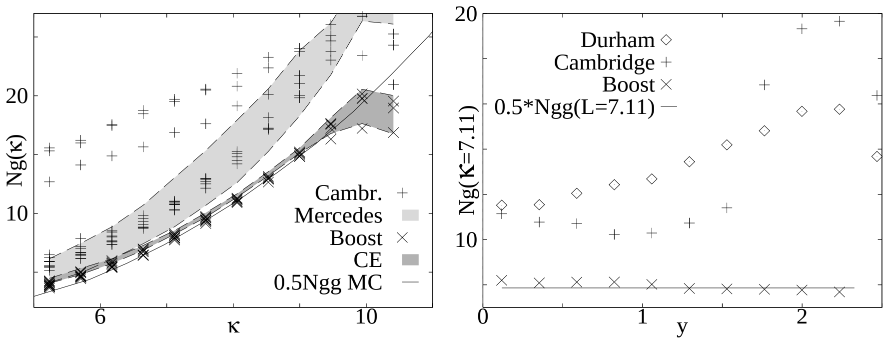

Figure 5.11: **a)** *Multiplicities in gluon jets as a function of κ. Results for several values of y are plotted, or the range of results are represented with shaded areas. The AO algorithms (*CAMBRIDGE *and Mercedes) have similar behaviours, and the multiplicity approaches* $0.5N^h_{\rm gg}$ *for low virtualities. The high values of the* CAMBRIDGE *algorithm corresponds to large y-values, where the gluon jet is not the softest one. The CE and Boost algorithms both give results independent of y which are in very good agreement with* $0.5N^h_{\rm gg}$ *also for higher transverse momenta.* **b)** *Multiplicities in gluon jets as a function of y for fixed κ. The* DURHAM *algorithm assigns coherently emitted particles to the gluon jet, and the multiplicity increases with y. The* CAMBRIDGE *result is more independent of y, as long as the gluon jet is the softest one.* $N^h_{\rm g}$ *of the Boost algorithms is very close to* $0.5N^h_{\rm gg}$ *for all y.*

They perform well at low transverse momenta, but start to show a y-dependence at higher virtualities. This is especially so for the Mercedes algorithm. The OSC algorithms (CE and Boost) give results independent of y and in very good agreement with $0.5N^h_{\rm gg}$.

In Fig 5.11b, the multiplicity of the gluon jet for fixed κ is presented as a function of gluon jet rapidity y. To allow the analysis to include large y, the "angle tag" method is used. With the Boost algorithm, $N^h_{\rm g}(\kappa)$ is independent of y and very close to the predicted $\frac{1}{2}N^h_{\rm gg}(\kappa)$. The result from the CAMBRIDGE algorithm is independent of y in a large range, but somewhat larger than $\frac{1}{2}N^h_{\rm gg}$. The steep rise of the CAMBRIDGE multiplicity at $y \sim 1.6$ reflects the different treatment of the gluon jet when it is not the softest one. A conventional cluster algorithm – in this case the DURHAM algorithm – assigns particles from the region of coherent emission to the gluon jet. For large y this region becomes larger and the DURHAM multiplicity increases.

In Fig 5.12 it is shown how the results using the very simple "soft tag" identification of gluon jets is in very good agreement with more sophisticated methods.

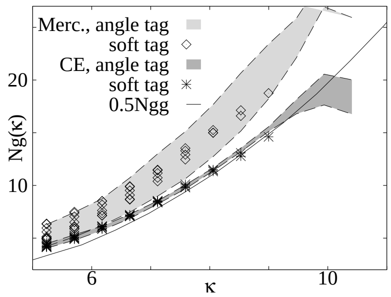

Figure 5.12: *Comparison of jet identification methods. The cluster algorithms presented are designed to properly construct gluon jets in a large part of phase space. Assuming the gluon jet to be softest (symbols) restricts the available phase space to some extent, but the result is in very good agreement with more sophisticated gluon tagging methods (shaded areas).*

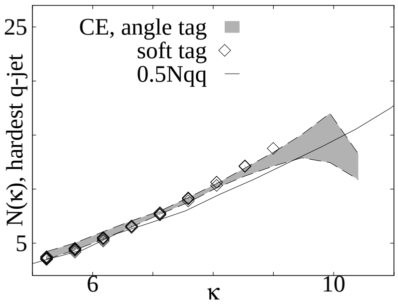

Figure 5.13: *Multiplicities in the hardest quark jet obtained by the Cone Exclusion method compared to half an e^+e^- annihilation event. Results are plotted for several values of y. The range of results is given by a shaded region for the "angle tag". A reliable analysis can be performed in the kinematical region where the gluon jet is predominantly the softest one.*

Multiplicities in Quark Jets

In the Cone Exclusion algorithm, the OSC is used to define one-scale dependent regions also for the quark and antiquark jet. The results for the hardest quark jet are presented in Fig 5.13. Again we note that jet mis-identifications in the "soft tag" method have little effect, and that this simple tagging procedure gives reliable results in a large kinematical region.

5.7.3 Two-Scale Dependence

The analysis required to compare data from fixed energy experiments with model predictions of the virtuality scale dependence is simple and straightforward. In Fig 5.14 the mean multiplicity in events where no gluon jet is found using a resolution scale κ_r, and in events where the hardest gluon jet is found at κ_r are presented. Since the full multiplicity of a two-jet or three-jet event is independent of how the particles are distributed among the jets, any $k_\perp$-based algorithm may be used. There is a fair agreement between MC simulations using the DURHAM algorithm, and the expectations from Eqs (5.25) and (5.26).

With the Mercedes and Boost algorithms, the multiplicities in quark jets are expected to be $0.5N^h_{\rm qq}(L+2y, \kappa < \kappa_r)$, where y and κ_r are the kinematical vari-

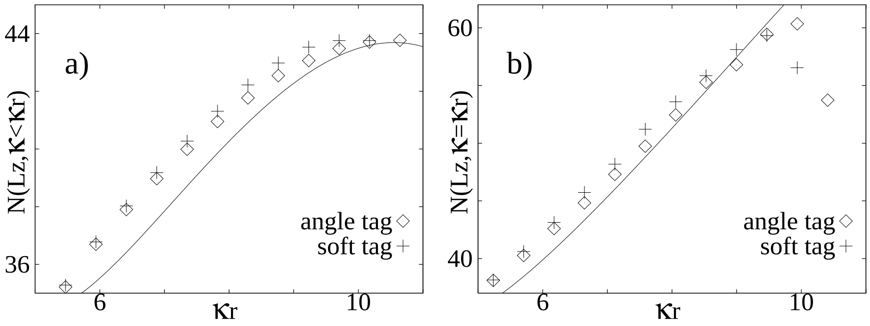

Figure 5.14: *MC results of the multiplicity dependence on the jet resolution scale κ_r for e^+e^- annihilation events with fixed CMS energy $\sqrt{s} = M_Z$. The gluon jet is identified both using the direction of the hardest gluon in the cascade and simply assuming the gluon jet to be softer than the quark jets. Solid lines are obtained using Eqs (5.25) and (5.26).* **a)** *The mean multiplicity in all events with no jet above κ_r* **b)** *The mean multiplicity in all events with the hardest gluon jet at κ_r.*

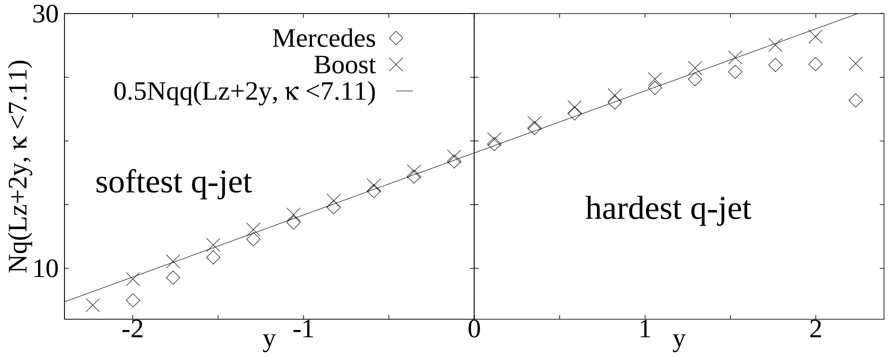

Figure 5.15: *With the Mercedes and Boost algorithms, the energy scales of the quark jets are well defined and equals $\ln(s/\Lambda^2) \pm 2y$, where the rapidity y of the gluon jet is defined by $y = \frac{1}{2}\ln[(1 - x_{\overline{\mathrm{q}}})/(1 - x_{\mathrm{q}})]$. Thus it is possible to study the energy dependence of the two-scale dependent multiplicity. MLLA predicts this dependence to be linear, which also is the result for the Boost algorithm, while the Mercedes algorithm (based on AO) deviates somewhat at large $|y|$.*

ables of the gluon jet. Thus the energy evolution of the two-scale dependence can be studied in a fixed-energy experiment. The expected linear dependence in y (cf. Eq (5.25)) is seen in Fig 5.15, especially for the OSC-based Boost algorithm.

5.8 Summary

The ratio of the hadron multiplicity in quark and gluon jets is predicted to be 4/9 at very high energies. Corrections to this values calculated in the Modified Leading Log Approximation (MLLA) cannot expalin the difference between experimental data and this asymptotic value. In this paper we estimate the contribution from recoil effects to the ratio $N_{\mathrm{q}}/N_{\mathrm{g}}$. Although formally of order $1/\ln s$ this contribution is quantitatively sizeable. Combined with the MLLA expression the result agrees well with MC simulations and with preliminary experimental data for jet energies equal to $M_Z/2$ [10, 11]. We also discuss gluon jet definitions by which the scale evolution of gluon jets can be studied, using data from a fixed energy e^+e^- experiment. These jet definitions thus should enable an extended analysis which would be interesting to combine with the results of [11].

Another important point in this paper is that multiplicities in jets depend on *two* scales, the energy and the virtuality or maximal allowed transverse momentum. We derive expressions for the two-scale dependence and note that it can be examined with simple methods: Using a $k_\perp$-based cluster algorithm to construct exactly three jets, the multiplicities can be examined as a function of jet transverse momentum.

We discuss the "One-Scale Criterion" (OSC), which states that a one-scale dependent jet will, in some Lorentz frame, correspond to one hemisphere of a two-parton event where the energy and transverse momentum scales coincide. The relevant scale for the jet is the energy of the corresponding hemisphere. Most of the commonly used cluster schemes of today concentrate on reproducing the jet energy and direction, and put less emphasis on the assignment of the soft particles to different jets. One exception is the CAMBRIDGE algorithm [9], which based on Angular Ordering (AO) arguments constructs jets with one-scale dependent multiplicities. We present a set of algorithms designed to construct one-scale dependent jets. These are based either on AO or explicitly on the OSC. We examine the algorithms by analysing MC-generated events and comparing the obtained multiplicities in the jets with complete MC-simulated events at corresponding energies.

Our study shows that all the presented algorithms perform well, but that the OSC methods are somewhat better than the AO ones for quantitative analyses of multiplicities in jets. With the OSC algorithms the gluon jet properties depend on only one scale. The treatment of quark jets differ, however. The "Boost algorithm" is particularly suited for studies of the two-scale dependence of quark jets, while the "Cone Exclusion" algorithm is designed for a study of one-scale jets, where the virtuality coincides with the energy of the jet.

We note that the algorithms can be used in a large kinematical region. We do not require the events to be Mercedes-like or Y-shaped. In events where one jet is significantly softer than the others, this jet is predominantly the gluon jet. Performing the analysis on these events makes it less important to identify the gluon jet via quark taggings.

Acknowledgments

This work was supported in part by the EU Fourth Framework Programme 'Training and Mobility of Researchers', Network 'Quantum Chromodynamics and the Deep Structure of Elementary Particles', contract FMRX-CT98-0194 (DG 12 - MIHT).

References

[1] DELPHI Collaboration, Preprint DELPHI 98-16, CONF 117;
TASSO Collaboration, *Z. Phys.* **C45** (1989) 193;
HRS Collaboration, *Phys. Rev.* **D34** (1987) 3304;
AMY Collaboration, *Phys. Rev.* **D42** (1990) 737;
DELPHI Collaboration, *Z. Phys.* **C70** (1996) 179;
P.Abreau, to be published in *Proc.* XXVIII *International Symposium on Multiparticle Dynamics,* Frascati, September 1997

[2] Ya.I. Asimov, Yu.L. Dokshitser, V.A. Khoze, S.I. Troyan, *Z. Phys.* **C27** (1985) 65

[3] Yu.L. Dokshitser, V.S. Fadin, V.A. Khoze, *Z. Phys.* **C15** (1982) 325;
ibid. **C18** (1983) 37;
A. Bassetto, M. Ciafaloni, G. Marchesini, *Phys. Rep.* **100** (1983) 201

[4] A.H. Mueller, *Nucl. Phys.* **B213** (1983) 85 [Erratum , **B241** (1984) 141];
ibid. **B228** (1983) 351;
Yu.L. Dokshitser, S.I. Troyan, *in* Proc. XIX Winter School LNPI, v.I. 144 (1984); preprint LNPI-922 (1984)

[5] Yu.L. Dokshitser, V.A. Khoze, A.H. Mueller and S.I. Troyan, Basics of Perturbative QCD, (*Editions Frontières, Gif-sur-Yvette, 1991*)

[6] D. Amati, G. Veneziano, *Phys. Lett.* **B83** (1979) 87

[7] For a review, see
L. Lönnblad, S. Moretti, T. Sjöstrand, *JHEP* **08** (1998) 001

[8] A.H. Mueller, *Phys. Lett.* **B104** (1981) 161;
B.I. Ermolaev, V.S. Fadin, *JETP. Lett.* **33** (1981) 269;
A. Bassetto, M. Ciafaloni, G. Marchesini, A.H. Mueller, *Nucl. Phys.* **B207** (1982) 189

[9] Yu.L. Dokshitser, G.D. Leder, S. Moretti and B.R. Webber, *JHEP* **08** (1997) 001

[10] OPAL Collaboration, *Phys. Lett.* **B388** (1996) 659;
OPAL Collaboration, *Eur. Phys. J.* **C1** (1998) 479

[11] OPAL Physics Note PN344, preliminary results, contributed paper 296 to the ICHEP'98 Conference, Vancouver

[12] ALEPH Collaboration, *Z. Phys.* **C76** (1997) 191;
DELPHI note 98-78, contributed paper 146 to the ICHEP'98 Conference, Vancouver

[13] G. Gustafson, *Phys. Lett.* **B175** (1986) 453;
G. Gustafson, U. Pettersson, *Nucl. Phys.* **B306** (1988) 746;
B. Andersson, G. Gustafson, L. Lönnblad, *Nucl. Phys.* **B339** (1990) 393

[14] G. Gustafson, *Nucl. Phys.* **B392** (1993) 251

[15] D. Amati, R. Petronzio, G. Veneziano, *Nucl. Phys.* **B140** (1978) 54;
ibid. **B146** (1978) 29

[16] G. Marchesini, L. Trentadue, G. Veneziano, *Nucl. Phys.* **B181** (1981) 335

[17] G. Marchesini, B.R. Webber, *Nucl. Phys.* **B238** (1984) 1

[18] B.R. Webber, *Nucl. Phys.* **B238** (1984) 492

[19] G. Marchesini et al., *Comp. Phys. Comm.* **67** (1992) 465

[20] B. Andersson, G. Gustafson, G. Ingelman, T. Sjöstrand, *Phys. Rep.* **97** (1983) 31

[21] B. Andersson, G. Gustafson, J.Samuelsson, *Z. Phys. C* **64** (1994) 653

[22] B. Andersson, P. Dahlquist, G. Gustafson, *Phys. Lett.* **B214** (1988) 604

[23] B. Andersson, P. Dahlquist, G. Gustafson, *Z. Phys.* **C44** (1989) 455,461

[24] L. Lönnblad, *Comp. Phys. Comm.* **71** (1992) 15

[25] M. Bengtsson, T. Sjöstrand, *Comp. Phys. Comm.* **39** (1986) 347;
T. Sjöstrand, *Comp. Phys. Comm.* **82** (1994) 74

[26] G. Gustafson, *Z. Phys.* **C15** (1982) 155

[27] C. Friberg, G. Gustafson, J. Häkkinen, *Nucl. Phys.* **B490** (1997) 289

[28] B.R. Webber, LEP2 QCD Working Group meeting, 19 May 1995;
L. Lönnblad, *Z. Phys.* **C70** (1996) 107;
J. Ellis, K. Geiger, *Phys. Rev.* **D54** (1996) 1967;
J. Ellis, K. Geiger, *Phys. Lett.* **B404** (1997) 230

[29] G. Gustafson, U. Pettersson, P.M.Zerwas, *Phys. Lett.* **B290** (1988) 90;
V.A. Khoze, T. Sjöstrand, *Z. Phys.* **C62** (1994) 291;
V.A. Khoze, T. Sjöstrand, *Phys. Rev. Lett.* **72** (1994) 28;
Yu.L. Dokshitser, V.A. Khoze, L.H. Orr, W.J. Stirling, *Nucl. Phys.* **B403** (1993) 65
G. Gustafson, J. Häkkinen, *Z. Phys.* **C64** (1994) 659;
Report of the Working Group on "W Mass and QCD", hep-ph/9709283 08 Sep 1997;
J.Häkkinen, M. Ringnér, *Eur. Phys. J.* **C5** (1998) 275

[30] DELPHI collaboration, *Phys. Lett.* **B401** (1997) 181;
OPAL collaboration, *Eur. Phys. J.* **C1** (1998) 395;
LEP2 preliminary results, contributed papers 287, 288, 391, 395, 506, 507, 894 and 909 to the ICHEP'98 Conference, Vancouver

[31] J.B. Gaffney and A.H. Mueller, *Nucl. Phys.* **B250** (1985) 109

[32] I.M. Dremin and V.A. Nechitailo, *Mod. Phys. Lett.* **A9** (1994) 1471

[33] Yu.L. Dokshitser, V.A. Khoze and S.I. Troyan, *Sov. J. Nucl. Phys.* **47** (1988) 881

[34] S. Catani, Yu.L. Dokshitser, M. Olsson, G. Turnock and B.R. Webber, *Phys. Lett.* **B269** (1991) 432